UNDERSTANDING AND TREATING EYE DISEASES: MECHANICAL CHARACTERIZATION AND PHOTOCHEMICAL MODIFICATION OF THE CORNEA AND SCLERA

Thesis by

Matthew Sanford Mattson

In Partial Fulfillment of the Requirements for the

degree of

Doctor of Philosophy

CALIFORNIA INSTITUTE OF TECHNOLOGY

Pasadena, California

2008

(Defended May 7, 2008)

© 2008

Matthew Sanford Mattson

All Rights Reserved

ACKNOWLEDGEMENTS

I would like to thank my mom and dad for all their support. Really without them, I never would have made it this far. I'd like to thank my brother and sister for their interest and fascination in what I am doing, and for always being a part of my life. I thank my relatives who always ask questions regarding my work and the progress we are making.

I thank those people who convinced me to apply to Caltech. You were right, California is fun. Caltech's a good school. I have enjoyed myself.

I extend a special thanks to everyone in the Kornfield group without whom I could not have completed this work. In addition I thank you for the wonderful conversations that make working in the lab more enjoyable.

I thank my friends, here in California, as well as in West Virginia and Virginia who remind me that I need to keep it real and relax.

I thank all of the collaborators who have made this work possible, and who have truly been fun to work with.

This project has continually been guided by the hands of my advisor, Julie Kornfield, and very close co-workers, Dan Schwartz, Scott Fraser, Bob Grubbs, CJ Yu, and Yang. Having regular interactions with you has been an eye opening experience.

I thank my friends at Church for all your helpful prayers and kindness. You are a blessing in my life.

I thank God for getting me through this ordeal and keeping me company no matter how things went.

ABSTRACT

Proper vision relies heavily on the eye's ability to maintain optical clarity and structural integrity under daily fluctuations in pressure, variations in humidity and temperature, constant muscular strain and sudden movements. Therefore, as is the case for many organs, proper function depends on the physical properties of eye tissues. Many diseases are associated with altered chemical and mechanical states of tissue and a resulting loss of functionality. Diseases that cause changes in visual acuity, such as degenerative myopia and keratoconus, may be treatable by engineering the mechanical properties of the sclera and cornea.

Degenerative myopia is the leading cause of untreatable blindness in China, Taiwan, and Japan, and is ranked 7th in the United States. The disease entails progressive stretching and thinning of the scleral tissues that leads to elongation of the eye and posterior staphyloma formation. While refractive errors are readily corrected for patients, there is an increased likelihood of visual loss due to stretching of the chorioretinal tissues. Retinal tears and detachments as well as choroidal neovascularization create debilitating problems. Currently, there is no treatment to retard or prevent the axial elongation of the globe in degenerative myopia.

Keratoconus affects nearly 1 in 2000 Americans and is identified by the conical shape that the cornea forms. The thinning and weakening of the cornea in this disease causes the cornea to bulge out under normal intraocular pressures. With increasing degrees of protrusion, correction by spectacles and contact lens wear becomes more and more difficult. Eventually 20% of patients will require corneal transplantation because refractive

correction is no longer possible. Further, patients with thin corneas are at high risk for complications after LASIK and similar refractive surgeries. Early clinical data supports the efficacy of ultraviolet light activation of topically applied riboflavin to increase the corneal modulus and prevent progression of the disease.

The use of riboflavin activated by ultraviolet light and the use of crosslinkers to treat tissue works on the presupposition that by increasing the strength and mechanical stability of the tissue, the disease progression may be halted. Our studies *in vitro* indicate that crosslinking can improve tissue mechanical stability and resistance to deformation.

Mechanical characterization of tissue has relied heavily on the use of the intact globe expansion method which we have developed. While other measurement techniques (uniaxial tensile tests, shear rheology) are used in the field of eye biomechanics, our evaluation of the testing methods and variability of the results indicates that considerable effort is required to achieve reliable results. The intact globe expansion test provides reliable measurements, with relatively few samples, and mimics the type and distribution of stresses inherent in the natural boundary conditions of the eye. Furthermore, application of high intraocular pressures provides a way to study shape changes of the sclera and cornea which are similar to those exhibited in myopia and keratoconus. Potential treatments that show an ability to prevent ocular distension in this method have a chance of preventing the deformations that occur *in vivo* in the diseases. Therefore, this method has been used to evaluate treatments developed in the course of this thesis.

Our treatment development has gained direction from the previous example of Wollensak and Speorl who pioneered the use of riboflavin and ultraviolet-light-induced crosslinking of tissue. Light activated crosslinking provides spatial and temporal control of treatments. The choice of different photoinitiator systems, such as Eosin Y (EY) and triethanolamine (TEOA) allows the use of visible light (525 ± 16 nm), and at the irradiation doses necessary to achieve stabilization of the eye mechanical properties *in vitro* (6–8 mW/cm^2), calculations indicate that treatments will be more than a factor of 6 under the thresholds set by ANSI guidelines.

Eye stabilization *in vitro* has been demonstrated through treatment of either the sclera or the cornea with the use of EY and TEOA. For myopia treatment, drug delivery *in vitro* used low concentrations (0.0289 mM EY, 90 mM TEOA) , while the switch to *in vivo* drug delivery by subconjunctival injection required the use of higher concentrations (0.298 mM EY, 90 mM TEOA) to achieve the same stabilization during *in vitro* expansion. Keratoconus treatments comparing the protocols for riboflavin that are used in the clinic to treatment with EY/TEOA demonstrate similar capabilities of eye stabilization. Further, penetration studies of EY/TEOA show the possibility of delivering drug to the stroma without removal of the epithelium. In combination with the reduced treatment time of the visible light treatment (10 minutes as opposed to 35 for the riboflavin/UV treatment), this could vastly improve the current treatment techniques.

Biocompatibility studies of the treatments indicate excellent tolerance to the light and drug in both rabbits and guinea pigs. Although we discovered that treatment with 0.09 mM EY/90 mM TEOA was not able to prevent development of form deprivation myopia in a

guinea pig model, there were no ill effects of the treatment seen during the life of the animals. Tests on normal growth of guinea pig eyes indicate that treatment with a higher dose (0.289 mM EY/90 mM EY) causes substantial changes to eye shape without toxicity. These changes are manifested in shifts in the refractive error and ocular length that persist for the duration over which the animals are monitored.

In summary, the mechanical measurement technique developed in this work has usefulness as a tool to characterize tissue strength and as a tool for screening and comparing treatment efficacy. The visible light system designed for the purposes of treating degenerative myopia and keratoconus shows an ability to stabilize eye shape *in vitro*, demonstrates biocompatibility, and does so with light doses that are deemed safe levels for clinical applications.

TABLE OF CONTENTS

Acknowledgements iii
Abstract v
Table of Contents ix
List of Illustrations and Tables xi
Symbols and Abbreviations xiv

Chapter I: Introduction
1.1 Importance of Vision I-1
1.2 Diseases of the Eye—Myopia & Keratoconus I-3
1.2.1 Degenerative Myopia I-5
1.2.2 Keratoconus I-6
1.2.3 Corneal and Scleral Structure I-7
1.3 Importance of Mechanical Properties—Diseases & Measurements .. I-9
1.4 Potential Treatments I-10
1.4.1 Crosslinking I-10
1.4.2 Photoactivated Crosslinking I-13
1.5 Outline of Thesis I-13
Bibliography I-15
Chapter II: Mechanical Measurements
2.1 Introduction to the Field of Biomechanics II-1
2.2 Principles Behind Measurements II-3
2.3 Techniques in the Field II-5
2.4 Strengths and Limitations of Alternative Techniques: Illustration in Cornea and Sclera II-9
2.4.1 Uniaxial Tensile Tests II-10
2.4.2 Oscillatory Shear Rheology II-21
2.4.3 Intact Globe Expansion Test II-35
Bibliography II-46
Chapter III: Photoactivated Treatment Using Visible Light
3.1 Introduction III-1
3.2 Photoinitiator Systems III-3
3.3 Temporal and Spatial Control of Treatments III-6
3.3.1 Temporal Control of Treatments III-6
3.3.2 Spatial Control of Treatments III-8
3.4 Light Safety and Clinical Relevance III-10
Bibliography III-14
Chapter IV: Interpenetrating Polymer and Tissue Networks
4.1 Tissue Engineering IV-1
4.2 Concentration and Oxygen Dependence of Increases in Scleral Modulus IV-3

4.3 Crosslinking Without PEGDM IV-7
4.4 *In Vivo* Treatment Comparison With and Without PEGDM IV-10
Bibliography IV-14
Chapter V: Treatment of Myopia
5.1 Introduction V-2
5.2 Materials and Methods V-6
5.2.1 In Vitro *Application &* In-Vitro *Expansion* *V-6*
5.2.2 Biocompatibility *V-8*
5.2.3 In Vivo *Application &* In-Vitro *Expansion* *V-9*
5.2.4 Animal Model of Myopia *V-12*
5.3 Results V-17
5.3.1 In Vitro *Application &* In-Vitro *Expansion* *V-17*
5.3.2 Biocompatibility *V-20*
5.3.3 In Vivo *Application &* In-Vitro *Expansion* *V-23*
5.3.4 Animal Model of Myopia *V-24*
5.4 Summary V-31
Bibliography V-32
Chapter VI: Treatment of Keratoconus
6.1 Introduction VI-1
6.2 Materials and Methods VI-3
6.2.1 Penetration of Molecules—Epithelial Barrier *VI-3*
6.2.2 In Vitro *Application and* In Vitro *Expansion* *VI-6*
6.3 Results VI-9
6.3.1 Penetration of Molecules—Epithelial Barrier *VI-9*
6.3.2 In Vitro *Application and* In Vitro *Expansion* *VI-10*
6.4 Summary VI-14
Bibliography VI-16

LIST OF ILLUSTRATIONS AND TABLES

Page

Chapter 1

Figure 1.1 Anatomy of the Eye I-3

Figure 1.2 Emmetropia, Hyperopia and Myopia I-4

Figure 1.3 Degenerative Myopia and Keratoconus I-6

Figure 1.4 Maillard Reaction I-12

Chapter 2

Figure 2.1 Ideal Materials II-3

Figure 2.2 Methods in Biomechanics II-6

Figure 2.3 Young-Laplace Equation II-7

Figure 2.4 Oscillatory Shear Measurement II-9

Figure 2.5 Stress-Strain Curves of Human Cornea II-11

Figure 2.6 Tissue Preparation for Tensile Measurements II-14

Figure 2.7 Clamping for Tensile Tests II-15

Figure 2.8 Stress-Strain Curves of Porcine Sclera II-17

Figure 2.9 Stress-Strain of GA Treated Porcine Sclera II-18

Figure 2.10 Stress-Strain Curves of Porcine Cornea II-20

Figure 2.11 Log Plot of Porcine Cornea Stress-Strain Curve II-20

Figure 2.12 Association of Modulus Values to Prestress II-21

Figure 2.13 Straightening Tissue for Loading II-23

Figure 2.14 Rheometry System for Biological Specimens II-25

Figure 2.15 Percent Compression During Loading II-25

Figure 2.16 GA Crosslinked Sclera II-28

Figure 2.17 NaCl-Concentration-Dependent Modulus II-30

Figure 2.18 In Situ NaCl-Concentration Dependence II-30

Figure 2.19 In Situ pH-Dependent Modulus II-32

Figure 2.20 In Situ pH-Reversible Effects II-33

Figure 2.21 In Situ Temperature-Dependent Modulus II-34
Figure 2.22 Button and Whole Eye Expansion II-36
Figure 2.23 Intact Globe Expansion Setup II-39
Figure 2.24 Variability from Initial Loading II-41
Figure 2.25 High- and Low-Pressure Expansion..... II-43
Figure 2.26 GA Crosslinking Prevents Expansion..... II-44

Table 2.1 Incubations in Different pH Solutions II-31
Table 2.2 Rabbit Eye Initial Dimensions II-41

Chapter 3
Figure 3.1 Photoinitiators III-5
Figure 3.2 Photorheology Setup..... III-7
Figure 3.3 Gelatin Modulus Change During Irradiation III-8
Figure 3.4 Spatial Control of Light-Activated Crosslinking..... III-10
Figure 3.5 Safe Light Doses for Posterior Illumination III-13

Table 3.1 Biocompatibility of Eosin Y III-5
Table 3.2 Light Absorption Values for Posterior Illumination III-12

Chapter 4
Figure 4.1 Concentration- and Oxygen-Dependent Polymerizations ... IV-6
Figure 4.2 Crosslinking With or Without PEGDM..... IV-9
Figure 4.3 Effect of PEGDM Crosslinking on Eye Expansion..... IV-11
Figure 4.4 Penetration of Fluorescein-PEGM Within Sclera..... IV-13

Table 4.1 Solutions for *In Vivo* Testing of PEGDM IV-10

Chapter 5
Figure 5.1 Setups for *In Vitro* Light Delivery V-7
Figure 5.2 *In Vivo* Drug and Light Delivery..... V-11

Figure 5.3 Controlled Subconjunctival Injection of Eosin Y V-14
Figure 5.4 Guinea Pig Irradiation Procedures V-15
Figure 5.5 Guinea Pig Form Deprivation Model V-16
Figure 5.6 Measurement of Ocular Dimensions V-18
Figure 5.7 Effect of 1x EY Treatment on Eye Expansion V-19
Figure 5.8 Effect of Light Source on Eye Expansion V-20
Figure 5.9 Rabbit Sclera Histology V-22
Figure 5.10 Effect of *In Vivo* Treatment on Eye Expansion V-24
Figure 5.11 Guinea Pig Sclera Histology V-25
Figure 5.12 Effect of 3x EY Treatment on Form Deprivation V-26
Figure 5.13 Effect of 10x EY on Normal Eye Growth V-28
Figure 5.14 Effect of 10x EY on Individual Ocular Components V-30

Table 5.1 *In Vivo* Rabbit Treatment Variables V-11
Table 5.2 *In Vivo* Guinea Pig Treatment Variables V-13

Chapter 6
Figure 6.1 Slit Lamp Apparatus for Fluorescent Imaging VI-4
Figure 6.2 Slit Lamp Images of Fluorescent Profiles VI-5
Figure 6.3 Penetration With or Without Intact Epithelium VI-10
Figure 6.4 Effect of Epithelium on Perimeters of Expanding Eyes VI-11
Figure 6.5 Effect of Epithelium on 1x EY Treated Eyes VI-12
Figure 6.6 Effect of Various Treatments on Eye Expansion VI-14

Table 6.1 Solutions for Penetration Studies VI-5
Table 6.2 Treatment Mixtures for Corneal Stability VI-7
Table 6.3 Keratoconus Treatment Results VI-14

SYMBOLS AND ABBREVIATIONS

AGE	Advanced Glycation Endproduct
CD	Corneal Diameter
CL	Corneal Length
CP	Corneal Perimeter
DPBS	Dulbecco's Phosphate-Buffered Saline
ED	Equatorial Diameter
EY	Eosin Y
G′	Storage Modulus
G″	Loss Modulus
GA	Glyceraldehyde
GAG	Glycosaminoglycan
HA	Hyaluronic acid
I2959	Irgacure 2959
PBS	Phosphate-Buffered Saline
SL	Scleral Length
SP	Scleral Perimeter
TEOA	Triethanolamine
η	Viscosity
σ	Shear Stress
γ	Shear Strain
$\dot{\gamma}$	Strain Rate

C h a p t e r 1

INTRODUCTION

1.1 Importance of Vision I-1
1.2 Diseases of the Eye—Myopia & Keratoconus I-3
1.2.1 Degenerative Myopia *I-5*
1.2.2 Keratoconus *I-6*
1.2.3 Corneal and Scleral Structure *I-7*
1.3 Importance of Mechanical Properties—Diseases & Measurements .. I-9
1.4 Potential Treatments I-10
1.4.1 Crosslinking *I-10*
1.4.2 Photoactivated Crosslinking *I-13*
1.5 Outline of Thesis I-13
Bibliography I-15

"There is no better way to thank God for your sight than by giving a helping hand to someone in the dark."—Helen Keller

1.1 Importance of Vision

Our culture recognizes the importance of vision, and it is an integral part of our lives and language. Vision allows processing of large amounts of information in a short period of time: "A picture is worth a thousand words." We associate the loss of sight with an inability to cope in the world: "Like the blind leading the blind." Our reluctance to lose the ability to see has driven the creation of a world of research, medicine, and business focused on restoring sight. Americans spend approximately $15 billion a year on eyewear,[1] and the National Eye Institute estimates that the economic cost associated with visual

disabilities in 2003 was nearly $63 billion.[3] Our research, like many other peoples' research, delves into the treatment of eye diseases in order to prevent eventual blindness.

To understand the nature of the two diseases we study (keratoconus and degenerative myopia), it is important to understand the role that individual ocular components play in allowing the eye to see. The eye is an amazing organ whose function is to collect light and transform it into signals interpretable by the brain. The cornea is the clear front of the eye and serves as window through which light enters the eye (Figure 1.1). The curvature of the cornea and its refractive index difference from air are responsible for nearly 2/3 of the eye's focusing power. Light that enters through the cornea then intercepts the iris. The iris acts as an aperture and controls the amount of light entering through the pupil. Its constriction restricts the amount of light in bright conditions, and its ability to dilate allows more light to enter in dark conditions. Immediately behind the pupil is a flexible crystalline lens. The ciliary muscle can change the shape of this lens, allowing adjustable focus of the world. Images are focused through the vitreous onto the retina. The vitreous is a collagen based gel that is nearly 99% water. This gel is thought to provide structural support, preventing damage to the eye's components during sudden movements or collisions. The retina is responsible for transforming light into chemical signals. Photoreceptors in the retina absorb light and transmit signals along nerves that exit the eye through the optic nerve, which connects to the brain. Around the whole eye, and connected to the cornea, is a tissue called the sclera, which is responsible for maintaining the proper shape of the eye.

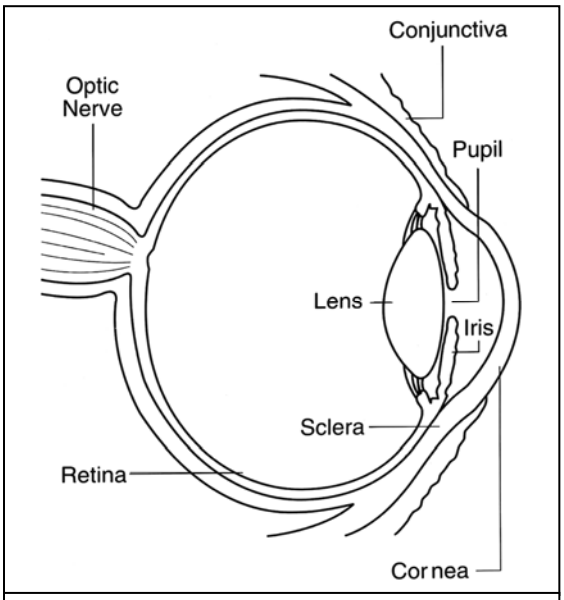

Figure 1.1. This illustration of the eye anatomy indicates the location of the cornea, sclera, and conjunctiva. Reproduced from the National Eye Institute, National Institutes of Health

1.2 Diseases of the Eye—Myopia and Keratoconus

If any one of the ocular components does not function properly, vision is impaired and in some cases, uncorrectable. The shape of the eye defined by the cornea and sclera plays a great role in the ability to see clearly. In the proper shape, incoming light is bent by the cornea and images are focused onto the plane of the retina. This state of vision is emmetropia (Figure 1.2a). If the corneal curvature changes to become flatter, it loses some of its power and images are focused behind the retina (Figure 1.2b). Steepening of corneal curvature increases its power and images are focused in front of the retina (Figure 1.2c). In these two cases, the eye becomes hyperopic or myopic, respectively. Likewise, changes in the shape of the sclera move the image focal plane off the retina. Shorter, hyperopic eyes

have light focused behind the retina, while longer myopic eyes have light focused in front of the retina. Without correction from spectacles, contacts, or surgery, vision is impaired resulting in farsightedness (hyperopia) or nearsightedness (myopia) (Figure 2.1.g, h).

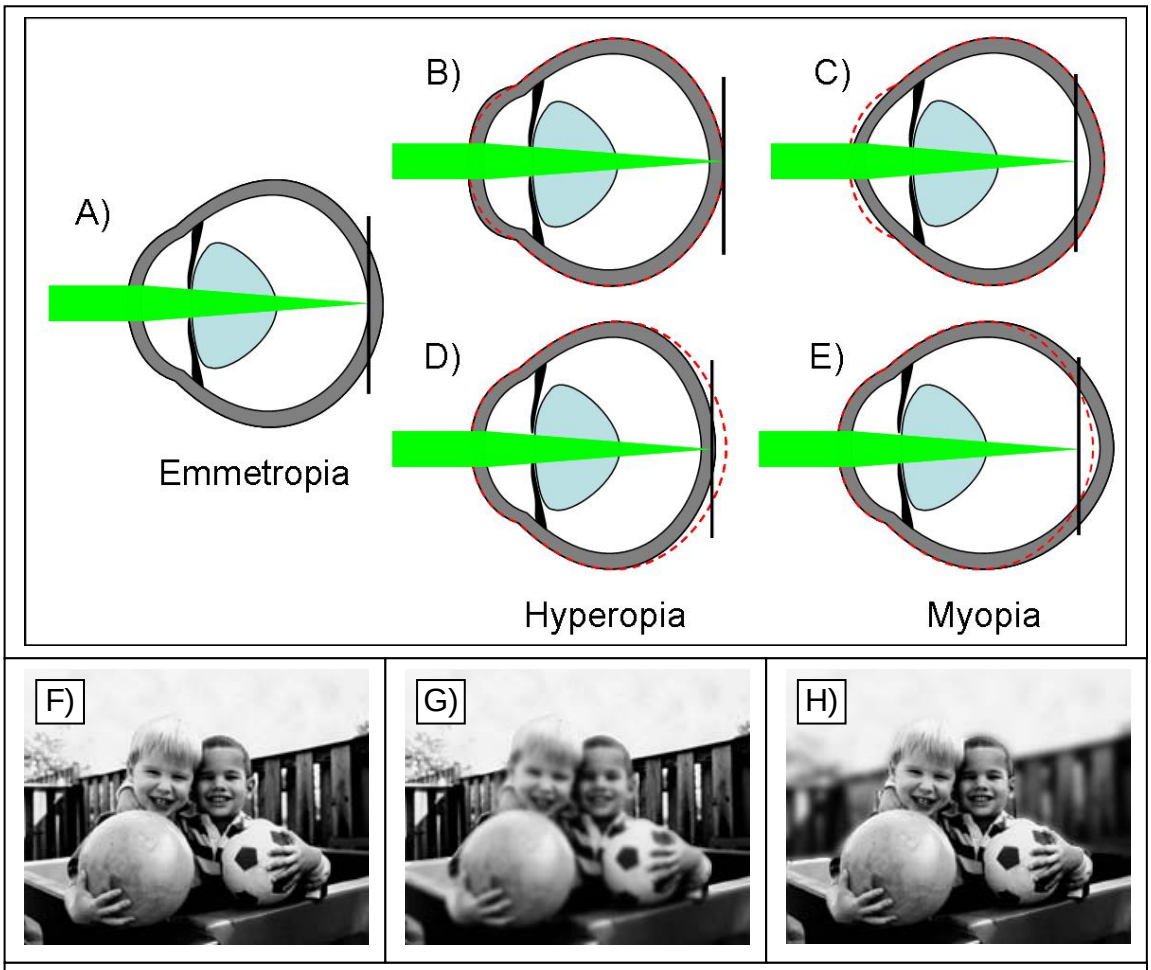

Figure 1.2. A) In the emmetropic state, images are focused onto the plane of the retina. In hyperopia, images are focused behind the plane of the retina, and in myopia they are focused in front of the retina. B) A flatter cornea focuses images behind the retina, while C) a steeper cornea focuses light in front of the retina. D) A shorter eye moves the retina in front of the focal plane and E) a longer eye moves the retina behind the focal plane. Images from the National Eye Institute, National Institutes of Health depict eyesight with F) emmetropia, G) hyperopia, and H) myopia.

Diseases that create shape changes in either the sclera or the cornea are bound to effect vision. Two diseases that we have studied in particular are degenerative myopia, which creates an elongated eye through the thinning and stretching of the sclera, and keratoconus, which creates a cone shaped cornea that bulges outward.

1.2.1 Degenerative myopia

Myopia affects 30% of the population in the U.S. and Europe, and 70–90% of the population in some Asian countries.[4-6] High myopia of greater than 8 diopters affects 0.2–0.4% of the US population and up to 1% of the population in Asian countries.[7-13] Degenerative myopia is classically defined as the form of myopia characterized by progressive stretching and thinning of scleral tissues leading to globe elongation and to posterior staphyloma formation (Figure 1.3a).[12] As scleral tissues stretch and thin, there is associated stretching of retinal and choroidal tissues that promotes visual loss. While visual loss from macular atrophy and choroidal neovascularization are most common in degenerative myopia, patients with this disease are also more prone to retinal detachment and macular hole formation. Although a large population is affected by this disease worldwide, there is currently no effective method to arrest progression and reduce the rate of visual loss.

The excessive axial enlargement of the globe that occurs in degenerative myopia occurs preferentially in the posterior pole. The causes of scleral thinning and stretching that occur during this elongation are incompletely understood, but reduction of collagen fibril diameter, enhanced turnover of scleral collagen, and alteration of scleral

glycosaminoglycans are contributory factors.[14] As the mechanical properties of the sclera are altered in myopia, it is hypothesized that the eye is prone to stretching due to the load effect of intraocular pressure.

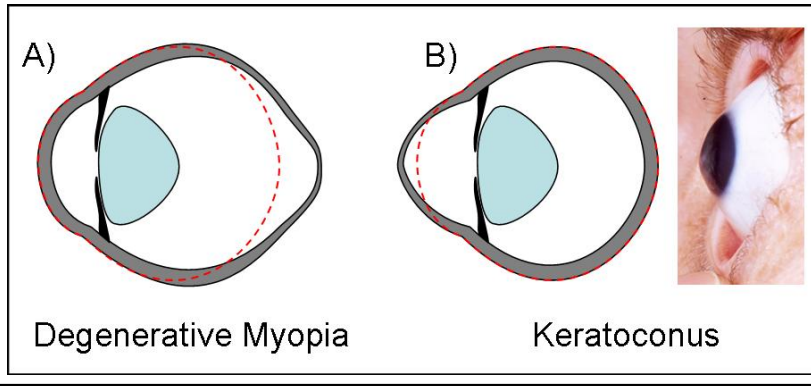

Figure 1.3. A) Thinning and stretching in the posterior pole characteristic of degenerative myopia. B) Conical shape of the cornea resulting from a thinning in keratoconus and photograph showing a keratoconus eye. Courtesy of Indiana University School of Medicine, Department of Ophthalmology

1.2.2 Keratoconus

Keratoconus is the most common corneal dystrophy, affecting approximately 1/2000 individuals with no gender or racial preference. The disease is nearly always bilateral and causes progressive paracentral corneal thinning.[15, 16] Patients usually present in their teens with increasing myopia and irregular astigmatism due to conical corneal steepening (Figure 1.3b). As the disease progresses, spectacles cannot correct the irregular astigmatism, and patients need to wear contact lenses to optimize their visual acuity. In approximately 20% of patients, penetrating keratoplasty (corneal transplantation) is required because of contact lens intolerance and/or loss in best corrected visual acuity. Keratoconus is one of the leading causes of penetrating keratoplasty in the US.

Clinical diagnosis of keratoconus is generally straightforward. In addition to progressive myopia and astigmatism, various changes are evident at the slit lamp including apical corneal thinning, iron line formation (Fleischer ring) at the base of the "cone", stromal scarring, and in some cases, corneal hydrops due to rupture of Descemet's membrane. Corneal topographical analysis has made it easier to quantify progression of keratoconus as well as to detect subclinical disease (forme fruste keratoconus).[17-19] The latter has come into increasing focus because patients with forme fruste keratoconus who undergo corneal refractive procedures, such as LASIK, can develop post-LASIK ectasia requiring corneal transplantation.[20-23] Given the growing frequency of corneal refractive surgery, forme fruste keratoconus is increasingly recognized as an important contraindication to excimer laser ablative procedures.

The genetic and molecular abnormalities underlying keratoconus are unknown. Increased extracellular matrix degradative enzyme activity has been reported,[24, 25] as has a mutation in superoxide dismutase (SOD1) that might increase oxidative damage to the cornea.[26]

1.2.3 Corneal and Scleral Structure

In keratoconus and myopia, changes to the extracellular matrix and thinning of the tissue result in a reduction of tissue strength and misshapen eyes. The corneal and scleral extracellular matrices are composed of very similar components. Both tissues are 75–78% water and the remaining mass consists mostly of collagen and glycosaminoglycans (GAGs).[27, 28] The majority of the dry mass is type I collagen. Collagen is a triple helix molecule with glycine located at every third position along the protein. Collagen self

assembles to form fibers of stacked molecules linked end to end, and these fibers aggregate to form fibrils which can be arranged in lamellae. In addition to collagen, the cornea and sclera also have GAGs, which are highly charged molecules formed of dissacharide subunits. These GAGs can also connect to protein cores forming very large, highly charged species—proteoglycans. These highly charged species attract water to the tissue. The collagen and proteoglycans interact to form the extracellular matrix.

While the basic components are similar, differences in fibril arrangement give the cornea and sclera distinct properties. The collagen fibers in the cornea have regular spacing between them, and have a very narrow distribution of fiber diameters. The fibrils are organized into layers with fibrils running parallel within the layer. Stacks of layers are arranged with sequential layers having orthogonal fibers. Such carefully controlled arrangement of the fibers creates the optically clear cornea. In the sclera, the fibers have a large distribution of diameters, have irregular spacing, and although organizing into ribbons of fibers, these ribbons interweave instead of stacking like in the cornea. All these differences contribute to the scattering properties of the sclera that make it white instead of clear.

Despite the differences in structure, the cornea and sclera are made of essentially the same components, and a treatment for one tissue could possibly work for the other. Based on the weakening of tissue in degenerative myopia and keratoconus, a way to alter the tissue and restore mechanical stability could be a suitable treatment.

1.3 Importance of Mechanical Properties—Diseases and Measurements

As discussed in the previous section, changes to the cornea and sclera during keratoconus and degenerative myopia result in changes of the mechanical properties of these tissues. With the disease, they are more susceptible to stresses, and undergo deformations that affect vision. The association of tissue mechanical state with proper function is seen in other areas of the eye and other parts of the body as well. A stiff lens prevents adjustable focus; a weakened lamina cribrosa contributes to pinching of the optic nerve in glaucoma. In other parts of the body, stiffening of collagen and elastin in the skin causes wrinkles, weakening of blood vessel walls can result in aneurysms, weakness of containing membranes can result in hernia, and weakened bones in osteoporosis can increase risk of bone fracture. While the healthy tissue has a mechanical state that allows proper function, diseased tissue with an altered mechanical state is susceptible to failure. Treatments can be developed with the goal of restoring proper mechanical state or replacing tissue with something that matches the natural tissue mechanics.

In order to characterize the healthy, diseased, and treated tissue, it is necessary to quantify the mechanical properties in each state. Ideally, tests on mechanical properties would be done *in vivo* without altering the tissue. Unfortunately this is often difficult and testing methods must be designed to mimic the types of stresses and strains experienced *in vivo*. Furthermore, it may be necessary to exaggerate the stresses and strains in order to obtain results that show a quantifiable difference between tissues within time limits imposed on laboratory work. Reliable methods would maintain a tissue's original condition as much as possible and provide repeatable results. In Chapter 2, we compare tensile, shear, and

expansion tests in order to evaluate variability of the methods and determine their usefulness for characterizing cornea and sclera. In addition, intact globe expansion tests provide a method of evaluating the treatments developed for keratoconus and myopia.

1.4 Potential Treatments

In our understanding of the disease state of keratoconus and degenerative myopia, we see that a loss of the mechanical stability of the tissue leads to deformations that cause visual problems. If however, there were methods of preventing the deformations, reinforcing the tissue, and restoring mechanical stability, then there would be the possibility of treating these diseases. Increasing the strength, or modulus, of the cornea and sclera might prevent ocular distension and reduce progression of keratoconus and degenerative myopia.

This section discusses the use of crosslinkers as viable treatment options and, in particular, discusses the merits of photoactivated systems. Such systems increase the ability to tailor treatments to individual patients by providing spatial localization and temporal control of crosslinking.

1.4.1 Crosslinking

Crosslinking in tissues occurs naturally with aging and is normally associated with undesirable changes.[2, 29-38] It causes stiffening of the skin, cartilage, heart, cornea, lens, lung, arteries, and nearly every tissue with an abundance of extracellular matrix. This stiffening is associated with wrinkling, osteoarthritis, cardiovascular disease, and vision

problems. Many of the crosslinks are advanced glycation end-products (AGEs) that result from the reaction of sugars with amine groups in proteins (Figure 3.1).[39-44]

An increased amount of AGEs is common in diabetics as a result of the inability to properly control sugar levels in the body. This predisposes diabetics to many problems, but interestingly, there is evidence that crosslinking of corneal collagen that occurs in diabetes provides protection against keratoconus.[45] Further, studies using common collagen crosslinkers such as glyceraldehyde, methylglyoxal, and glutaraldehyde within the cornea and sclera indicate that strength of the tissue is increased after crosslinking.[46-50] Our experiments with glyceraldehyde crosslinking show a greater than 300% increase in shear modulus after crosslinking of sclera (Figure 2.16), and demonstrate the ability of crosslinked eyes (cornea and sclera) to resist expansion at elevated intraocular pressures (Figure 2.26).

The ability to use crosslinking agents to strengthen ocular tissues and prevent expansion is not attractive clinically. The extent of crosslinking produced by a given dose of crosslinker using the "Maillard reaction" (Figure 1.4) may prove difficult to control and monitor. The initial reaction is reversible and does not necessarily lead to the formation of crosslinks: the Schiff base undergoes modification, typically forming more stable Amadori products, which tend to accumulate over time and through further modification may form crosslinks or stable pendant adducts. The transition from Amadori product to AGE can take from minutes to days, so that even after removal of excess sugars, continued crosslinking of tissue occurs. This effect is evident in the additional 50% increase of the shear modulus observed over the first 24 hours after rinsing excess glyceraldehyde from the sclera (Figure

2.16). A further aspect of the lack of control over the crosslinking reaction is the fact that there is no way to turn on and off the reactivity of the reducing sugars. Protein modification is more likely in areas of high crosslinker concentration, and these small molecules spread quickly by diffusion—both into the intended tissue and surrounding tissues. This poses a danger in the eye where crosslinking in sensitive areas, such as the retina, should be avoided.

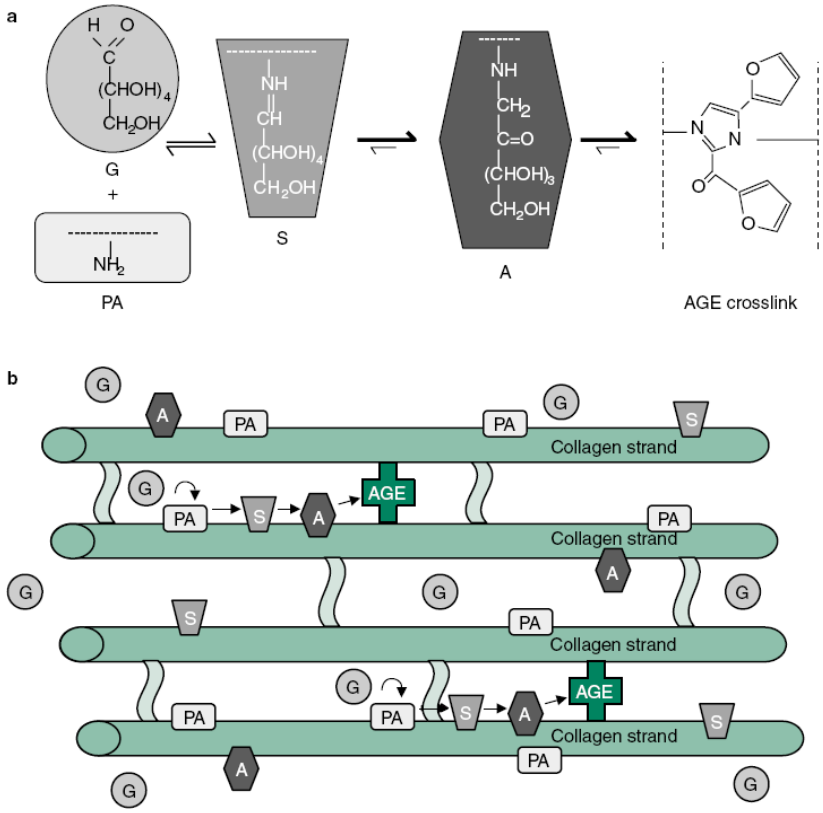

Fig. 1. (**a**) The Maillard reaction occurs when a reducing sugar (glucose) reacts with an amine group to form an unstable Schiff base that transforms to an Amadori product, which can further rearrange to form advanced glycation endproducts (AGEs) capable of crosslinking proteins. (**b**) Schematic of the formation of collagen-collagen AGE crosslinks. The Maillard reaction occurs in two places (arrows) to form AGE crosslinks (dark green) between strands of collagen, which are also functionally enzymatically crosslinked for strength (light green). **A** = Amadori product; **G** = glucose; **PA** = protein amine; **S** = Schiff base.

Figure 1.4. Reproduced from Zieman & Kass[2]

1.4.2 Photoactivated Crosslinking

Photoactivated crosslinking provides a high degree of control that enables precise treatments to avoid damaging sensitive areas of the eye, or even surrounding tissues. Light-activated compounds could be delivered in the dark and allowed to diffuse to the correct locations in tissue. Those locations could be selectively exposed to irradiation, inducing crosslinking locally while adjacent tissue is unexposed and safe from crosslinking. Further, the use of light activation could provide the ability to start crosslinking with light exposure, and after achieving the desired level of crosslinks, stop further reactions by turning off the light. Treatment location and strength could be customized specifically for individual patients.

1.5 Outline of Thesis

The measurement techniques typically used for mechanical characterization of the cornea and sclera have individual advantages and disadvantages that we evaluate in Chapter 2. Our work has led to an improved intact globe expansion method that uses relatively simple loading procedures, has low variability, and provides the ability to discriminate between treatments that are developed specifically for keratoconus and degenerative myopia.

Chapters 3 and 4 discuss the treatment development process. Chapter 3 discusses advantages of photoactivated systems including temporal and spatial control of the reaction. The search for a biocompatible system that uses safe levels of light led to the choice of a visible light-activated system using Eosin Y and triethanolamine. Chapter 4 presents the use of interpenetrating polymer networks to enhance mechanical properties of

the tissue. Surprisingly, results show that polymer interpenetrating networks are not necessary because crosslinking with initiator alone achieves comparable degrees of tissue stabilization.

Chapters 5 and 6 illustrate the strengthening of sclera and cornea for the treatment of myopia and keratoconus respectively. In Chapter 5, intact globe expansion tests are used to determine the potential for treatments to stabilize eye shape *in vivo* and animal testing provides biocompatibility as well as *in vivo* treatment responses. In Chapter 6, penetration studies are used to demonstrate that treatment without removal of the epithelium may be possible, and intact globe expansion tests show the visible-light-activated treatment produces equivalent stabilization of the cornea compared to methods that are currently in clinical trials.

BIBLIOGRAPHY

1. Shoemaker, J.A. Vision Problems in the U.S. Prevalence of Adult Vision Impairment and Age-Related Eye Disease in America. (Prevent Blindness America, 2002).
2. Zieman, S.J., Kass, D.A. Advanced glycation endproduct crosslinking in the cardiovascular system - Potential therapeutic target for cardiovascular disease. *Drugs* **64**, 459-470 (2004).
3. Ellwein, L.B. *Updating the Hu 1981 Estimates of the Economic Costs of Visual Disorders and Disabilities.* (National Eye Institute, 2004).
4. Chow, Y.C., Dhillon, B.B., Chew, P.T., Chew, S.J. Refractive errors in Singapore medical students. *Singapore Medical Journal* **45**, 470-474 (1990).
5. Lin, L.L.K., Shih, Y.F., Hsiao, C.K., Chen, C.J., Lee, L.A., Hung, P.T. Epidemiologic study of the prevalence and severity of myopia among school children in Taiwan in 2000. *Journal of the Formosan Medical Association* **100**, 684-691 (2001).
6. Wong, T.Y., Foster, P.J., Hee, J.J., Ng, T.P., Tielsch, J.M., Chew, S.J., Johnson, G.J., Seah, S.K. Prevalence and risk factors for refractive errors in adult Chinese in Singapore. *Investigative Ophthalmology & Visual Science* **41**, 2486-2494 (2000).
7. Tokoro, T. On the definition of pathologic myopia in group studies. *Acta Opthalmol Suppl* **185**, 107-108 (1998).

8. Sperduto, R.D., Seigel, D.D., Roberts, J.J., Rowland, M.M. Prevalence of myopia in the United States. *Archives of Ophthalmology*, 405-407 (1983).

9. Tano, Y. Lix Edward Jackson memorial lecture - Pathologic myopia: Where are we now? *American Journal of Ophthalmology* **134**, 645-660 (2002).

10. Xu, L., Wang, Y.X., Li, Y.B., Wang, Y., Cui, T.T., Li, J.J., Jonas, J.B. Causes of blindness and visual impairment in urban and rural areas in Beijing - The Beijing eye study. *Ophthalmology* **113**, 1134-1141 (2006).

11. Hsu, W.M., Cheng, C.Y., Liu, J.H., Tsai, S.Y., Chou, P. Prevalence and causes of visual impairment in an elderly Chinese population in Taiwan - The Shihpai Eye Study. *Ophthalmology* **111**, 62-69 (2004).

12. Curtin, B.J. *The myopias : basic science and clinical management*. (Lippincott Williams & Wilkins, 1985).

13. Iwase, A., Araie, M., Tomidokoro, A., Yamamoto, T., Shimizu, H., Kitazawa, Y., Grp, T.S. Prevalence and causes of low vision and blindness in a Japanese adult population - The Tajimi Study. *Ophthalmology* **113**, 1354-1362 (2006).

14. McBrien, N.A., Gentle, A. Role of the sclera in the development and pathological complications of myopia. *Progress In Retinal And Eye Research* **22**, 307-338 (2003).

15. Krachmer, J.H., Feder, R.S., Belin, M.W. Keratoconus And Related Noninflammatory Corneal Thinning Disorders. *Survey Of Ophthalmology* **28**, 293-322 (1984).

16. Rabinowitz, Y.S. Keratoconus. *Survey Of Ophthalmology* **42**, 297-319 (1998).

17. Buhren, J., Kuhne, C., Kohnen, T. Defining subclinical keratoconus using corneal first-surface higher-order aberrations. *American Journal of Ophthalmology* **143**, 381-389 (2007).

18. Rabinowitz, Y.S., Garbus, J., Mcdonnell, P.J. Computer-Assisted Corneal Topography in Family Members of Patients with Keratoconus. *Archives of Ophthalmology* **108**, 365-371 (1990).

19. Salabert, D., Cochener, B., Mage, F., Colin, J. Keratoconus and Corneal Familial Topographic Abnormalities. *Journal Francais D Ophtalmologie* **17**, 646-656 (1994).

20. Binder, P.S., Lindstrom, R.L., Stulting, R.D., Donnenfeld, E., Wu, H., McDonnell, P., Rabinowitz, Y. Keratoconus and corneal ectasia after LASIK. *Journal of Cataract and Refractive Surgery* **31**, 2035-2038 (2005).

21. Faraj, H.G., Gatinel, D., Chastang, P.J., Thanh, H.X. Corneal ectasia after LASIK. *Journal of Cataract and Refractive Surgery* **29**, 220 (2003).

22. Randleman, J.B. Post-laser in-situ keratomileusis ectasia: current understanding and future directions. *Current Opinion in Ophthalmology* **17**, 406-412 (2006).

23. Randleman, J.B., Russell, B., Ward, M.A., Thompson, K.P., Stulting, R.D. Risk factors and prognosis for corneal ectasia after LASIK. *Ophthalmology* **110**, 267-275 (2003).

24. Smith, V.A., Easty, D.L. Matrix metalloproteinase 2: involvement in keratoconus. *European Journal of Ophthalmology* **10**, 215-226 (2000).

25. Smith, V.A., Hoh, H.B., Littleton, M., Easty, D.L. Over-Expression of a Gelatinase a Activity in Keratoconus. *Eye* **9**, 429-433 (1995).

26. Udar, N., Atilano, S.R., Brown, D.J., Holguin, B., Small, K., Nesburn, A.B., Kenney, M.C. SOD1: A candidate gene for keratoconus. *Investigative Ophthalmology & Visual Science* **47**, 3345-3351 (2006).

27. Oyster, C.W. *The Human Eye: Structure and Function*. (Sinauer Associates, Inc., Sunderland, Massachusetts, 1999).

28. Watson, P.G., Young, R.D. Scleral structure, organisation and disease. A review. *Experimental Eye Research* **78**, 609-623 (2004).

29. Bailey, A.J. Molecular mechanisms of ageing in connective tissues. *Mechanisms of Ageing and Development* **122**, 735-755 (2001).

30. Forrester, J.V. Aging and vision. *British Journal of Ophthalmology* **81**, 809-810 (1997).

31. Monnier, V.M., Mustata, G.T., Biemel, K.L., Reihl, O., Lederer, M.O., Dai, Z.Y., Sell, D.R. Cross-linking of the extracellular matrix by the Maillard reaction in aging and diabetes - An update on "a puzzle nearing resolution". *Maillard Reaction: Chemistry at the Interface of Nutrition, Aging, and Disease* **1043**, 533-544 (2005).

32. Peppa, M., Uribarri, J., Vlassara, H. Advanced glycoxidation. A new risk factor for cardiovascular disease? *Cardiovasc Toxicol* **2**, 275-87 (2002).

33. Singh, R., Barden, A., Mori, T., Beilin, L. Advanced glycation end-products: a review. *Diabetologia* **44**, 129-146 (2001).

34. Singh, R., Barden, A., Mori, T., Beilin, L. Advanced glycation end-products: a review (vol 44, pg 129, 2001). *Diabetologia* **45**, 293 (2002).

35. Stitt, A.W. Advanced glycation: an important pathological event in diabetic and age related ocular disease. *British Journal of Ophthalmology* **85**, 746-753 (2001).

36. Verzijl, N., DeGroot, J., Ben Zaken, C., Braun-Benjamin, O., Maroudas, A., Bank, R.A., Mizrahi, J., Schalkwijk, C.G., Thorpe, S.R., Baynes, J.W., Bijlsma, J.W.J., Lafeber, F.P.J.G., TeKoppele, J.M. Crosslinking by advanced glycation end products increases the stiffness of the collagen network in human articular cartilage - A possible mechanism through which age is a risk factor for osteoarthritis. *Arthritis and Rheumatism* **46**, 114-123 (2002).

37. Wautier, J.L., Guillausseau, P.J. Advanced glycation end products, their receptors and diabetic angiopathy. *Diabetes & Metabolism* **27**, 535-542 (2001).

38. Cai, W.J., Zhu, L., Chen, X., Uribarri, J., Peppa, M. Association of advanced glycoxidation end products and inflammation markers with thrombosis of arteriovenous grafts in hemodialysis patients. *American Journal of Nephrology* **26**, 181-185 (2006).

39. Booth, A.A., Khalifah, R.G., Todd, P., Hudson, B.G. In vitro kinetic studies of formation of antigenic advanced glycation end products (AGEs) - Novel inhibition of post-Amadori glycation pathways. *Journal of Biological Chemistry* **272**, 5430-5437 (1997).

40. Cho, S.J., Roman, G., Yeboah, F., Konishi, Y. The road to advanced glycation end products: A mechanistic perspective. *Current Medicinal Chemistry* **14**, 1653-1671 (2007).

41. Price, D.L., Rhett, P.M., Thorpe, S.R., Baynes, J.W. Chelating activity of advanced glycation end-product inhibitors. *Journal of Biological Chemistry* **276**, 48967-48972 (2001).

42. Reihsner, R., Pfeiler, W., Menzel, E.J. Comparison of normal and in vitro aging by non-enzymatic glycation as verified by differential scanning calorimetry. *Gerontology* **44**, 85-90 (1998).

43. Shangari, N., Chan, T.S., Chan, K., Wu, S.H., O'Brien, P.J. Copper-catalyzed ascorbate oxidation results in glyoxal/AGE formation and cytotoxicity. *Molecular Nutrition & Food Research* **51**, 445-455 (2007).

44. Tessier, F.J., Monnier, V.M., Sayre, L.M., Kornfield, J.A. Triosidines: novel Maillard reaction products and cross-links from the reaction of triose sugars with lysine and arginine residues. *Biochemical Journal* **369**, 705-719 (2003).

45. Seiler, T., Huhle, S., Spoerl, E., Kunath, H. Manifest diabetes and keratoconus: A retrospective case-control study. *Graefes Archive For Clinical And Experimental Ophthalmology* **238**, 822-825 (2000).

46. Mattson, M., Schwartz, D.M., Kornfield, J.A. Mechanical measurements of sclera for screening myopia treatments. *Investigative Ophthalmology & Visual Science* **46** (2005).

47. Spoerl, E., Boehm, A.G., Pillunat, L.E. The influence of various substances on the biomechanical behavior of lamina cribrosa and peripapillary sclera. *Investigative Ophthalmology & Visual Science* **46**, 1286-1290 (2005).

48. Spoerl, E., Boehm, A.G., Valtink, M., Pillunat, L.E. Changes of biomechanical properties of lamina cribrosa and of peripapillary sclera by glyceraldehyde. *Investigative Ophthalmology & Visual Science* **45**, U789 (2004).

49. Tessier, F.J., Tae, G., Monnier, V.M., Kornfield, J.A. Rigidification of corneas treated in vitro with glyceraldehyde characterization of two novel crosslinks

and two chromophores. *Investigative Ophthalmology & Visual Science* **43**, U892 (2002).

50. Tae, G., Dickinson, M.E., Louie, A., Kornfield, J.A., Park, J.Y., Lambert, R.W., Rich, K.A., Karageozian, H.L. Crosslinking effects of glycerose on rabbit and human corneas: Rheological and microscopical studies. *Investigative Ophthalmology & Visual Science* **41**, S693 (2000).

C h a p t e r 2

MECHANICAL MEASUREMENTS

2.1 Introduction to the Field of Biomechanics II-1
2.2 Principles Behind Measurements II-3
2.3 Techniques in the Field II-5
2.4 Strengths and Limitations of Alternative Techniques:
Illustration in Cornea and Sclera II-9
2.4.1 Uniaxial Tensile Tests II-10
2.4.2 Oscillatory Shear Rheology II-21
2.4.3 Intact Globe Expansion Test II-35
Bibliography II-46

This work includes contributions from Joyce Huynh, Muzhou Wang, and Meredith Wiseman. Undergraduates Muzhou Wang and Meredith Wiseman contributed to the method development necessary for tensile tests and intact globe expansion, respectively. Graduate student Joyce Huynh assisted with intact globe expansion experiments during her first year.

2.1 Introduction to the Field of Biomechanics

The field of biomechanics has arisen from a desire to understand how living things work. One of the earliest texts relating to biomechanics came from Aristotle's writing "On the Parts of Animals" (394–322 B.C.). Other contributors to the field include Galileo Galilei, Robert Hooke, Isaac Newton, and Thomas Young. Contributions from them and many others help us understand things ranging from blood flow and respiration to locomotion and talking.

Findings related to the human body have greatly advanced medicine. Respirators assist with breathing, artificial heart valves replace faulty ones, and bones and joints are replaced with prosthetic devices. Advances within medicine have relied on methodology of engineering and biomechanics to understand problems associated with diseased, injured, or broken systems in relation to healthy working systems. Characterization of bones has lead to earlier detection of osteoporosis, better joint materials, and even injectable materials to fill the holes and gaps in damaged bones.

In relation to the eye, there are obvious mechanical changes of the sclera and cornea associated with degenerative myopia and keratoconus (Chapters 1, 5, & 6). Characterization of these changes could be useful for understanding and diagnosing the diseases. Understanding the changes that occur could also lead to new insights for treating or preventing the diseases. In addition, clinical treatments aimed at modifying the mechanical properties of the cornea and sclera can be evaluated using methods of biomechanics.

In this chapter we present methods used for the characterization of the cornea and sclera, and we evaluate the reliability of the methods based on the variability of results and the relationship to *in vivo* conditions. Our findings indicate that results are often method-dependent, and for studies related to keratoconus and degenerative myopia, there are advantages in using an intact globe method that maintains an almost natural configuration of the tissue.

2.2 Principles Behind Measurements

In order to understand the tissue, we are interested in studying the forces imposed on and the mechanical responses of the system. Although biomaterials are typically complex inhomogeneous materials, our understanding of them has been built up from very basic understandings of ideal solids and liquids.

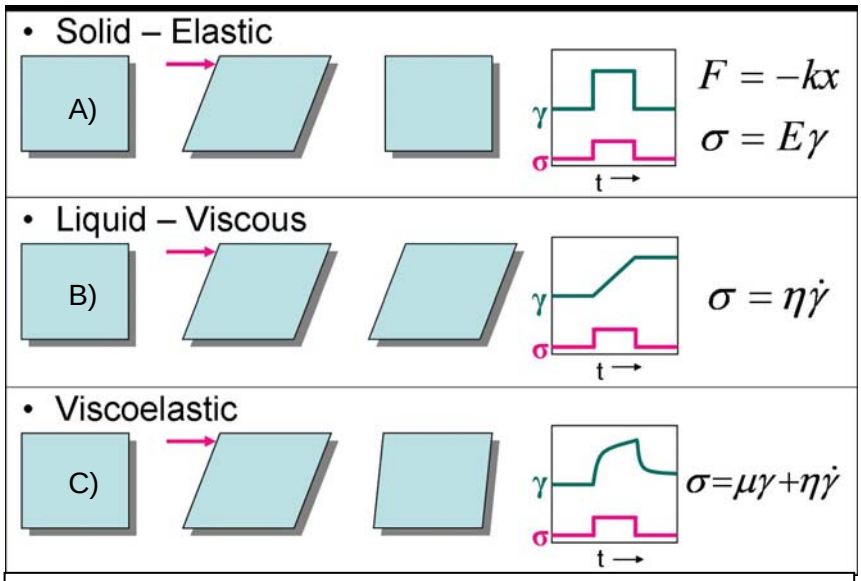

Figure 2.1. A) Mechanical response of ideal solids to imposed stress with equations representing Hooke's law, B) response of ideal liquids with equation representing Newtonian fluids, and C) example response of viscoelastic material exhibiting characteristics between solids and liquids with equation for Voigt model. σ: stress, γ: strain, $\dot{\gamma}$: strain rate, η: viscosity, k: spring constant, μ: modulus, E: Young's modulus

Ideal or Hookian solids can be thought of as isotropic homogeneous materials that behave like springs. Applying a force to the solid induces a deformation. Upon removal of the force, the solid returns to its original shape (Figure 2.1a). This behavior can be described by the restoring force of the spring F = -kx. The restoring force (F) is in the opposite

direction of the imposed deformation (x) and the magnitude of the force depends on material properties of the spring, which are defined by the spring constant (k). Because samples are often different sizes, it is essential to look at the forces relative to sample size in order to isolate the material properties. For this, we examine the stress (σ, force per unit cross-sectional area) that is proportional to strain (γ, a dimensionless measure of deformation). Higher strains create higher stress in the material, or application of higher stresses creates larger strains. The proportionality of stress and strain contains information regarding the material properties and is named Young's modulus, or the elastic modulus (E).

For ideal or Newtonian liquids, it is helpful to think of water flowing through a pipe. If you apply a force to it, water flows along the pipe. If you stop applying a force, then flow stops. There is no restoring force causing the water to return through the pipe (Figure 2.1b). In this case, the amount of deformation is dependent on how long the force is applied; the force is proportional to the deformation rate. As we increase the stress on the liquid, it deforms at a higher strain rate ($\dot{\gamma}$), or if we increase the strain rate, we increase the stress in the liquid. The material properties governing this relation are defined in η, which is the viscosity of the liquid. Under the same stress, a more viscous liquid (honey) flows slower than a less viscous liquid (water).

Most materials cannot be accurately described by either the ideal solid or ideal liquid, but are more appropriately described by a combination of these. Silly Putty™ demonstrates the combination of elastic and viscous properties. If you throw a ball of Silly Putty against the floor it will bounce up retaining its normal shape. During the interaction with the floor, it

acts like a solid, deforming as it hits, but using a restoring force to bounce back. If you slowly pull on Silly Putty it will stretch and elongate. When you stop pulling, the Silly Putty has flowed or creeped and will not return to its original shape. Materials such as Silly Putty, which behave like solids under some conditions and liquids under others, are classified as viscoelastic.

The cornea and sclera are viscoelastic materials that typically exhibit elastic behavior while under physiological stresses. However, under normal intraocular pressures, the cornea and sclera creep in keratoconus and degenerative myopia. This creep is what results in the corneal bulging and axial elongation characteristic of the diseases. Characterization of the elastic and viscous properties of the tissues is essential for understanding the diseases and developing appropriate treatments.

2.3 Techniques in the Field

The ability to characterize the mechanical properties of biomaterials lies in the ability to make measurements of the material response to stress and strain. Typically, this is done by applying one (e.g., stress) and recording the other (e.g., strain or strain rate). The way in which this is done depends in large part on the type of behavior that is being analyzed. The bones and spinal column bear compressive forces due to the weight of the body, tendons are subjected to cyclic tensile stresses, the skin is stretched over the body, blood vessels expand and contract with the pumping of blood, and bones shear past one another in the joints. Because of the variety of forces and deformations to study, there are many

techniques used in biomechanics (Figure 2.2). Also, some testing techniques are developed specifically to replicate the *in vivo* conditions.

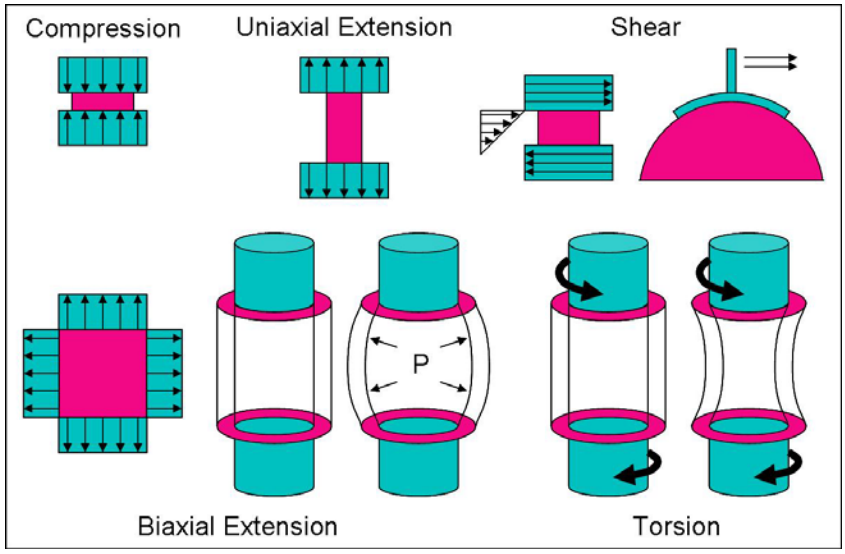

Figure 2.2. Some example methods and geometries used in biomechanics. Compression—samples are sandwiched between plates (e.g., bone). Uniaxial Extension—samples are stretched along one axis (e.g., tendon, ligaments). Biaxial Extension—samples are stretched along two axes (e.g., skin), or as in arterial wall experiments, pressure is used to expand the blood vessel. Shear—samples are sheared between two plates (e.g., mucus), and some geometries mimic the naturally occurring curvature (e.g., joints, cornea). Torsion—samples are torqued along an axis (e.g., vessels, bone).

In vivo, the eye is subject to an intraocular pressure that keeps the cornea and sclera stressed. In order to relate this natural state of the eye to types of mechanical testing we can do, it is useful to introduce the Young-Laplace equation (Figure 2.3). The Young-Laplace equation describes the surface tension (γ) of a membrane that experiences a pressure differential (ΔP) across the two sides of the membrane. The curvature of the membrane at any point can be described by the radius of curvature ($R_{x \text{ or } y}$) along the x- or

y-axis. By approximating the eye as a sphere ($R_x = R_y = R_s$), we are able to simplify this expression to relate the stress in the cornea and sclera to the intraocular pressure (IOP), knowing the radius and thickness of the eye. In a human eye with intraocular pressures of 18–25 mmHg, radius ~12.5 mm, and thickness ~1 mm the biaxial stress would be 15–21 KPa. When considering the strip geometry used in uniaxial extension, people often convert this to a tensile force determined by the stress and cross-sectional area of the sample. Samples with a width of ~5 mm and a thickness of ~1 mm have a 5 mm^2 cross-sectional area, giving a tensile load of 0.075–0.10 N.

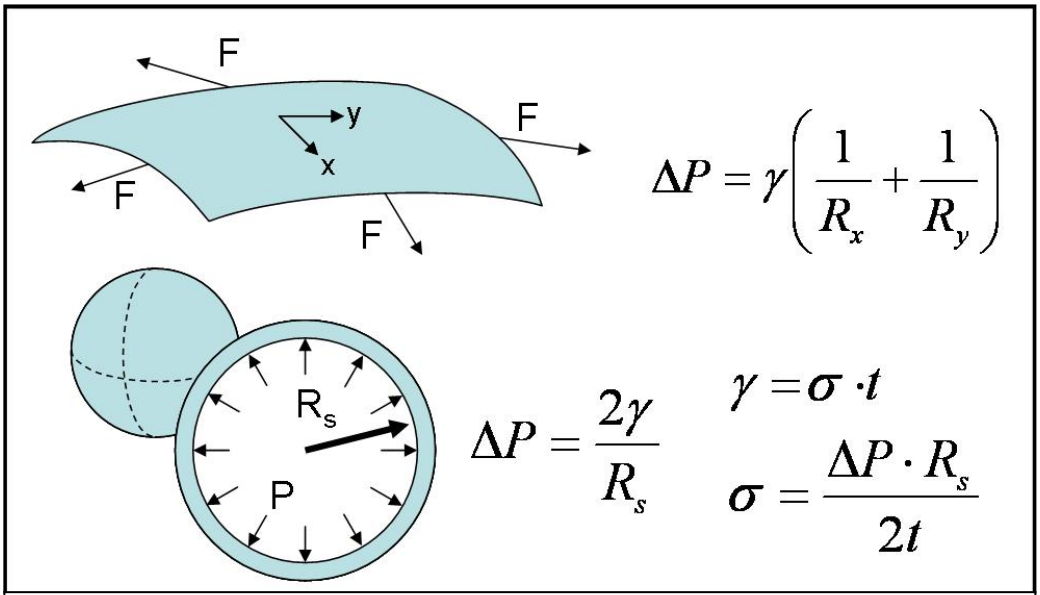

Figure 2.3. The Young-Laplace equation to describe the pressure differential (ΔP) across a curved membrane with surface tension (γ) can be used to approximate the stresses that occur in an eye. By assuming the eye is a spherical shell with ($R_x = R_y = R_s$), the relation of intraocular pressure (ΔP), radius (R_s), and thickness (t) can be used to determine stresses (σ). This relation becomes useful for the comparison of biomechanical testing methods.

Cutting tissue samples for biomechanical testing removes the intraocular pressure and natural stress from the specimen. Groups often condition samples to restore the specimen to a state similar to *in vivo*. For example, application of a pre-stress equivalent to that calculated using the Young-Laplace equation is used as a physiological starting point for measurements. A load (e.g., ~0.1 N) is applied for a specified time and the tissue extends under this stress. Unfortunately, the stress distribution in uniaxial tension (where this method is often used) is different than that in biaxial tension and cannot properly simulate *in vivo* conditions. Another method of conditioning the specimens is the application of cyclic stresses to realign molecules within the sample, and in tensile tests it is often repeated until the hysteresis in the stress-strain curves disappears. Removal of hysteresis implies that the stresses are large enough to cause structural changes in the specimen.

While the application of cyclic stresses is used to precondition tissue, application of small oscillatory stresses can be used to probe the tissue without generating structural changes. Small deformation oscillatory shear rheology oscillates the tissue around zero stress and zero deformation (Figure 2.4). The components of the measured shear stress and strain that are in phase contribute to the magnitude of the storage modulus (G′), which is related to the elastic properties of the tissue. The components that are out of phase contribute to the magnitude of the loss modulus (G″), which is related to the viscous properties of the tissue. If the stress and strain were large, it would be possible to monitor the structural changes of the specimen, however the use of small stresses and deformations allows gentle probing of the tissue.

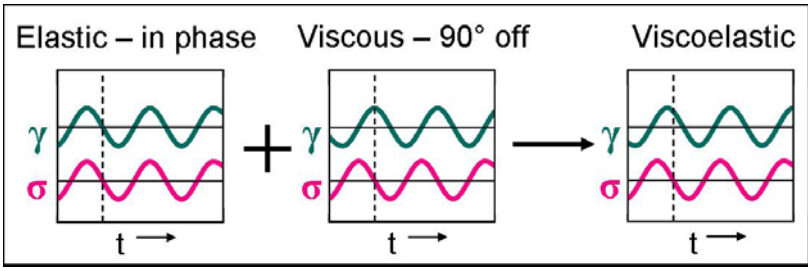

Figure 2.4. Oscillatory shear about a zero stress and zero deformation provides a method to characterize the elastic and viscous properties of tissue. The material properties given in the storage modulus (G', elastic property) and loss modulus (G", viscous property) govern the relationship of stress (σ), strain (γ_o), and frequency (ω). $\sigma=\gamma_o[G'\sin(\omega t)+G''\cos(\omega t)]$

2.4 Strengths and Limitations of Alternative Techniques: Illustration in Cornea and Sclera

An ideal goal of mechanical measurements would be to monitor the properties of tissue while under physiological conditions and stresses. The cornea and sclera are under stress due to the intraocular pressure of the eye, which results in tension of the tissue. During blinking the cornea experiences shear forces, and during eye movement, the sclera experiences shear, compression, and tension. When looking at the mechanical behavior of cornea and sclera, the majority of literature focuses on uniaxial tensile measurements. While this method has its use, other methods such as shear rheology and biaxial expansion can be used to further understand these tissues. In this section, we discuss some of the limitations and advantages of each method and how it applies to the particular problem of studying cornea and sclera.

2.4.1 Uniaxial Tensile Tests

Extensive literature on tensile tests of cornea and sclera provides the majority of knowledge regarding the mechanical properties of these tissues.[1-23] However, there are surprising differences between research groups' reported stress-strain curves and modulus values (e.g., Figure 2.5). Modulus values for human cornea were reported from 3.81±0.40 MPa by Zeng[2], up to 57±4.1 MPa by Andreassen.[3] Friberg has reported values for human sclera that differ from 2.9±1.4 MPa for anterior sclera and 1.8±1.1 MPa for posterior sclera[7], and Wollensak reported values as high as 22 MPa.[22] The differences in modulus values are due to differences in the particular measurement techniques and protocols used. While tensile measurements appear straightforward—cut a rectangular strip of tissue and apply tension—the variations in the sample preparation, clamping, pulling, stress history, and hydration all play a role in the experimental outcome.

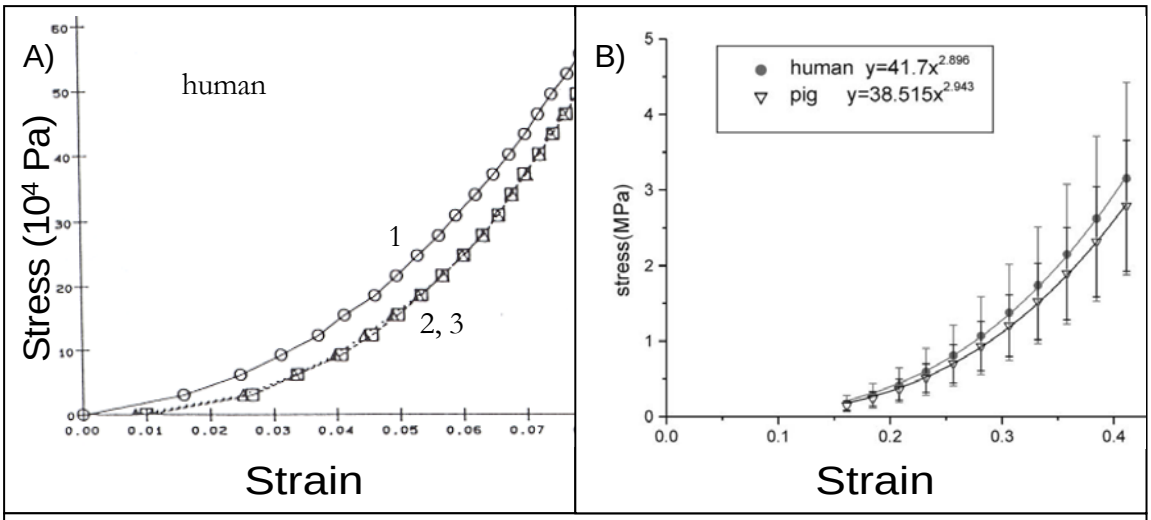

Figure 2.5. Results from (A) Hoeltzel[1] and (B) Zeng[2] showing the stress-strain response of human cornea after cyclic conditioning. Hoeltzel demonstrates that 3 cycles removes hysteresis from the testing and Zeng shows results after 3 cycles. Note that results from Hoeltzel range from 0–7% strain and 0–0.5 MPa stress while Zeng ranges from 15–40% stress and up to 3 MPa. This is exemplary of the vast differences that exist in current literature regarding mechanical testing of cornea and sclera.

Much of the variability comes from the difficulties associated with loading samples. The tissue hydration is important to consider, as tissue stiffness decreases as hydration increases, and swollen tissue may be more prone to failure. Different methods employ the use of dry or moist atmospheres, saline baths, and oil baths as ways of controlling the hydration.

In order to apply tension to the samples, the ends must be secured. Methods of securing the samples include clamping, gluing or pinning. Challenges associated with clamping result from slip of the sample in the grips and tissue damage near the ends due to deformation inherent in clamping. Challenges associated with glues include modification of tissue properties produced by glue that diffuses into the tissue and hardens. Lastly, pins cause further damage to the already cut samples. With all three fastening methods, further

uncertainty in the measurement results from variability in configuration of the tissue between the fixtures. Ideally, the sample should be parallel to the direction of tension, and neither slack nor taut at the point of zero extension.

Unfortunately, samples are often slack upon loading, so there is uncertainty of the true length of the tissue. Several methods have been used to provide a self-consistent zero extension point for a set of measurements. For example, common practices include 1) alignment of data, 2) pre-stressing, and 3) minimal initial stress. Alignment of data uses features in the stress-strain curve (such as the elbow region) as registration points among a data set to shift individual curves on top of each other. After the curves are aligned, a zero-extension point is selected. Pre-stressing a sample involves imposing a specific, small stress for a specified time, after which the desired test condition is imposed (typically a specified crosshead speed or a specified load that is greater than the pre-stress load). The length at the end of the "pre-stress period" is taken to be zero extension and calculations of strain during the experiment relative to that length. The "minimal initial stress" method uses the extension at which the stress reaches a small, specific value during tension as the zero-extension point. In the experiments below, the minimal initial stress method was used.

The variability in loading methods, tissue preparation, and testing procedures all add to the uncertainty of results. The following experiments examine the variability of data that is seen under conditions that minimize the variability, namely low stress (< 1 MPa) and low strain (< 20%). To place the observed uncertainty in context, we compare two groups of specimens: sclera specimens held for 12 hours in saline (making them somewhat softer

than their initial state) and specimens held for 12 hours in glyceraldehyde solution (making them much stiffer than their initial state). The experiments demonstrate the inability of this method to characterize the changes that result from fairly extreme crosslinking with glyceraldehyde.

Method: Eyes from 3–4 month old swine were ordered from Sierra for Medical Science and stored in saline on ice until use within 72 hours post mortem. Orbital tissues were removed and strips of either 3 or 5 mm width and approximately 20 mm length were cut from the cornea or the posterior sclera using parallel scalpel blades. The strips of cornea ran from superior to inferior across the center of the cornea (Figure 2.6a). The cornea was ~14 mm in length, and surrounded on each side by ~3 mm of sclera. The strips of sclera ran superior to inferior and were temporal to the optic nerve (Figure 2.6b). The control samples were stored in Dulbecco's phosphate-buffered saline (DPBS), while the treated samples were stored in a 2% glyceraldehyde solution (GA). After 12 hours in solution at room temperature, the samples were tested on an Instron 5542 Universal Materials Testing Machine (Instron Corp., MA). The tissue sections were laid across the 6 mm gap of the testing apparatus as shown in Figure 2.7. To prevent slippage of the sample, pieces of Kimwipe were placed between the sample and the metal clamp, providing a higher friction surface. A permanent marker was used to mark where the tissue touched the clamp, and was observed for any movement that would indicate slip. After clamping, the samples were loaded vertically into the Instron and pulled at a rate of 1.0 mm/min (cornea) or 1.5 mm/min (sclera) while recording the stress. The samples were in air at ~48% humidity and ~20 ºC. The instrument stopped pulling when a maximum load of 5 N was reached. Zero

extension was taken as the point where the instrument first recorded a non-zero apparent stress (0.005 MPa = F/A, where F is the measured load and A is the initial cross-sectional area) in the sample.

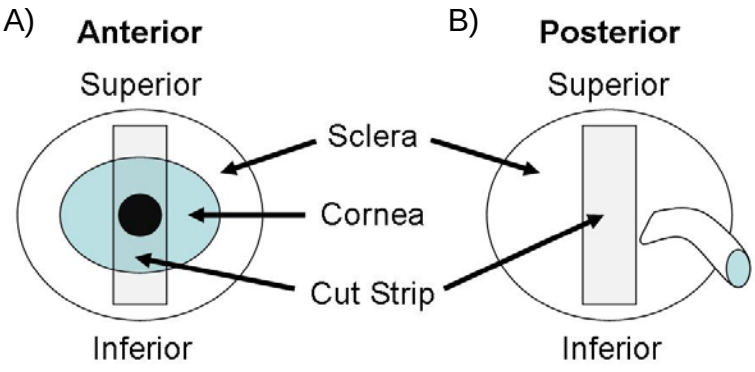

Figure 2.6. Strips of tissue were cut from porcine eyes using parallel scalpel blades. A) The section of cornea was ~14 mm long within a ~20 mm section cut from superior to inferior, containing the center of the cornea. B) The section of sclera was ~20 mm long and cut from the posterior globe running from superior to inferior, temporal to the optic nerve. The strips were either 3 mm or 5 mm in width and thickness varied from 0.83–2.06 mm depending on the animal.

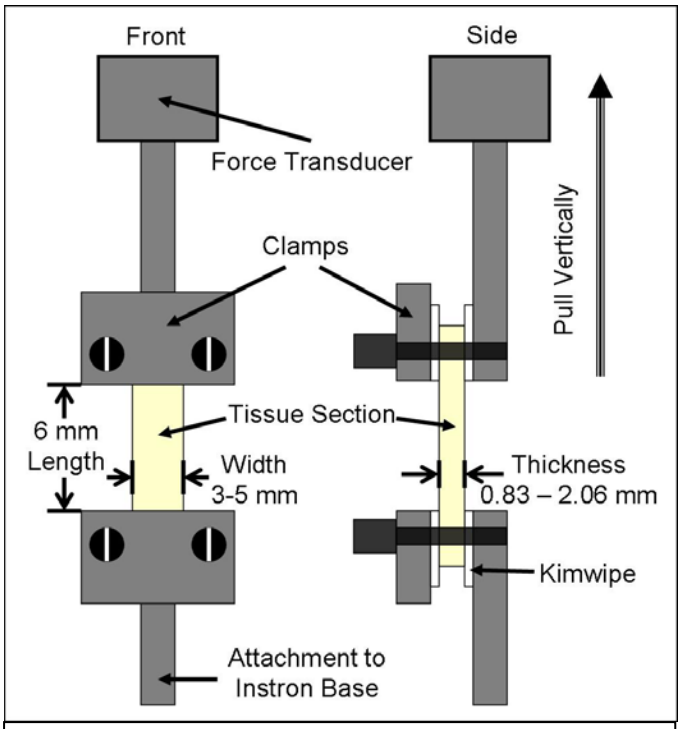

Figure 2.7. Tissue sections were mounted for testing on an Instron 5542. The specimens were laid across a 6 mm gap and clamped securely. Kimwipe between the clamps and tissue provided enhanced friction to prevent slipping. The clamp fixture was mounted vertically on the Instron and pulled at 1.0 mm/sec (cornea) or 1.5 mm/sec (sclera) while the force transducer recorded the load.

Results: Stress-strain curves of the scleral strips show large variability between different sections, as depicted in the scattered curves of control data (Figure 2.8a, b). Curves from 3 mm sections exhibit more scattering than those of 5 mm sections, but still exhibit a similarly shaped curve. The experimental soak with GA is extreme and generates changes in the tissue that are observable by eye and touch (tissue sections have browned and hold a curved shape during loading). It is expected that tensile tests would measure such differences, however, plotting the average results shows that there is no difference between

the treated and control groups (Figure 2.9). In fact, the only significant difference is exhibited in low strain (0–5%) where the 2% GA sections have less stress at the same strain as controls (significance determined from t-tests with p values $p < 0.05$). These results are contrary to observation and contrary to the known effects of GA. Because of the large variability that results from cutting, loading, clamping, and testing of samples, this method is not able to measure the change in modulus that results from GA treatment. This GA treatment would be more extreme than treatments planned for use in keratoconus or degenerative myopia. Because of the inability of this method to monitor large changes in treated tissue, other methods of characterizing tissue are discussed in the sections below.

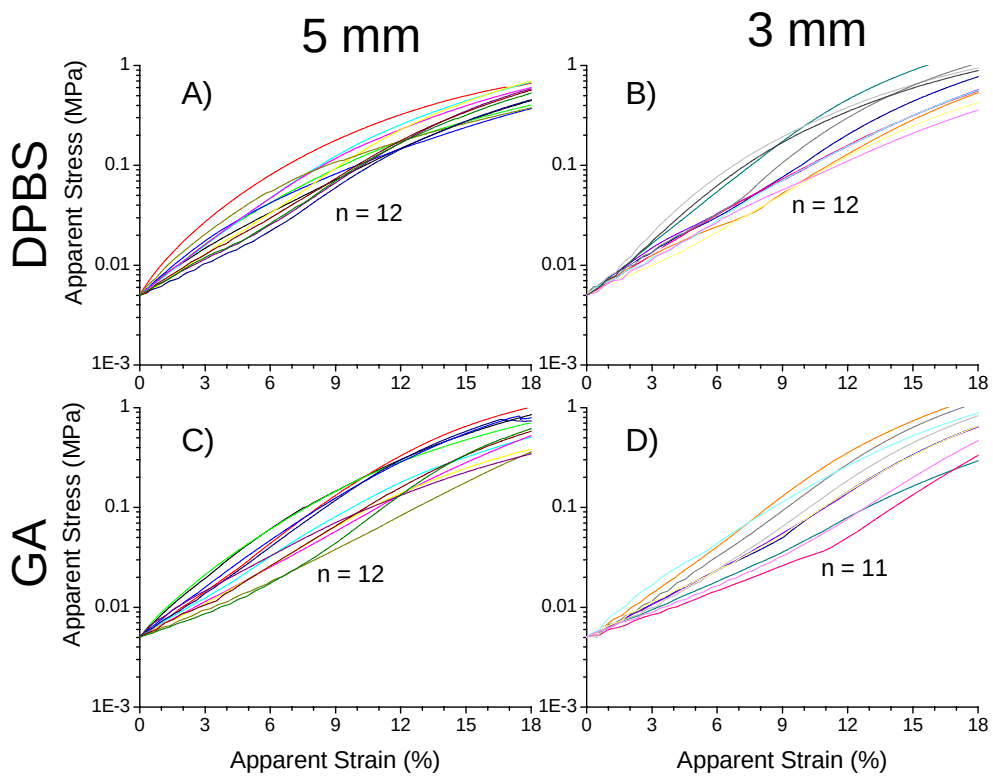

Figure 2.8. Plots of apparent stress-apparent strain curves of individual porcine sclera sections showing the results of incubations in DPBS or GA for 12 hours prior to measurement. There appears to be greater scatter in 3-mm-wide sections than in 5-mm-wide sections, and all curves show similar responses to strain.

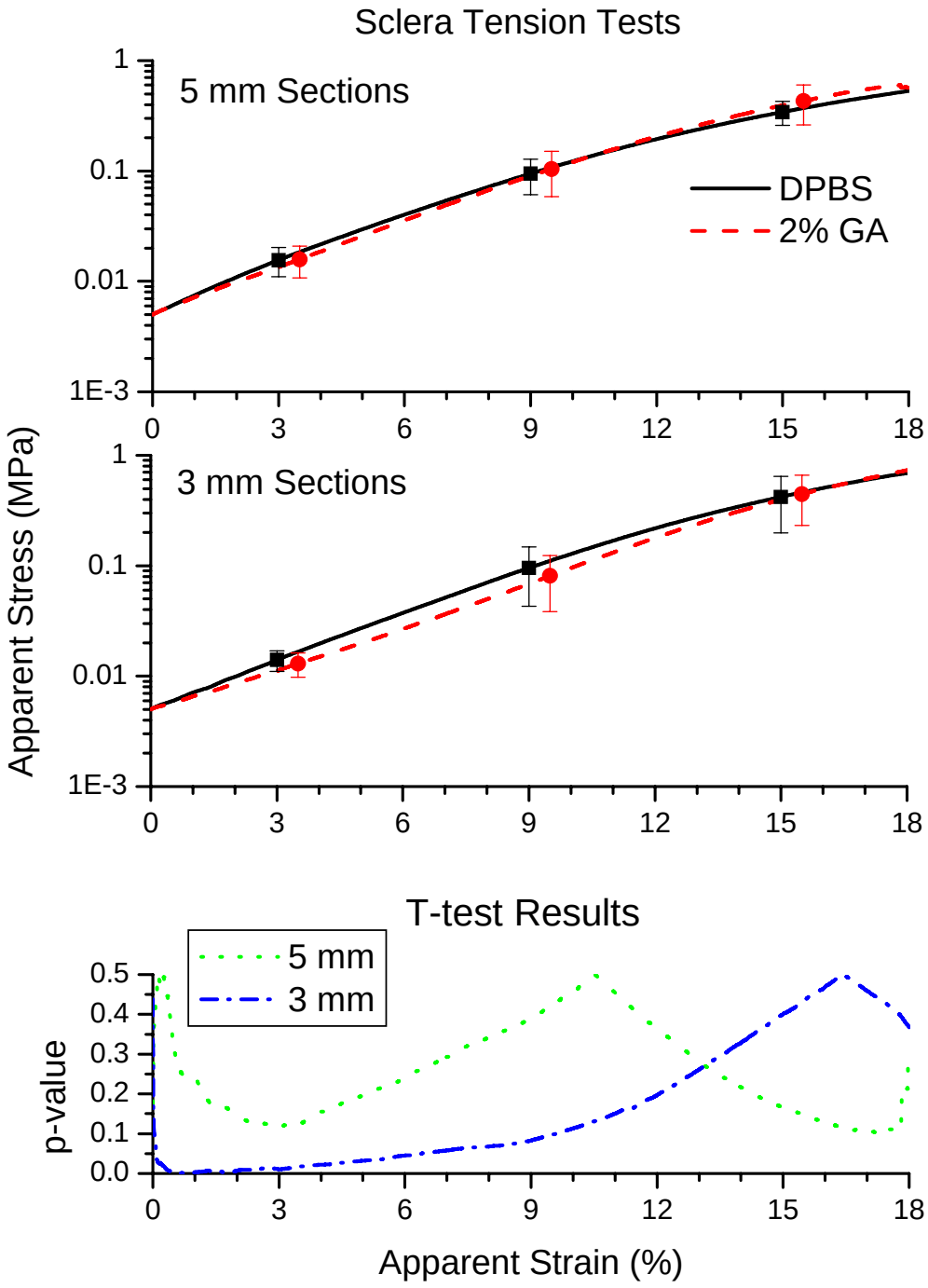

Figure 2.9. Averages of results displayed in Figure 2.8 indicate that there is no measureable difference in GA crosslinked sclera and control sclera. Although t-test results indicate that the GA treatment results in less stiff sclera for strains 0–5%, this does not remain so for higher strains and is contrary to physical observation. These results are unreliable even when comparing groups of size n = 11 and 12.

The measured stress-strain curves for cornea are typical of those reported in literature and the graphs in Figure 2.10a demonstrate similar curves as in Figure 2.5. Out of 8 cornea strips tested, 5 did not have problems from loading, and individual curves are shown in Figure 2.10b. Cornea 2 shows little increase in stress above 10% strain, indicating either slippage, or failure of the tissue. Cornea 6 shows a bump at 17% strain which could also be explained by tissue slippage or failure. Although no signs of slippage could be seen from movement of the markings on the cornea, the individual curves indicate possible slippage. There is no way to determine if this is truly slip, so the data cannot be disregarded. With this in mind, the average and standard deviation that is displayed in Figure 2.10a could be unreliable and gives us uncertainty in the reliability of results published in literature. The same results are presented in Figure 2.11 with stress on a log scale. This scaling method allows examination of behavior at small strains, comparison to the porcine data, and it reveals that the scatter is increasing with strain rather than remaining a constant percentage of the stress. This scatter observed here is similar to the scatter reported for cornea in the introduction of this section.

Further examination of the variability due to different loading methods (specifically different prestresses) is easy to do using our extension curves. By changing the "minimal stress" used as a threshold for calculating zero extension, we change the observed curves (Figure 2.12). The curves become steeper and the tissue undergoes less strain before failure. The steepness of the curves is related to the elastic modulus, and from this example it is possible to see how having a higher prestress results in higher modulus values. The range of reported modulus values in literature can in part be attributed to the differences in

prestress and loading techniques. It would be useful for future researchers to study the relative merit of different methods of securing samples and determining the initial sample length.

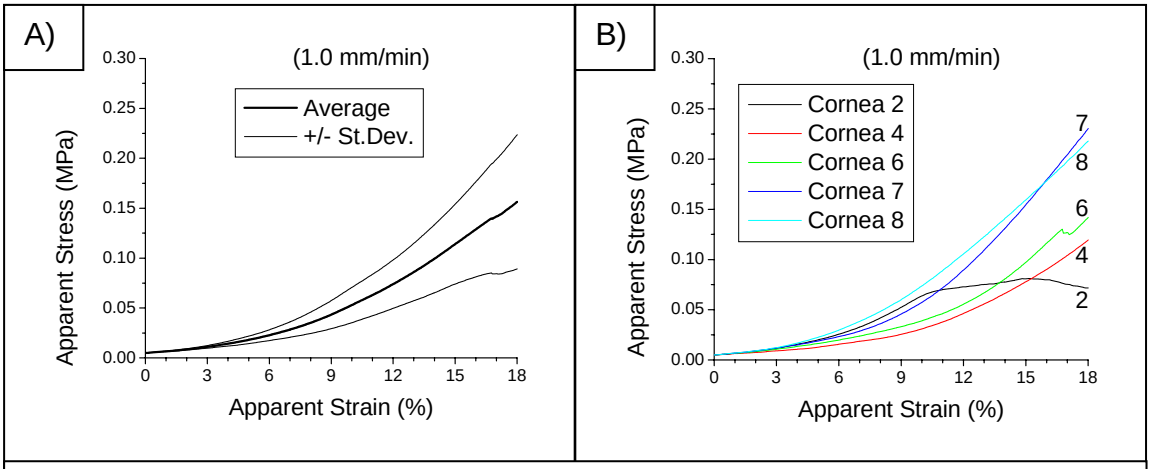

Figure 2.10. A) The average results of tensile tests for 5-mm-wide cornea sections (n = 5) reveal stress-strain relations similar to those reported in literature (Figure 2.5). B) The plots of individual curves (5 out of 8 corneas) indicate the variability of this method, as well as the potential slippage of samples. Because no slipping was visibly observed, these samples have all been included in the average.

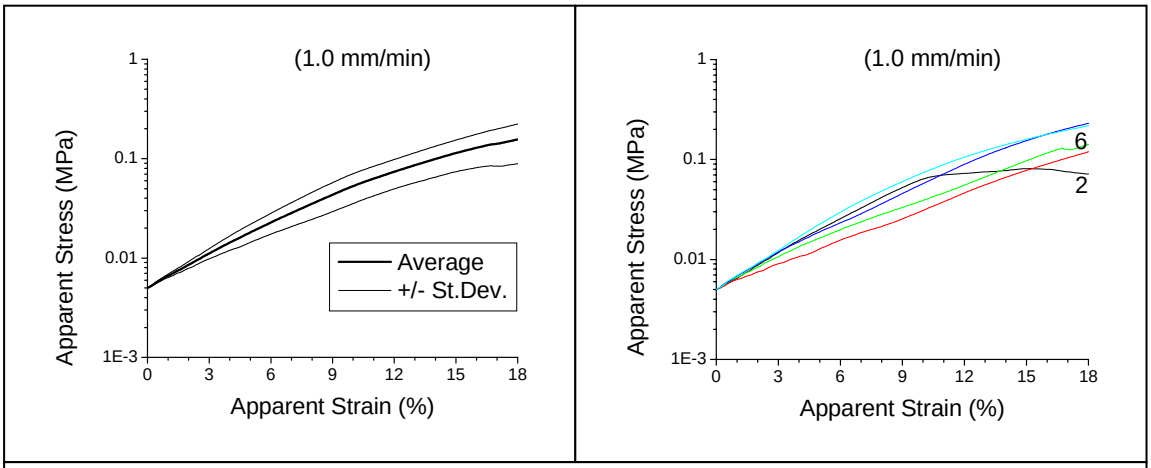

Figure 2.11. The same results presented in Figure 2.10 are shown here on a log scale. This scaling method helps demonstrate that scatter is increasing with increasing percent strain.

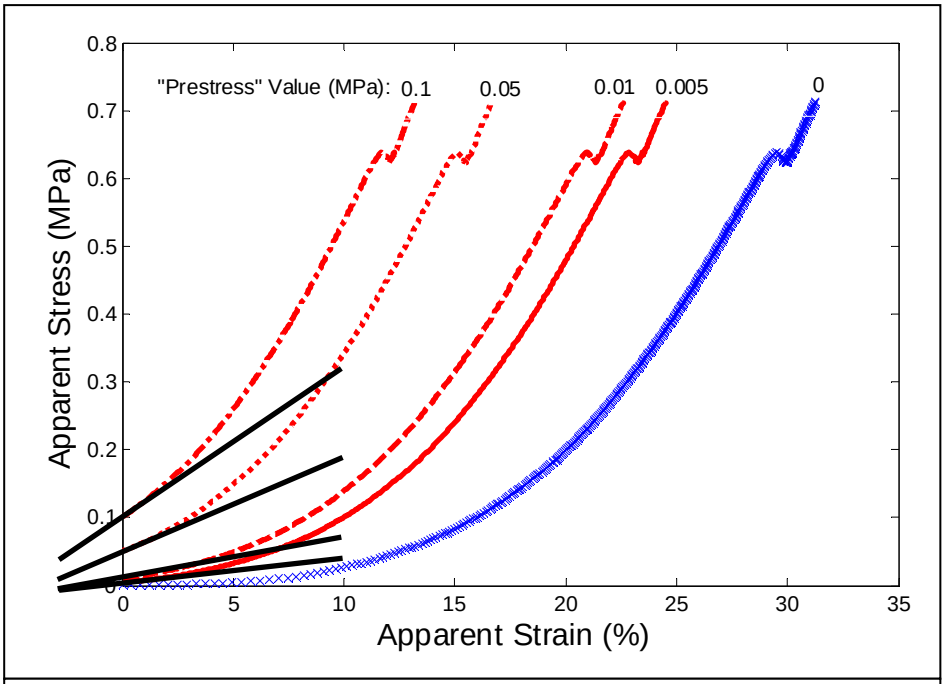

Figure 2.12. Changing the "minimal stress" or "prestress" that is used to calculate zero extension changes the stress-strain curves. Using the results of porcine sclera, we demonstrate the effects of changing the initial stress threshold from 0 to 0.1 MPa. As the prestress increases, curves become steeper, indicating higher modulus values.

2.4.2 Oscillatory Shear Rheology

Shear provides complimentary information to elongation tests. Both the cornea and the sclera may be viewed as fiber-reinforced composites in which relatively tough, inextensible collagen fibrils are embedded in a soft hydrogel matrix. The fibrils are preferentially oriented in the plane of the tissue, with a greater degree of alignment in cornea than in the sclera. Under tension, the stress buildup occurs in fibers, while under shear the fibers are more prone to slide past one another. Therefore the apparent rigidity of the tissue is expected to be greater under tension than in shear. This hypothesis is referred to in

literature about modeling the cornea and sclera[24], but there is limited literature which tests this hypothesis[25].

Unfortunately, many of the sources of uncertainty encountered in tensile testing above are also confronted using shear; there are inherent difficulties in keeping tissue properly hydrated, avoiding structural damage while loading and testing, and imposing a well-defined deformation to a slippery specimen. Here we use a thermostated bath to control tissue hydration. We use a sample of radius 4 mm to analyze specimens cut from porcine eyes of radius 12 mm, so that only small deformation is required to load the slightly dome-shaped specimen into the disc-shaped geometry of the rheometer tools (Figure 2.13). To prevent slip, cleated tools developed in our laboratory[26-29] are employed, providing superior results compared to smooth plates, roughened plates, or grooved plates. With these methods, reproducible measurements of the dynamic moduli were obtained. That is, oscillatory shear was imposed with such a small strain amplitude that the deformation did not perturb the structure or properties of the tissue. The present method allows for repeated measurement of storage modulus on the same scleral section (e.g., before and after crosslinking), and also enables in-situ monitoring of environmental effects on the modulus (e.g., effects of NaCl concentration, pH, and temperature).

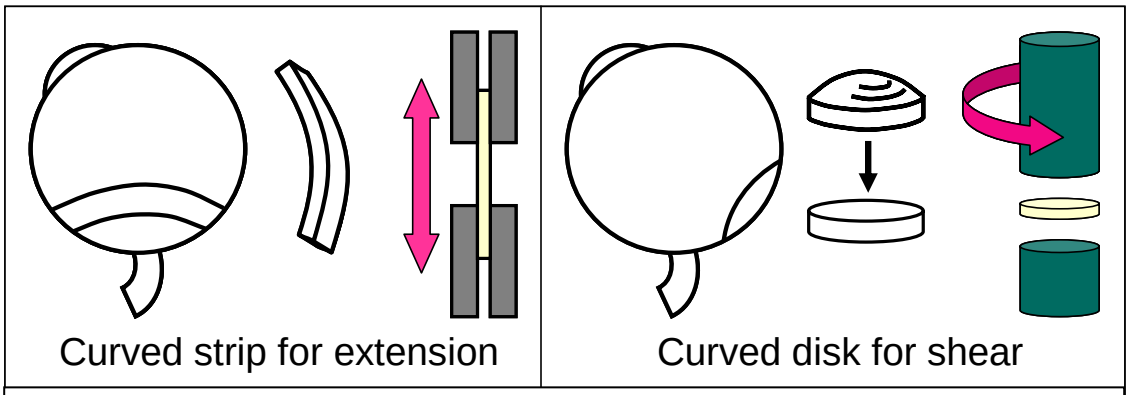

Figure 2.13. Strips cut for either tensile or shear measurements must be straightened before testing. Straightening the tissue introduces stresses in addition to those imposed by the measurement technique.

Materials: Dulbecco's phosphate-buffered saline (DPBS) was purchased from Sigma Aldrich (pH 7.5, 0.9% NaCl). Solutions of varying salt concentration (0–2% by weight) were prepared by mixing NaCl in deionized water and adjusting the pH to 7.5 using NaOH or HCl. A series of 0.9% saline solutions with pH ranging from 5 to 10 were prepared from 10 mM PBS buffer—4 g NaCl, 0.72 g Na_2HPO_4, and 0.12 g NaH_2PO_4 (Sigma Aldrich) dissolved in distilled water for a final volume of 500 mL—with pH adjusted using NaOH or HCl.

Porcine eyes were acquired from Sierra for Medical Science and were stored in 0.9% saline on ice until use within 72 hours of enucleation. The fat and muscle from all eyes were removed with scissors to expose the sclera. An equatorial incision was used to separate the posterior sclera from the anterior hemisphere of the eye. The vitreous, retina, and choroid were removed and 8 mm circular sections were cut using a trephine punch (Katena). The center of the circular section was located ~10 mm from the optic nerve and in some cases

multiple sections were cut from one eye. The following studies used approximately 60 eyes.

Procedures: Circular sections were tested in an 8 mm parallel plate geometry modified with cleats on an AR1000 (TA Instruments) Stress Controlled Rheometer (Figure 2.14). The sample was placed on the lower geometry, and then the upper geometry was lowered to contact the sclera. Experiments monitoring the effect of normal force and tissue compression on the modulus were used to determine the appropriate forces to achieve good contact (Figure 2.15). Good contact was made when the instrument registered a 0.1 N normal force. The tool position is then fixed and the gap between the tips of the cleats on the two tools was used to compute the shear strain from the observed torsional displacement. A small oscillatory stress was imposed on the sample such that the native structure of the tissue was not perturbed. The amplitude and phase of the resulting oscillatory deformation reveal the elastic and dissipative character of the material, which is typically a function of the frequency of the imposed oscillation. The elastic character of the tissue is manifested in the storage modulus, $G'(\omega)$. Because the sclera is solid, at low frequency its behavior is primarily elastic and the modulus becomes insensitive to frequency. Oscillatory shear measurements were done using a stress amplitude of 5 Pa and a frequency of 1 rad/sec. Temperature was controlled using a Peltier plate and the solution surrounding the tissue was prevented from evaporating by using a solvent trap. The solvent trap had a port that could be accessed to change the solution around the tissue.

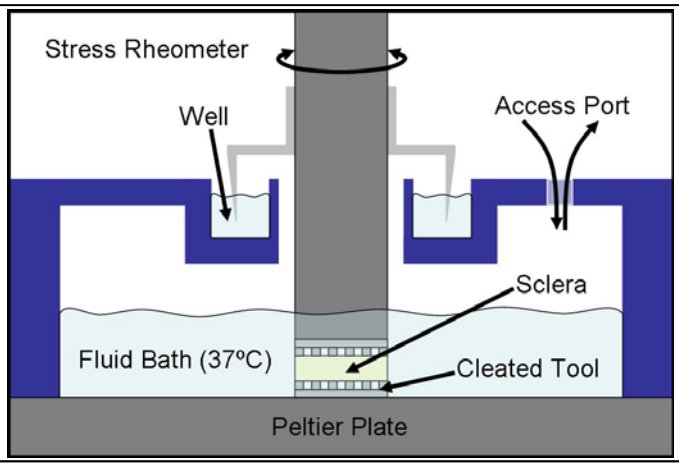

Figure 2.14. Rheometry system for characterizing ocular tissues. An 8-mm-diameter disc-shaped specimen, is loaded between parallel disc cleated tools. Significantly, the cleated tools are loaded without the application of significant normal force or compression of the tissue. A chamber around the sample is used to control the environment (appropriate saline solution). Temperature is controlled from below with a peltier plate. The tools and chamber are used on a stress rheometer (TA Instruments AR1000).

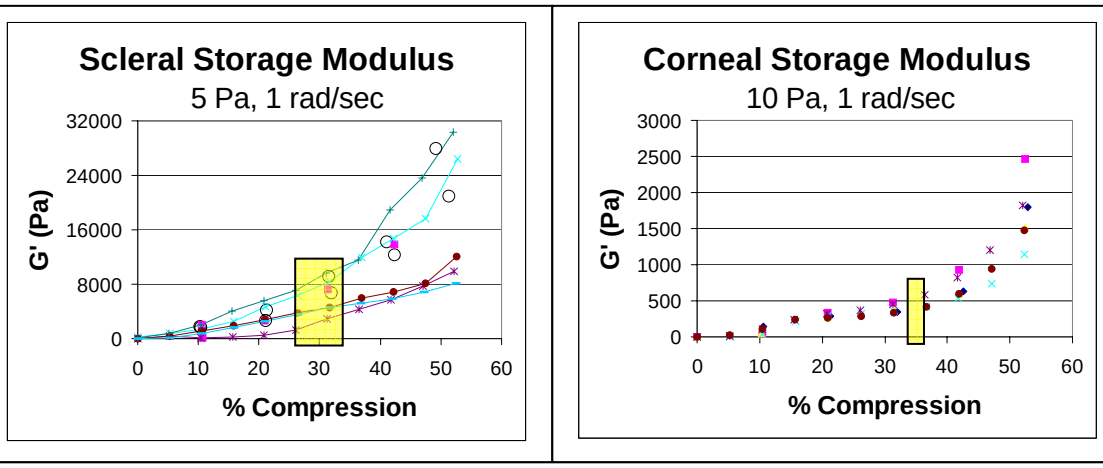

Figure 2.15. Modulus values increase as tissue is compressed. At low compression, the tissue is prone to slip, while at high compression residual stress builds in the tissue, artificially increasing the modulus. Loading with a normal force of ~0.1 N compresses the sclera by 30 ± 4.3 % (n = 12) and compresses the cornea by 35 ± 1.6 % (n = 3). These regions of compression are indicated in the highlighted boxes on each of the graphs. Tissue was compressed to this point in order to ensure good contact and reliable modulus measurements without tissue slippage.

Samples were tested using two different methods. First, the gentle nature of our loading protocol allows samples to be characterized pre- and post-incubation: with negligible damage, each sample can be loaded, measured for initial modulus, unloaded, incubated in a treatment solution, and measured on the rheometer again. Second, the effects of salt, pH, and temperature on the modulus were measured in situ while leaving the sample loaded.

GA crosslinking: Using the incubation method, tissue sections were tested for changes in modulus due to GA crosslinking by measuring an initial modulus, soaking the tissue for 24 hours in 2% GA, measuring the modulus after treatment, rinsing for 24 hours in DPBS, and then measuring the modulus after treatment.

NaCl concentration: Testing for the effects of salt concentration was done using both an incubation protocol and an in situ transient protocol. For the incubation protocol, samples were soaked in DPBS for 24 hours, measured for initial modulus, incubated in 0–2% NaCl (pH 7.5) for 24 hours, and then measured for final modulus. An in-situ measurement of NaCl effects was conducted by continuously measuring the modulus while the bath fluid was changed (0–60 min 0.9% NaCl, 60–120 min 0% NaCl, 120–180 min 0.9% NaCl).

pH: The effects of pH on the scleral modulus were determined using both an incubation protocol and an in-situ protocol. The incubation method consisted of soaking samples in DPBS for 24 hours, measuring initial modulus, incubating in a 10 mM PBS solution of a selected pH (5, 6, 7.4, 8, or 9) for 24 hours, and then measuring a final modulus. In-situ measurement of pH dependence was done by continuously measuring the modulus while

changing the surrounding solution (0–120 min DPBS at pH 7.5 and 120–140 min, 10 mM PBS of a selected pH [5, 6, 7, 7.4, 9, or 10]).

Temperature: Temperature dependence was monitored in situ by continuously measuring the sclera at 37ºC for 1 hour, lowering the temperature to 5ºC for 1 hour, and raising the temperature back to 37ºC for the final hour.

Results: The initial storage modulus of pig sclera as measured using a stress amplitude of 5 Pa and frequency of 1 rad/sec is 4500 ± 1400 Pa (n = 66 specimens cut from 22 eyes) in DPBS at 37ºC. While our measurements of shear modulus were on the order of $5x10^3$ Pa, measurements of Young's modulus are of the order of 10^6 Pa for sclera (previous section). In contrast to homogeneous isotropic materials, which have tensile modulus E only 3-fold greater than their shear modulus G, the sclera show $E \approx 100G$ consistent with the known structural anisotropy and inhomogeneity of the tissue noted earlier. While fibers are able to slide past one another in shear, the resistance to this motion arises from the components between collagen fibers and bundles (glycosaminoglycans, proteoglycans, and collagen connectors). Shear has the potential to provide information regarding the interaction of these components and how they contribute to strength.

GA crosslinking: Although the change in Young's modulus upon crosslinking with glyceraldehyde could not be successfully measured using tensile tests, shear measurements readily reveal an approximately 3-fold increase in modulus after a 24 hour incubation period (328 ± 112.0 % increase in G′, Figure 2.16, left). In contrast, the control specimens are slightly softer after their 24 hour incubation in DPBS. After a further 24 hour rinse in

DPBS, the modulus continues increasing to 379 ± 133.1 % of its original value. The reason that GA crosslinking continues even after free glyceraldehyde is extracted and its implications regarding a clinical procedure are discussed in Chapter 3. The control specimens show a small further softening following their second 24 hour incubation in DPBS (Figure 2.16, right).

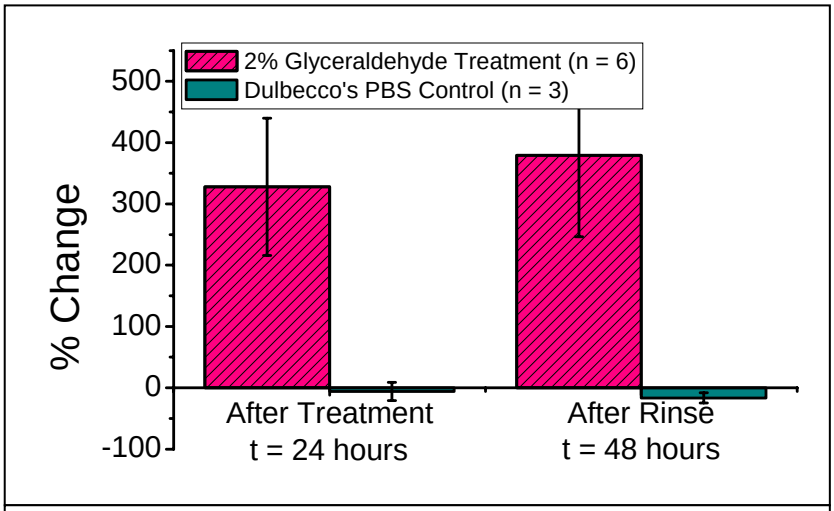

Figure 2.16. Glyceraldehyde crosslinking of sclera for 24 hours increases the modulus over 300% while control values slightly decrease. Even after rinsing residual glyceraldehyde from the tissue, crosslinking continues increasing the modulus over the next 24 hours.

NaCl concentration: The effect of the salt concentration in the incubation solution on the change of modulus is pronounced at low salt concentrations (Figure 2.17). In particular, the shear modulus increases at least 4-fold when specimens are incubated in solution with ≤0.1% salt for 24 hours. Control eyes in DPBS show a slight decrease in storage modulus (28 ± 8.0%) upon the second measurement 24 hours after the first. Increasing the salt

concentration causes an asymptotic decrease in modulus, reaching a 50 ± 1.0% reduction in modulus at 2% NaCl.

In-situ measurements of shear modulus when the NaCl concentration is changed from 0.9% to 0% and back to 0.9% (Figure 2.18) demonstrate that change in modulus is reversible. In addition, the transient effect seen after changing the solution from 0.9% to 0% appears to plateau after ~1 hour. The transient effect upon replacing the 0.9% NaCl solution occurs rapidly, with most of the effect occurring within 30 minutes. Permeability of the bovine sclera to sodium ions is large (4.6×10^{-5} cm/sec),[30] and the transient response seen in the porcine sclera is likely due to diffusion of ions in and out of the tissue. The change in modulus is not accompanied by a change in normal force, which would indicate swelling of the bulk tissue.

The changes in modulus that occur with changes in salinity are most likely explained by the electrostatic screening effects of salt on the highly charged molecules within the sclera. Glycosaminoglycans are repeating units of disaccharides and are highly charged. Proteoglycans are protein cores with attached glycosaminoglycan chains. These molecules may be considered flexible while in high salinity, but as free electrolytes are removed, the glycosaminoglycan side chains expand, causing the proteoglycans to take on a stiff, "bottle brush" like conformation. Grodzinsky has proposed that the stiffening of molecules within the tissue (e.g., cartilage or sclera) would create stresses that are manifested as an increase in modulus.[31]

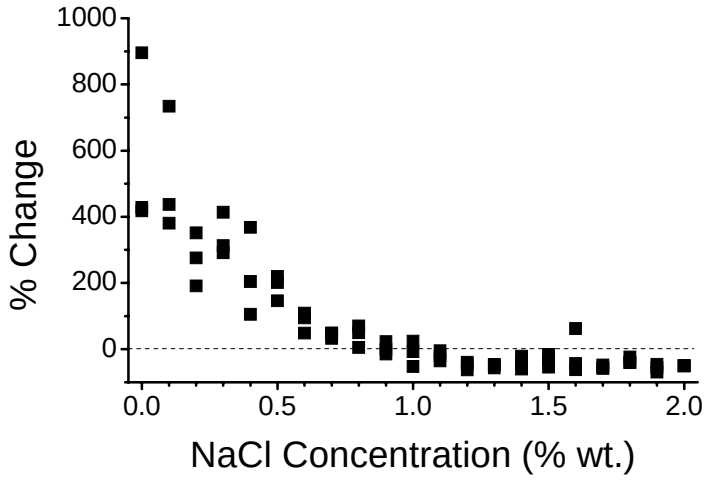

Figure 2.17. All samples were initially measured in DPBS at 37°C and then placed in their respective salinity solutions for 24 hours. The % change is calculated for each specimen with % change = $(G'_{final} - G'_{initial})/ G'_{initial}*100$. Variability from specimen to specimen was large ($G'_{initial}$ = 4500 ± 1400 Pa for n = 60 samples from 20 eyes) compared to the reproducibility of the change in modulus for each specimen.

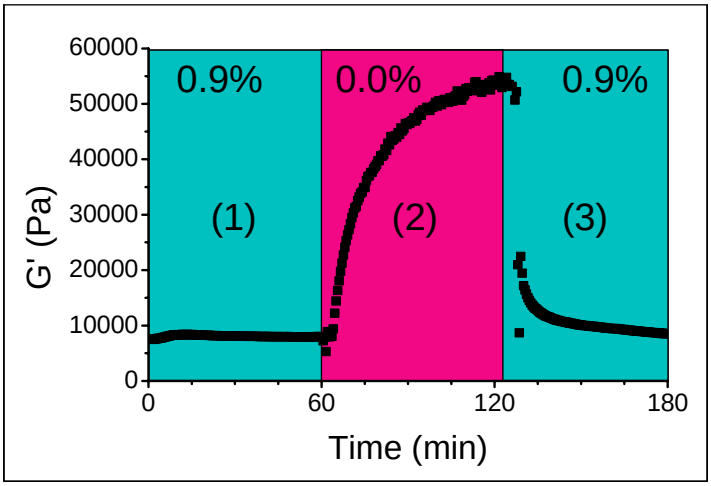

Figure 2.18. In-situ measurement of changing salt concentration shows the rapid change in modulus associated with ions diffusing into the sclera. The ~6-fold change in modulus from ~8,000 Pa to ~55,000 Pa falls within the range of values measured for incubations in ~0% solution.

pH: Electrostatic interactions of the constituent molecules are also influenced by changes in pH. Incubations of scleral discs in different pH solutions yield results given in Table 2.1. Increasing the pH does not cause any measurable differences as compared to controls at physiological pH of 7.4. However, decreasing the pH causes stiffening of the tissue, with a 48 ± 40.1% increase in modulus at pH 5. Note that the uncertainty present at pH 7.4 contains variability of reloading, as well as sample-to-sample variability. The uncertainty of these measurements is large compared to the changes and makes conclusive observations difficult.

pH	% Change Avg ± Stdev	# of Samples
5	48 ± 40.1	9
6	44 ± 68.4	6
7.4	-21 ± 23.6	6
8	-24 ± 17.1	9
9	-24 ± 19.3	6

Table 2.1: 24 Hour Incubation Experiments

In-situ measurements remove the error associated with reloading a sample and definitively show the effects of altering the pH. Lowering the pH increases the modulus while increasing the pH has little effect on the modulus (Figure 2.19). Within two hours, there is no change in modulus at pH 7.4, 9, or 10. Although the modulus does not reach a plateau value within the 2 hours of this test, lowering the pH to 6 increases the modulus by 18 ± 5.4% and lowering to 5 increases the modulus by 62 ± 12.8%. Based upon diffusion of ions in the NaCl studies, we would expect the transient response for pH changes to also near completion within 1 hour. Because the transient timescale is more than twice as long, we hypothesize that some form of remodeling occurs in the sclera. However, the modulus

changes were reversible for all tested pH values, and Figure 2.20 demonstrates the reversibility with pH 7.4, 5, and 9.

The pKa of sulfate, carboxyl, and amine groups that are relevant to proteoglycans and collagen in the cornea and sclera are 2–2.5[32], 4.1[33], and 9.3[33] respectively. As pH approaches these values, we expect to see changes in the mechanical properties. While we would expect large effects close to these values, it is interesting to notice that there is no response when passing the pKa for amines. At lower pH, the sulfate and carboxyl groups are expected to become protonated, reducing charge in the tissue. A reduction in charges could reduce the stress of the molecules in the tissue and reduce the modulus, so the increase in modulus at pH 5 and 6 is counterintuitive. Future research into the interactions within the sclera is necessary to explain these results.

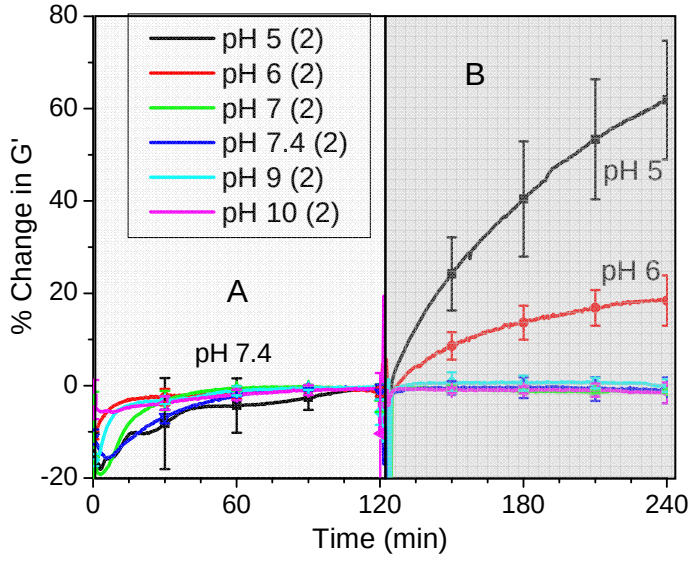

Figure 2.19. Changing solutions from (A) DPBS to (B) a different pH causes changes in modulus for decreasing pH. These values do not plateau within 2 hours, in contrast to the plateau near 1 hour seen in NaCl tests.

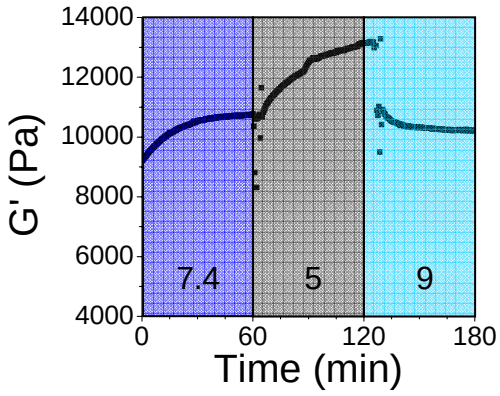

Figure 2.20. While decreasing the pH from 7.4 to 5 causes an increase in modulus, increasing the pH around the same sample from 5 to 9 causes a decrease in modulus. This demonstrates that pH in this range has not permanently altered the sclera.

Temperature: Cooling of samples from 37ºC down to 5ºC causes more than a 60% increase in modulus (Figure 2.21). This finding is in agreement with prior literature regarding the softening of tissue with increasing temperature.[25, 34]

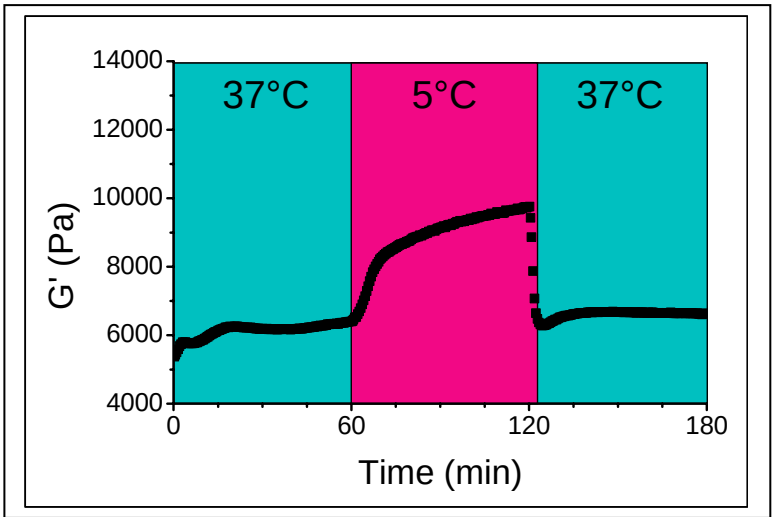

Figure 2.21. The modulus increases as temperature is decreased and causes stiffening of the tissue. Returning the temperature to physiological levels restores the modulus to its original value.

In-situ monitoring helps eliminate some of the variability associated with repeated loading and unloading of a sample, and provides a more accurate method to study the effects of environmental factors on the tissue. Shear measurements are subject to similar variability of cutting and loading specimens as tensile tests. This is clear from the large scatter in initial modulus measurements (G = 4500 ± 1400 Pa). The ability to non-destructively measure and remeasure samples provides a way to remove some sample-to-sample variability. Samples used for measurements of NaCl concentration effects show remarkable similarities in % change. Changing from repeated measurements to in-situ monitoring further reduces the variability by eliminating errors introduced by reloading the sample. In-situ monitoring very clearly shows the time course of changes that happen in individual specimens.

2.4.3 Intact Globe Expansion Tests

The uniaxial tensile tests and shear tests mentioned above do not accurately simulate the loading geometry that occurs *in vivo*. The sclera and cornea are under tension due to the IOP, which imposes an approximately biaxial stress, not a uniaxial one. Shear stress can be imposed during blinking and eye movement, but it is in addition to the biaxial tension that is constantly acting on the cornea and sclera. To more closely mimic the physiologic stresses, researchers have used button and intact globe expansion tests.[34-49]

Button tests consist of removing a portion of the eye and clamping it to a pressurizable chamber (Figure 2.22a). The clamps around the specimen periphery are to ensure a fixed boundary condition as the interior surface expands under pressure. Because of the cutting and mounting of specimens, this method has disadvantages similar to the tensile and shear tests.

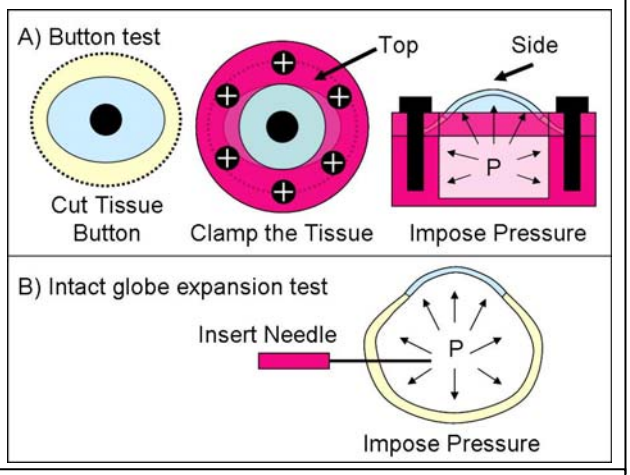

Figure 2.22. A) Buttons of tissue cut from the eye are mounted on a fixture with a circular hole that allows tissue to expand outward. The tissue is clamped down and the pressure inside the fixture is elevated to cause expansion. B) The entire eye is kept intact and a needle is inserted to control intraocular pressure.

Intact globe expansion experiments use the eye without cutting the tissue (Figure 2.22b). The fibril structure is not disturbed by cutting or clamping, and there is an attempt to maintain the natural boundary conditions of the eye. Most importantly, the type of stresses imposed in this intact globe expansion test provide a model for conditions that more closely resemble *in vivo* stresses. Some research groups have glued eyes to fixtures, or pierced eyes with several needles in order to hold them steady while testing. In our experiments, whole eyes are set upon a ring support and pierced through the posterior pole with a single needle that is used to control IOP. In this manner, there is only minimal damage at the site of the needle. The eyes are not clamped or glued to the ring support, so they are free to expand along any ocular dimension. To measure ocular dimensions, groups have used lasers, interferometry, ultrasound, calipers, and photography. With current advances in

technology, cheap cameras are able to provide high-resolution images (~28 micron/pixel in this study) and even video. Using this method, we are able to keep the eye submersed in a physiological bath and remotely monitor the shape change. By minimizing tissue disturbance, variability is reduced to that associated with animal-to-animal variability.

In degenerative myopia and keratoconus, there are shape changes that occur gradually under a normal intraocular pressure. While creep occurs in the weakened, diseased tissue *in vivo*, we are able to use intact globe tests to induce creep of cornea and sclera by imposing elevated intraocular pressures in distensible rabbit eyes *in vitro*. By inducing creep, we are able to study the deformation of the tissue, and are able to study treatments for their ability to prevent deformation. We demonstrate eye creep at low and high IOPs and demonstrate stabilization of eye shape using crosslinking with GA.

Materials: Eyes from New Zealand White rabbits were provided by Keith Duncan at University of California, San Francisco. Because young eyes are more distensible (collagen fibrils are not completely matured), we have used rabbit kit (2–3 weeks old) globes for these experiments. The eyes were stored in saline on ice until use within 48 hours of enucleation. The fat and muscle from all eyes were removed with scissors to expose the sclera. Twelve rabbits were used in this study.

Procedures: Enucleated eyes used for the study of elevated pressure and creep were placed in DPBS at room temperature (~22ºC) for 30 minutes prior to loading. GA crosslinking was done by removing the corneal epithelium, soaking for 12 hours in 2% GA, rinsing for

12 hours in DPBS, and then loading. Eyes were loaded in a transparent plexi-glass observation cell filled with DPBS. The eyes were aligned with the major axis of the equator parallel to the imaging plane. Two holes at the bottom of the cell were used for the insertion of hypodermic needles (30 gauge) that regulate the IOP (Figure 2.23b). The needles were inserted into the eyes through the posterior sclera, and they were fed from a DPBS reservoir held a certain height h above the apparatus, thus providing an IOP governed by hydrostatic pressure ($IOP = \rho gh$; ρ = density, g = gravitational acceleration). The eyes were equilibrated in the cell for 15 minutes without any control of IOP. The pressure valve was then opened, and the eyes were maintained at an initial IOP of 22 mmHg for 1 hour, and then maintained at either 22 or 85 mmHg for 24 hours. Photographs of the eyes were taken every 15 minutes throughout the experiment and then analyzed for changes in ocular dimensions using MATLAB (Scleral Perimeter—SP, Equatorial Diameter—ED, Scleral Length—SL, Corneal Perimeter—CP, Corneal Diameter—CD, Corneal Length—CL, and Axial Length—AL, Figure 2.23c). The Canon Powershot G3 used in these experiments gave a resolution of ~28 microns per pixel. For the 24 hours preceding the experiments, the DPBS was set out at room temperature so that dissolved gasses could escape and eliminate bubbles that interfere with measurements. To minimize bacterial growth during the experiment, several antibiotic eyedrops (Bausch & Lomb neomycin, polymyxin B sulfate and gramicidin ophthalmic solution USP) were added to the solution in the observation cell.

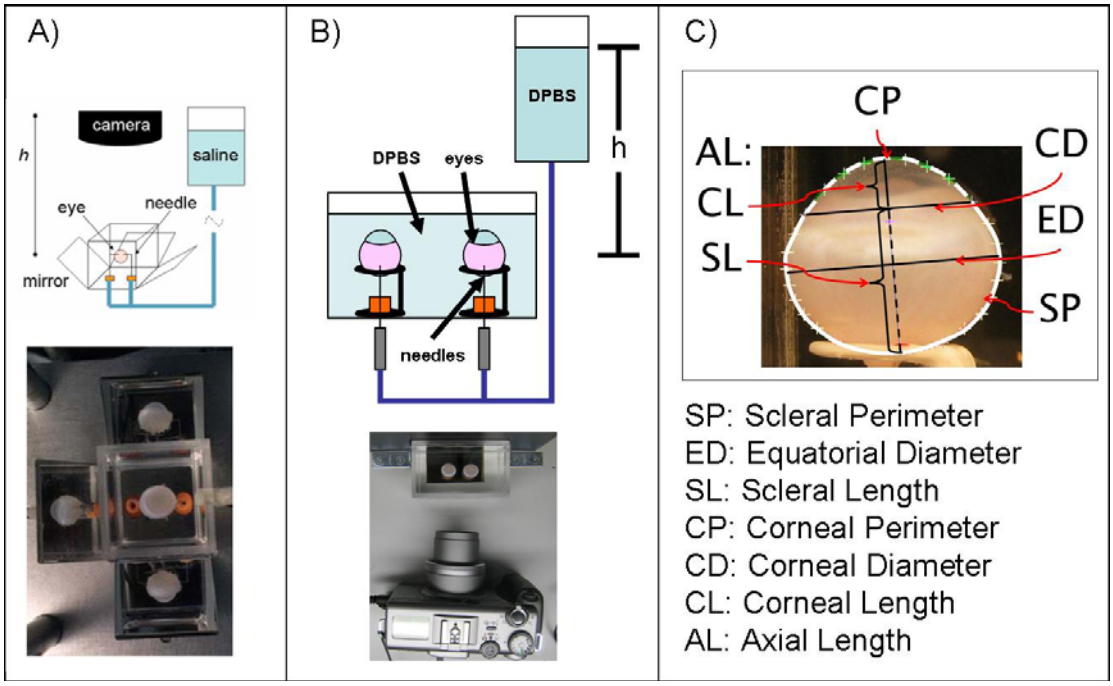

Figure 2.23. A) Initial setup using mirrors for photographing an eye from multiple angles to give a more complete record of eye expansion. This was traded for the simplicity of the setup in B) which uses a pair of eyes for internal control and a ring stand that allows free expansion of the eye. C) Ocular dimensions are measured using custom MATLAB software.

Results: Because the enucleated rabbit eyes are taken from saline and loaded without application of pressure, they are initially in a slack, unknown configuration. After turning on the low pressure (22 mmHg), the eyes have a fast expansion that takes place within the first 30 minutes and is mostly complete by the time 1 hour has elapsed (Figure 2.24a). As an example, results for CP of 5 eyes show a jump in length from the second to third data points, coinciding with the application of pressure. It is interesting to note that eyes 1 and 2 (belonging to the same animal) have initial differences in shape that are reduced after pressure is applied. The difference within animals (1&2, or 3&4) is much smaller than the variability of the entire group, indicating that fellow eyes provide a good control for these studies. Looking at the percent change in shape from the onset of low pressure

demonstrates that there is large scatter in the end results, with measurements ranging from 6–22% after 24 hours (Figure 2.24b). For studies of creep, which are applicable to keratoconus and degenerative myopia, we are interested in the changes that occur after the initial expansion period. The creep is determined from the changes occurring after 1 hour of low pressure application (Figure 2.24c). We see that creep of the eyes has small variability (0–6% change) compared to the expansion from the initial shape. All but one of the eyes fall in the range of 4–6% change. The method of applying a low pressure for a specified time is similar to applying a prestress in tensile tests. However, the boundary conditions of a whole eye ensure the prestress is distributed similarly to *in vivo* stresses. This prestressed configuration (1 hour at 22 mmHg) is taken as the starting point for further analysis of creep. Measurements of eye dimensions after 1 hour of low pressure give a baseline for the initial size of the rabbit eyes (Table 2.2). Equatorial diameter (ED) is larger than the axial length, indicating the oblate shape of the eyes.

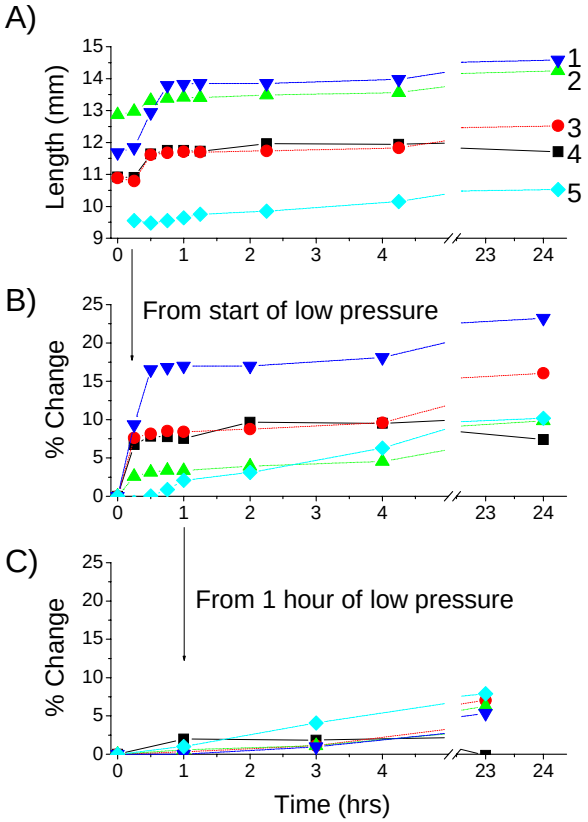

Figure 2.24. Measurements of CP are illustrated for 5 eyes undergoing expansion at a low pressure of 22 mmHg for 24 hours. The pressure is turned on 15 minutes from the start of measurements. A) Initial differences in size between eyes 1 & 2 of rabbit 1 decrease with application of pressure, whereas eyes 3 & 4 from rabbit 2 already start out as similar size. B) Starting calculation of % change from the start of low pressure shows similar variability as measurements of length. This is due to the initially unknown conformation of the eyes. C) Calculating % change from the time point 1 hour after low pressure provides a method of removing the initial uncertainty in eye size and eliminates scatter in the results.

Ocular Dimensions 1 Hour at 22 mmHg (n = 11 eyes)	
Measurement	Avg. ± SD. (mm)
SP	28.53 ± 1.270
ED	13.78 ± 0.655
SL	9.60 ± 0.413
CP	12.21 ± 1.112
CD	10.08 ± 0.802
CL	3.00 ± 0.373
AL	12.60 ± 0.573

Table 2.2: Measurements of Prestressed Rabbit Eyes

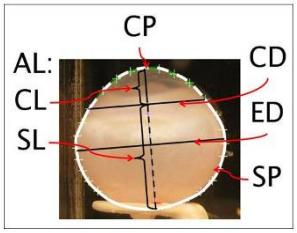

SP: Scleral Perimeter
ED: Equatorial Diameter
SL: Scleral Length
CP: Corneal Perimeter
CD: Corneal Diameter
CL: Corneal Length
AL: Axial Length

After applying the initial prestress, maintaining the eyes at low pressure for up to 24 hours induces less creep than maintaining the eyes at high pressure (Figure 2.25). The cornea and sclera behave differently, as can be expected from tensile tests which demonstrate the sclera has a higher modulus. At low pressure, it is apparent that the sclera is less susceptible to creep than the cornea (SP, ED, & SL change < 1% while CP, CD, & CL change 4, 2, and 10% respectively). Together, the cornea and sclera contribute to the changes in AL (2%). The changes in CP, DP, CL, and AL do not appear linear and may reach plateau values in a period longer than 24 hours. For the high pressure, the creep rates appear linear from 8–24 hours.

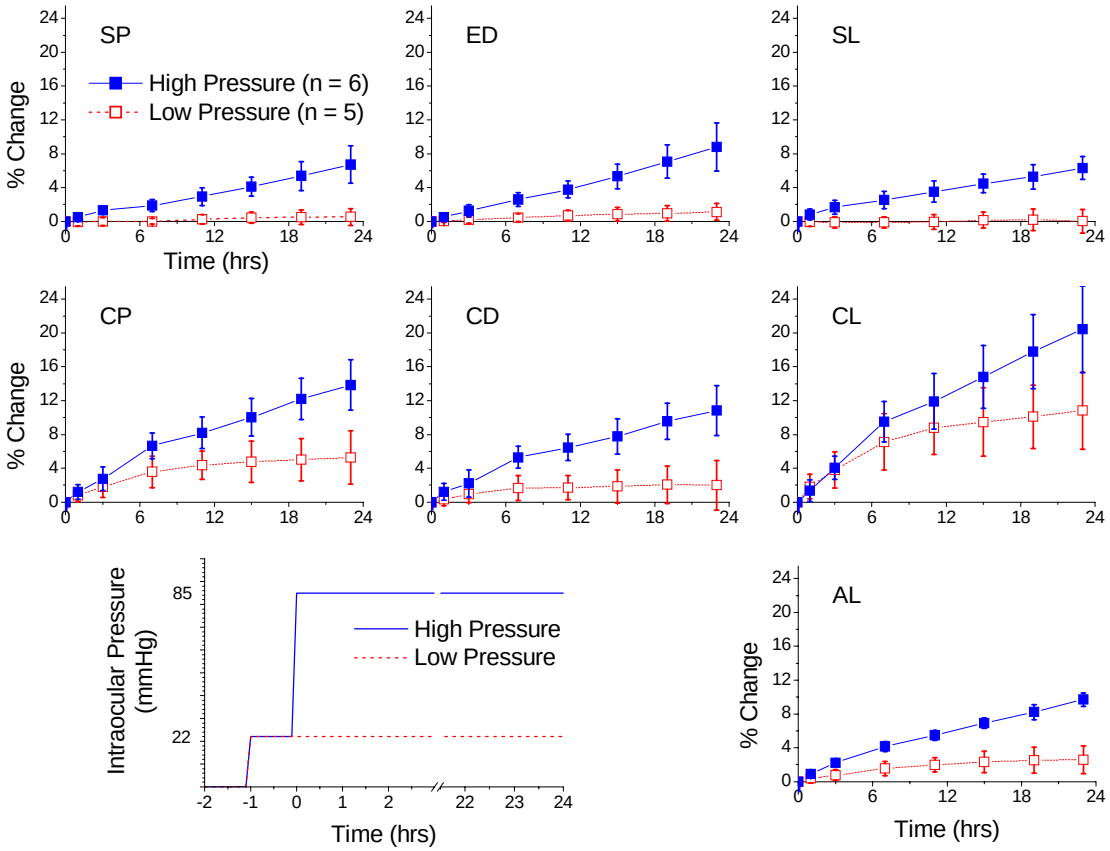

Figure 2.25. Rabbit eyes subjected to low (22 mmHg) and high (85 mmHg) pressures for up to 24 hours show the susceptibility of the cornea and sclera to creep. At low pressure, the sclera remains stable (top row) while the cornea expands to nearly a plateau value (middle row). At high pressure, the cornea and sclera both expand and the creep rate appears linear from 8–24 hours. For values of the overall dimensions, refer to Table 2.2.

The continuous creep experienced in the high-pressure eyes is useful for the study of keratoconus and degenerative myopia where we are trying to examine tissue that progressively changes shape. Further, treatments that successfully prevent expansion of eyes due to creep could have potential as therapeutic agents. Eyes soaked in 2% GA treatment became hard and yellow, indications that crosslinking had occurred. After 24 hours at the high pressure, none of the treated eyes expanded, while control eyes expanded in all dimensions (Figure 2.26).

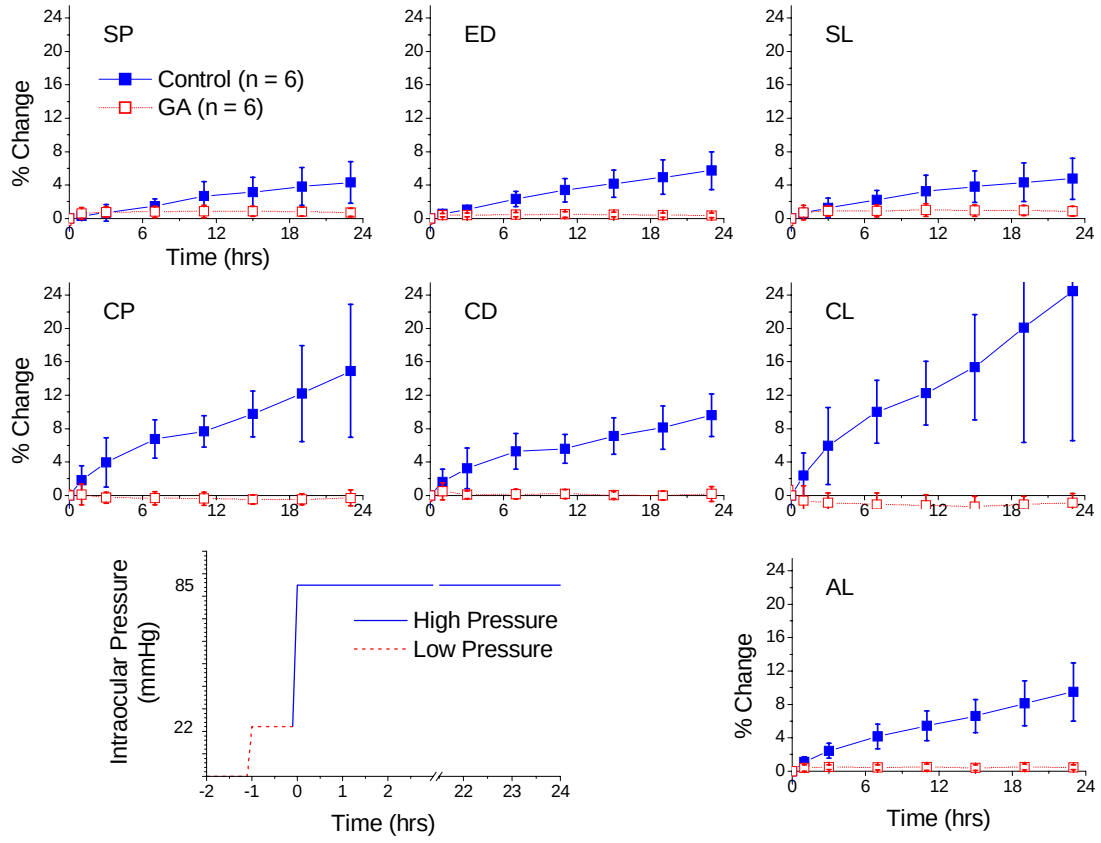

Figure 2.26. Glyceraldehyde (GA) crosslinking of whole eyes stiffens the tissue and noticeably changes the response of the intact eyes to high pressure. While control eyes expand along every dimension, the treated eyes show little expansion along any of the dimensions.

Treatments that prevent expansion of the eyes *in vitro* show the potential to strengthen the tissue and prevent distension *in vivo*. Using the intact globe method, we are able to screen potential treatments with relatively few animals as compared to the tensile and shear tests. By using a test that has resemblance to physiological stresses, we are more likely to probe conditions that are relevant to stopping corneal and scleral shape changes in keratoconus and degenerative myopia. For these reasons, the intact globe method has been chosen to demonstrate treatment efficacy in later chapters.

The expansion studies developed here could also find application in the study of eyes with altered mechanical properties. Currently, we use the tests to induce deformation in normal tissue, but studies of diseased tissue may show increased susceptibility to distension with worsening disease state. While this has been studied with tensile measurements, we believe that this method will provide a fuller characterization of the changes. Studies of molecules such as retinoic acid, which is known to cause increased axial growth in chicks, could provide insight to the mechanisms by which changes occur in the sclera (cell signaling, or direct effects on collagen). Such future work with this model is likely to yield new insights to the field of eye biomechanics.

BIBLIOGRAPHY

1. Hoeltzel, D.A., Altman, P., Buzard, K., Choe, K.I. Strip Extensiometry for Comparison of the Mechanical Response of Bovine, Rabbit, and Human Corneas. *Journal of Biomechanical Engineering-Transactions of the ASME* **114**, 202-215 (1992).
2. Zeng, Y.J., Yang, J., Huang, K., Lee, Z.H., Lee, X.Y. A comparison of biomechanical properties between human and porcine cornea. *Journal of Biomechanics* **34**, 533-537 (2001).
3. Andreassen, T.T., Simonsen, A.H., Oxlund, H. Biomechanical Properties of Keratoconus and Normal Corneas. *Experimental Eye Research* **31**, 435-441 (1980).
4. Bryant, M.R., Szerenyi, K., Schmotzer, H., Mcdonnell, P.J. Corneal Tensile-Strength in Fully Healed Radial Keratotomy Wounds. *Investigative Ophthalmology & Visual Science* **35**, 3022-3031 (1994).
5. Curtin, B.J. Physiopathologic aspects of scleral stress-strain. *Trans Am Ophthalmol Soc* **67**, 417-61 (1969).
6. Downs, J.C., Suh, J.K.F., Thomas, K.A., Bellezza, A.J., Burgoyne, C.F., Hart, R.T. Viscoelastic characterization of peripapillary sclera: Material properties by quadrant in rabbit and monkey eyes. *Journal Of Biomechanical Engineering-Transactions Of The ASME* **125**, 124-131 (2003).
7. Friberg, T.R., Lace, J.W. A Comparison of the Elastic Properties of Human Choroid and Sclera. *Experimental Eye Research* **47**, 429-436 (1988).

8. McBrien, N.A., Gentle, A. Role of the sclera in the development and pathological complications of myopia. *Progress In Retinal And Eye Research* **22**, 307-338 (2003).

9. Nash, I.S., Greene, P.R., Foster, C.S. Comparison of Mechanical-Properties of Keratoconus and Normal Corneas. *Experimental Eye Research* **35**, 413-424 (1982).

10. Nyquist, G.W. Rheology of Cornea - Experimental Techniques and Results. *Experimental Eye Research* **7**, 183-188 (1968).

11. Pandolfi, A., Manganiello, F. A model for the human cornea: constitutive formulation and numerical analysis. *Biomechanics and Modeling in Mechanobiology* **5**, 237-246 (2006).

12. Phillips, J.R., Khalaj, M., McBrien, N.A. Induced myopia associated with increased scleral creep in chick and tree shrew eyes. *Investigative Ophthalmology & Visual Science* **41**, 2028-2034 (2000).

13. Phillips, J.R., McBrien, N.A. Form Deprivation Myopia - Elastic Properties Of Sclera. *Ophthalmic And Physiological Optics* **15**, 357-362 (1995).

14. Reichel, E., Miller, D., Blanco, E., Mastanduno, R. The Elastic-Modulus of Central and Perilimbal Bovine Cornea. *Annals of Ophthalmology* **21**, 205-208 (1989).

15. Shchukin, E.D., Izmailova, V.N., Larionova, N.I., Krasnov, M.M., Gurov, A.N., Bessonov, A.I., Afanas'eva, G.N. Creep of the eye sclera. *Materials Research Innovations* **2**, 147-149 (1998).

16. Siegwart, J.T., Norton, T.T. Regulation of the mechanical properties of tree shrew sclera by the visual environment. *Vision Research* **39**, 387-407 (1999).

17. Spoerl, E., Boehm, A.G., Pillunat, L.E. The influence of various substances on the biomechanical behavior of lamina cribrosa and peripapillary sclera. *Investigative Ophthalmology & Visual Science* **46**, 1286-1290 (2005).

18. Spoerl, E., Boehm, A.G., Valtink, M., Pillunat, L.E. Changes of biomechanical properties of lamina cribrosa and of peripapillary sclera by glyceraldehyde. *Investigative Ophthalmology & Visual Science* **45**, U789 (2004).

19. Spoerl, E., Hellmund, K., Schreiber, J., Seiler, T. In vivo-stiffening of the rabbit cornea by riboflavin plus UV-irradiation and glutaraldehyde. *Investigative Ophthalmology & Visual Science* **40**, S339 (1999).

20. Spoerl, E., Huhle, M., Seiler, T. Induction of cross-links in corneal tissue. *Experimental Eye Research* **66**, 97-103 (1998).

21. Spoerl, E., Seiler, T. Techniques for stiffening the cornea. *Journal Of Refractive Surgery* **15**, 711-713 (1999).

22. Wollensak, G., Spoerl, E. Collagen crosslinking of human and porcine sclera. *Journal Of Cataract And Refractive Surgery* **30**, 689-695 (2004).

23. Wollensak, G., Spoerl, E., Seiler, T. Stress-strain measurements of human and porcine corneas after riboflavin-ultraviolet-A-induced cross-linking. *Journal Of Cataract And Refractive Surgery* **29**, 1780-1785 (2003).

24. Pinsky, P.M., Datye, D.V. A microstructurally-based finite element model of the incised human cornea. *Journal of Biomechanics* **24**, 907-909 (1991).

25. Soergel, F., Muecke, S., Pechhold, W. Corneal Viscoelasticity Spectra as a Result of Dynamic Mechanical Analysis. in *Advances in Corneal Research: Selected Transactions of the World Congress on the Cornea IV* (ed. J. H. Lass) 257-272 (1997).

26. Mattson, M., Schwartz, D.M., Kornfield, J.A. Mechanical measurements of sclera for screening myopia treatments. *Investigative Ophthalmology & Visual Science* **46**(2005).

27. Nickerson, C.S., Karageozian, H.L., Park, J., Kornfield, J.A. The mechanical properties of the vitreous humor. *Investigative Ophthalmology & Visual Science* **45**, U113 (2004).

28. Nickerson, C.S., Karageozian, H.L., Park, J., Kornfield, J.A. Chemical resilience of the vitreous and vitreoretinal interface. *Investigative Ophthalmology & Visual Science* **46**, 5165 (2005).

29. Nickerson, C.S., Kornfield, J.A. A "cleat" geometry for suppressing wall slip. *Journal Of Rheology* **49**, 865-874 (2005).

30. Prausnitz, M.R., Noonan, J.S. Permeability of cornea, sclera, and conjunctiva: A literature analysis for drug delivery to the eye. *Journal Of Pharmaceutical Sciences* **87**, 1479-1488 (1998).

31. Jin, M.S., Grodzinsky, A.J. Effect of electrostatic interactions between glycosaminoglycans on the shear stiffness of cartilage: A molecular model and experiments. *Macromolecules* **34**, 8330-8339 (2001).

32. Kuettner, K.K.E., Lindenbaum, A.A. Analysis of mucopolysaccharides in partially aqueous media. *Biochimica et biophysica acta* **101**, 223-5 (1965).

33. Nishiyama, N., Suzuki, K., Nagatsuka, A., Yokota, I., Nemoto, K. Dissociation States of Collagen Functional Groups and their Effects on the Priming Efficacy of HEMA Bonded to Collagen. *J Dent Res* **82**, 257-261 (2003).

34. Greene, P.R., Mcmahon, T.A. Scleral Creep Vs Temperature and Pressure Invitro. *Experimental Eye Research* **29**, 527-537 (1979).

35. Arciniegas, A., Amaya, L.E. Mechanical-Behavior of the Sclera. *Ophthalmologica* **193**, 45-55 (1986).

36. Cahane, M., Bartov, E. Axial Length and Scleral Thickness Effect on Susceptibility to Glaucomatous Damage - a Theoretical-Model Implementing Laplaces Law. *Ophthalmic Research* **24**, 280-284 (1992).

37. Forster, W., Kasprzak, H., Vonbally, G. Measurement of Elastic-Modulus of the Central Bovine Cornea by Means of Holographic-Interferometry .2. Results. *Optometry and Vision Science* **71**, 27-32 (1994).

38. Girard, M., Downs, J.C., Burgoyne, C.F., Suh, J.K.F. Experimental surface strain mapping of porcine peripapillary sclera under Intraocular pressure. *Investigative Ophthalmology & Visual Science* **46**, 1271 (2005).

39. Greene, P.R. Mechanical Considerations in Myopia - Relative Effects of Accommodation, Convergence, Intraocular-Pressure, and the Extra-Ocular Muscles. *American Journal of Optometry and Physiological Optics* **57**, 902-914 (1980).

40. McEwen, W.K., Sthelen, R. Rheology Of Human Sclera - Unifying Formulation Of Ocular Rigidity. *Ophthalmologica* **150**, 321-346 (1965).

41. Phillips, J.R., McBrien, N.A. Pressure-induced changes in axial eye length of chick and tree shrew: Significance of myofibroblasts in the sclera. *Investigative Ophthalmology & Visual Science* **45**, 758-763 (2004).

42. Pierscionek, B.K., Widlicka, M., Schachar, R.A. The effect of changing intraocular pressure on the corneal and scleral curvatures in the fresh porcine eye. *Br J Ophthalmol*, bjo.2006.110221 (2006).

43. Purslow, P.P., Karwatowski, W.S.S. Ocular elasticity - Is engineering stiffness a more useful characterization parameter than ocular rigidity? *Ophthalmology* **103**, 1686-1692 (1996).

44. Richards, R.D., Tittel, P.G. Corneal and Scleral Distensibility Ratio on Enucleated Human Eyes. *Investigative Ophthalmology* **12**, 145-151 (1973).

45. Sampson, W.G., Girard, L.J. The coefficient of scleral rigidity. Effect of variation of the intraocular volume. *Am J Ophthalmol* **52**, 789-99 (1961).

46. Sthelen, R., McEwen, W.K. Rheology Of Human Sclera .1. Anelastic Behavior. *American Journal Of Ophthalmology* **52**, 539-548 (1961).

47. Sthelen, R., McEwen, W.K. Rheology Of Human Sclera. *American Journal Of Ophthalmology* **51**, 328 (1961).

48. Tittel, P.G., Richards, R.D. Distensibility Measurements of Rabbit Eye. *Investigative Ophthalmology* **10**, 800-809 (1971).

49. Woo, S.L.Y., Schlegel, W.A., Kobayash, A.S., Lawrence, C. Nonlinear Material Properties of Intact Cornea and Sclera. *Experimental Eye Research* **14**, 29-39 (1972).

Chapter 3

PHOTOACTIVATED TREATMENT USING VISIBLE LIGHT

3.1 Introduction III-1
3.2 Photoinitiator Systems.....III-3
3.3 Temporal and Spatial Control of Treatments III-6
3.3.1 Temporal Control of Treatments III-6
3.3.2 Spatial Control of Treatments.....III-8
3.4 Light Safety and Clinical Relevance III-10
Bibliography III-14

This work has been done in collaboration with CJ Yu, Dennis Ko, and Muzhou Wang. Dr. CJ Yu synthesized PEGylated Eosin Y. Undergraduates Dennis Ko and Muzhou Wang assisted with spatial control and temporal control experiments respectively.

3.1 Introduction

Treatment of keratoconus and degenerative myopia have been proposed that aim to prevent tissue deformation by reinforcing the tissue, using crosslinking, which has been shown to increase tissue modulus and strength (Chapter 2). Wollensak, Seiler, Spoerl, and co-workers have developed a photoactivated crosslinking system as a potential treatment to arrest progression of keratoconus.[1-14] Through a series of laboratory and clinical studies, these investigators have demonstrated the efficacy of this treatment for keratoconus, and examined the possibility of using this treatment for degenerative myopia. A photosensitizing agent (riboflavin) is administered to the cornea then activated by excitation with ultraviolet light (UV-A), inducing crosslinking within the tissue. *In vitro*

study of UV-A irradiation after treatment with riboflavin showed an increase in modulus greater than 3 times for human corneal strips[8] and human sclera specimens.[20] *In vivo* experiments in a rabbit model showed that UV-A/riboflavin treatment of the cornea caused a 12% increase in collagen fiber diameter, an effect that may contribute to the increase in corneal modulus.[14] FDA clinical trials are currently underway to determine the safety of UV-A/riboflavin treatment for keratoconus.

Photoactivated crosslinking systems such as UV-A/riboflavin have advantages in temporal and spatial control over traditional crosslinking agents or reducing sugars. First, traditional crosslinkers begin to react as soon as they contact the tissue and create intermediary products that can continue reacting for minutes to days after removal of the excess reducing sugars. This effect is evident in the additional 50% increase of the shear modulus observed over the first 24 hours after rinsing excess glyceraldehyde from the sclera (Figure 2.16). Ideally, a photoactivatable solution could be delivered to an area and then allowed to diffuse into tissue before activation. Then upon activation, crosslinking would commence. After irradiation, no further modification would occur, giving the ability to precisely control the degree of crosslinking. Second, traditional crosslinking is mediated by small molecules that spread quickly by diffusion—both into the intended tissue and surrounding tissues. In the eye, there is the potential that crosslinking agents will be swept away in tears and in circulation, and there is a potential hazard that agents like GA will continue creating crosslinks as they move through the body. This poses a danger in the eye where crosslinking in sensitive areas, such as the retina, should be avoided. Photoactivated crosslinking can be localized to the intended area by selective irradiation.

While crosslinking with UV-A/Riboflavin does provide greater control than crosslinking with glyceraldehyde or other reducing sugars, the UV irradiation lasts 30 minutes and has potential toxicity, especially when combined with photoinitiator activation. Indeed, toxic effects on keratocytes have been observed during keratoconus treatment;[7] and upon testing on rabbit sclera *in vivo*, "serious side-effects were found in the entire posterior globe with almost complete loss of the photoreceptors, the outer nuclear layer and the retinal pigment epithelium (RPE)."[27]

Our present study examines alternative photoactivated systems that maintain the advantages of temporal and spatial control achieved with UV-A/riboflavin. We examine several systems to test for photoactivated strengthening of tissue. The results demonstrate a means to avoid the potential toxicity of UV light by using a visible light activated system of Eosin Y (EY) and triethanolamine (TEOA). This visible light system combines a strong record of biocompatibility with crosslinking ability under irradiation doses that are clinically relevant (conforming to ANSI safety standards).

3.2 Photoinitiator Systems

Photoactivated systems rely on light and a photosensitizer—a molecule that is able to generate a radical through the absorption of light. Such systems have been extensively developed for use in coatings and adhesives, and in tissue-engineering applications (Chapter 4). The wavelength of light acceptable in the application guides the selection of the appropriate photosensitizer system. In addition, water solubility, lipophilicity, and cytotoxicity are considered in biological systems.

During the course of this research, three photoinitiator systems have been used (Figure 3.1): two UV photoactivated systems were used for proof of concept. For convenience and solubility in water, preliminary experiments used (4-benzoylbenzyl)trimethylammonium bromide (Figure 3.1a). The demonstration of oxygen inhibition of PEGDM polymerization within the tissue in Chapter 4 uses this initiator. To avoid cytotoxicity, we next examined Irgacure 2959 (I2959, Figure 3.1b), which showed low toxicity over a range of mammalian cell lines relative to other UV-photoinitiators, including Irgacure 184, Irgacure 907, Irgacure 651, CQ/4-N,N-dimethylaminobenzoate, and CQ/Triethanolamine.[28, 29] I2959 is used to demonstrate spatial control of photoactivated crosslinking in this chapter, and to demonstrate strengthening with and without creation of an integrated polymer network in the tissue. Moving toward our goal of eliminating the potential cytotoxic effects of UV light, we devoted the greatest effort to an initiator system for use with visible light, EY with TEOA (Figure 3.1c), which has a well-established track record of biocompatibility in a range of applications (Table 3.1) and has gained FDA approval for use in the human body in the lung sealant FocalSeal® (Genzyme Biosurgical, Cambridge, MA).

EY is a water-soluble xanthene dye and is a common stain for collagen, the main component of the cornea and sclera. EY's absorption peak at 514 nm allows efficient activation with visible light. Upon irradiation, it becomes excited to the triplet state and undergoes electron transfer with TEOA, generating radicals. The combined characteristics of low-toxicity light (green light) and low-toxicity initiator (EY/TEOA) were incorporated in the design of treatment protocols for the majority of *in vitro*, and all of the *in vivo* studies. We use this system to illustrate temporal control of crosslinking in this chapter, to

demonstrate stabilization of eye shape using integrated polymer networks created *in vivo* in Chapter 4, and it is the system used for development toward a treatment of degenerative myopia (Chapter 5) and treatment of keratoconus (Chapter 6).

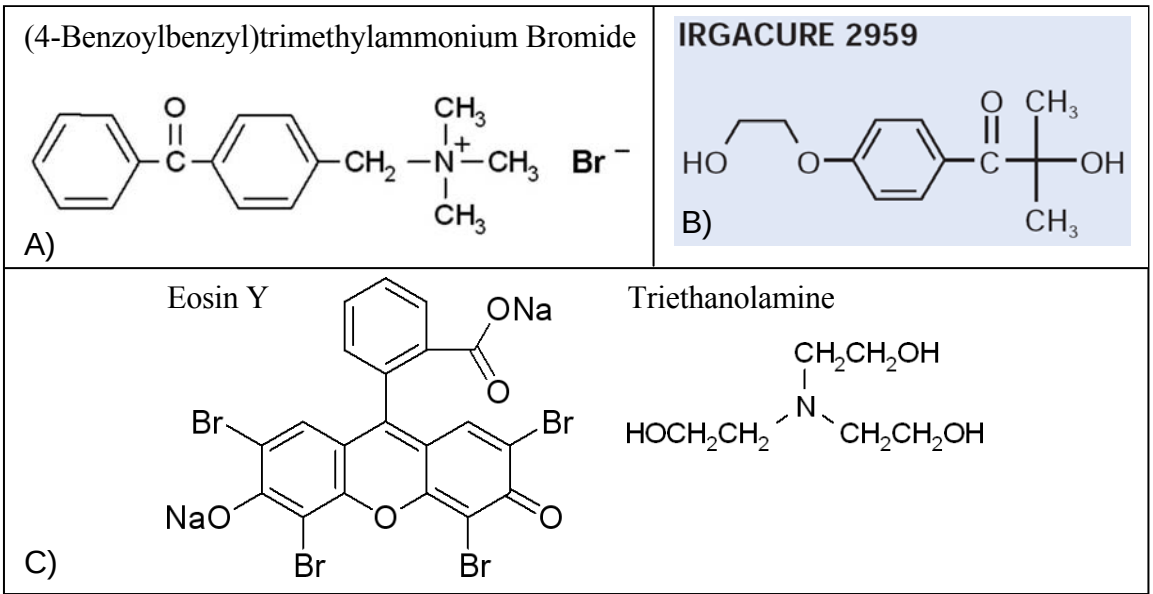

Figure 3.1. A) (4-Benzoylbenzyl)trimethylammonium Bromide and B) Irgacure 2959 are UV activated photoinitiators, and C) Eosin Y/TEOA is a visible light activated system

Authors	Application
Nakayama et al.[15]	Hemostasis of Liver Tissue
Orban et al[16]	Cardiovascular Applications
Cruise et. al., Pathak et al., Desmangles et al.[17-19]	Islet Cell Encapsulation / Microencapsulation
Elisseeff et al.[21]	Transdermal Polymerization
Luman et al. Carnahan et al.[22, 23]	Close Linear Corneal Incisions, Secure Lasik flaps
Alleyne et al.[24]	Dural Sealant in Canine Craniotomy (FocalSeal)
West et al.[25, 26]	Thrombosis Inhibition

Table 3.1. Literature Demonstrating Biocompatibility of Eosin Y

3.3 Temporal and Spatial Control of Treatments

The following *in vitro* experiments illustrate the ability to control the degree of crosslinking using the duration of irradiation, and to achieve spatial control of photoactivated treatments. Collagen gels are used in lieu of cornea or sclera specimens to establish the relationship between irradiation time and extent of crosslinking. Irradiation of porcine sclera through a mask is used to demonstrate spatially resolved activation.

3.3.1 Temporal Control of Treatments

Methods: We have built custom photorheology equipment that allows us to record changes in mechanical properties of specimens during irradiation. Using this, we record the modulus of collagen gels with time before, during, and after irradiation.

For these experiments, 8-mm-diameter circular sections of 1-mm-thick slabs of 20% gelatin with 0.0289 mM Eosin Y and 90 mM TEOA were mounted on the center of the shear rheometer (AR1000, TA Instruments) modified to allow measurement of light-induced changes (Figure 3.2). The sample was subjected to oscillatory shear with a stress amplitude of 30 Pa and frequency of 0.3 rad/sec, at which the initial storage modulus is approximately 3000 Pa. The dynamic moduli were recorded every 48 seconds for 20 minutes prior to irradiation, during 20 minutes of irradiation, and then monitored for 20 minutes while in the dark (Figure 3.3). Light emitting diodes (LEDs) at 525 ± 16 nm were used to give an irradiance at the sample of 1–3 mW/cm^2.

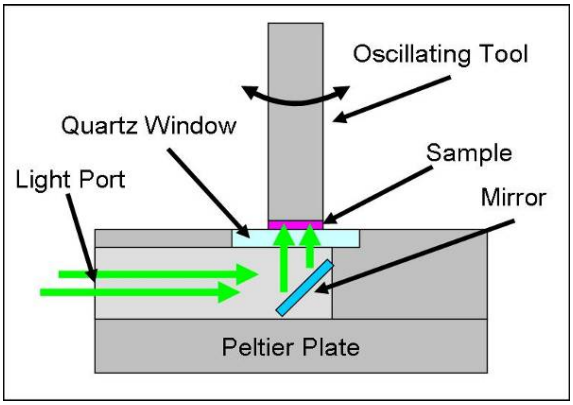

Figure 3.2. Setup for measuring real-time changes in sample modulus while exciting with light on a shear rheometer

Results: Control samples that receive no light (0 mW/cm^2) do not show any increase in modulus throughout the experiment (Figure 3.3). The change in modulus increases approximately linearly with time at each of the three flux levels examined (1, 2, and 3 mW/cm^2). Further, the increase in modulus does not continue after cessation of irradiation. Therefore, the degree of crosslinking can be controlled using the duration of light exposure. Note that the modulus change may asymptotically approach a maximum rate, and increasing the light intensity beyond a certain value (~3 mW/cm^2) will simply deposit excess energy in the system without increasing the rate. Also note that 5 minutes of irradiation is used in the *in vitro* and *in vivo* experiments described in Chapters 5 & 6. The storage modulus of the model gel increases approximately 5% after 5 minutes of irradiation with a flux in the saturated regime (3 mW/cm^2). Because the increase in modulus is controlled by factors (light intensity and exposure time) that can be easily controlled in the clinic, a treatment can be modified to suit an individual patient. Also, the ability to deliver

the drug to the proper location and then activate it with light will ensure that the proper area is treated.

Photorheological monitoring of crosslinking in collagen gels takes advantage of relatively simple techniques that can be used to screen the effects of light intensity, wavelength, EY concentration, TEOA concentration, and the interactions of these parameters without the use of animals. Future drug optimization experiments requiring animals can then be more intelligently designed based on these test results.

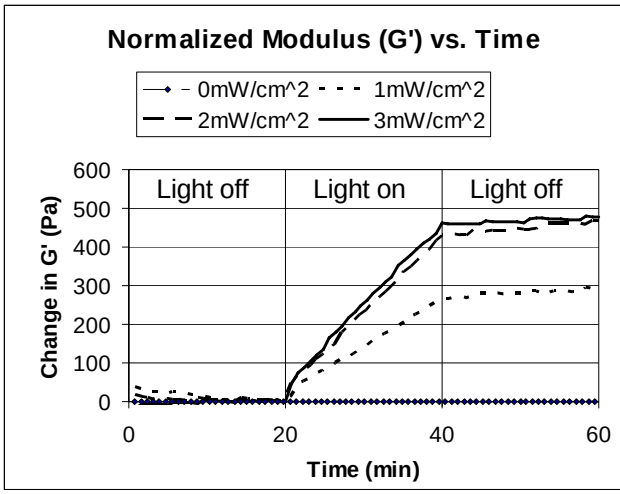

Figure 3.3. The change in storage modulus G' as a function of time prior to irradiation (t = 0–20 minutes), during irradiation (t = 20–40 minutes), and in the dark after irradiation (t = 40–60 minutes) with 525 nm LEDs at the flux indicated in the legend

3.3.2 Spatial Control of Treatments

Because the photoinitiator system is only activated upon irradiation with light, it should be possible to selectively activate regions of interest within the tissue. Clinically, this means that drug may be applied to a broad area, and then activated precisely where needed. In

order to determine where treatments are activated, Dr. C.J. Yu synthesized a Fluorescein-PEG-methacrylate (Fluor-PEGM) molecule that is fluorescent and capable of coupling to tissue upon reaction with radicals generated by the photoinitiator (Figure 3.4a). A porcine eye was immersed in a treatment solution (Fluor-PEGM—fluorescent & Irgacure 2959—which does not have visible fluorescence) for 5 minutes, then the surface was wiped clean of excess material. A mask was used during irradiation so that only 3 slits of light fell on the posterior sclera. The eye was rinsed in DPBS for 48 hours to allow free Fluor-PEGM to diffuse out of the tissue, and then examined under a black light to visualize fluorescence. Three fluorescent bands were evident (Figure 3.4b). The location of the three fluorescent bands that persist on the sclera correspond to the irradiated regions, indicating activation of the photoinitiator and crosslinking of Fluor-PEGM (Figure 3.4b). The dark bands coincide with areas that did not receive light through the mask.

Treatment of degenerative myopia will likely involve an injection behind the eye, where solution may diffuse into periorbital fat and neighboring muscles. Activation of crosslinking only where light is directed (i.e., onto the sclera) will protect these other tissues. Strengthening of cornea and sclera can also be directed selectively to areas of thinned or weakened tissue without crosslinking healthy areas. Thus, the combined advantages of temporal and spatial control provided by photoinitiator systems increase the ability to tailor treatments to individual patients.

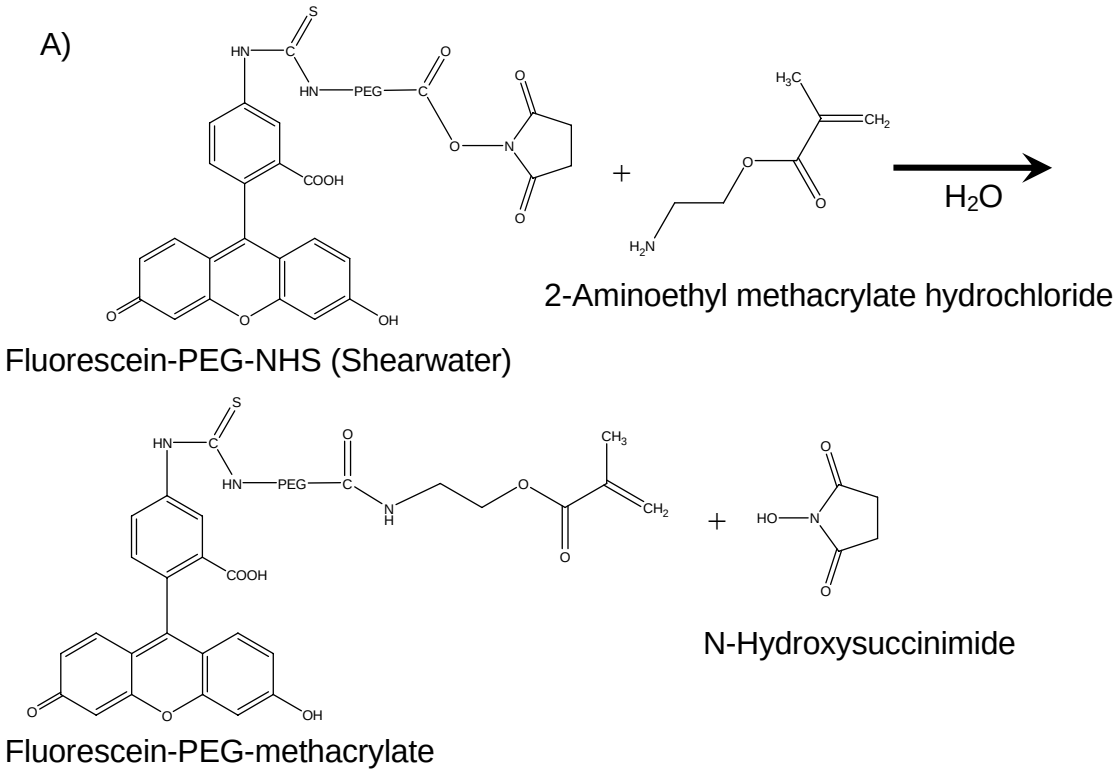

Figure 3.4. A) fluorescent molecule capable of binding to tissue after light-activated crosslinking (Fluorescein-PEG-methacrylate) was prepared from a precursor fluorescein-PEG-NHS (2000 dalton) and 2-aminoethyl methacrylate hydrochloride by reacting overnight in H_2O in the dark. The reactive methacrylate group is capable of binding to tissue upon activation by radicals and B) the fluorescent molecule has been crosslinked to form three bright green bands on the posterior sclera of a porcine eye, demonstrating the ability to localize treatment.

B)

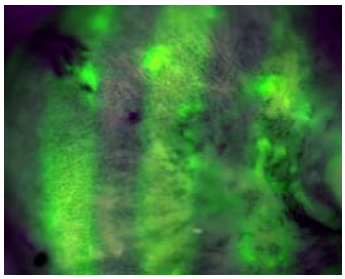

3.4 Light Safety and Clinical Relevance

We hypothesized that visible-light irradiation would facilitate activation of photoinitiator systems using safe levels of irradiation within the cornea and sclera. In view of the experimental results, we compare the irradiation dose that is used above (525 ± 16 nm LEDs, and 6–8 mW/cm^2 at the plane of the tissue) and is used for eye stabilization in

Chapters 5 and 6 to existing standards for safe exposure. The American National Standards Institute (ANSI) provides the American National Standard for Safe Use of Lasers[30], and although we are using an LED light source instead of lasers, these standards provide a guideline for the safe irradiation of the eye. Because of reduced photochemical hazards at longer wavelengths, the maximum permissible exposure (MPE) of the retina to green light (525 ± 16 nm) is approximately 30 times greater than the MPE for blue light (400 nm). We use the MPE for blue light (2.7 J/cm^2) to make a conservative estimate for irradiation safety. The safety thresholds for clinical treatment of keratoconus are more stringent than those for degenerative myopia due to the potential exposure of the retina to the treatment irradiation.

For keratoconus treatment, light directed onto the cornea is transmitted through the cornea, lens, and vitreous and to the retina with minimal loss. Using the MPE for retinal irradiance (E_R), we can calculate the maximum permissible source radiance (L_S):

$$L_S = \frac{4 \cdot E_R \cdot f^2}{\pi \cdot \tau \cdot d_P^2}, \quad [31]$$

where τ is the transmission through the ocular media (conservatively taken to be 100%), f is the focal length of the eye (1.7 cm), and d_P is the diameter of the pupil (0.7 cm). This gives L_S of 20 J/(cm^{2}sr). Calculating the exposure at the cornea can be done using the geometry of the light source, which can be taken as 1 cm in diameter (D_S) a distance 1 cm from the cornea (r). The irradiance at the cornea is:

$$E_C = L_S \cdot \frac{\pi \cdot D_S^2}{4 \cdot r^2} = 15.7 \text{ J/cm}^2.$$

For a 300 second exposure, this would correspond to a maximum permissible irradiation of 52 mW/cm^2, which is 6.5 times greater than the irradiation (8 mW/cm^2) used in the *in vitro* keratoconus studies in Chapter 6.

For treatment of degenerative myopia, light delivered from the outside of the eye must pass through the sclera and the choroid before reaching the retina. To obtain conservative safety criteria, calculations here are based upon the minimum thickness and minimum absorption coefficients of the sclera and choroid, neglecting scattering in the sclera and choroid. On this basis, less than 5 % of light incident on the sclera will irradiate the retina (Table 3.2). The MPE for retina remains the same as above (2.7 J/cm^2). Although ANSI does not provide an MPE value for the sclera, exposure of the skin to visible light of duration > 10 seconds should not exceed 200 mW/cm^2. Based on these limits, the irradiation (6–8 mW/cm^2) used in studies on degenerative myopia (Chapter 5) with visible light falls well below the safety limits (by a factor of 25, Figure 3.5).

Tissue	Absorption Coefficient, μ (mm^{-1})	Thickness, l (mm)	Transmittance $I/I_{incident} = e^{-\mu l}$
Choroid	15[32]	0.2	0.05
Sclera	0.39 (for 500 nm)[33]	0.39[34]	0.86

Table 3.2 Calculation of Light Absorbed by the Choroid and Sclera

Calculations yield margins of safety with factors of at least 6.5 and 25 for treatment of keratoconus and degenerative myopia, respectively. The safety of this irradiation on rabbit and guinea pig sclera has been verified during *in vivo* biocompatibility studies (Chapter 5).

In relation to clinical application, considerations beyond safety may motivate further reduction of the irradiation dose. The MPE values from ANSI are below known hazardous levels for creation of retinal lesions. Thus, the calculations above indicate that the irradiation used should not damage any ocular tissues; it may still be uncomfortable to view or cause perturbed color perception for a period of time after treatment. Further reduction in intensity may increase patient comfort.

The key factors that led to the decision to use EY/TEOA for development of a clinically relevant treatment in Chapters 5 and 6 are: 1) efficacy with irradiation that is considered safe with respect to ANSI standards, 2) previously demonstrated biocompatibility of EY/TEOA, and 3) temporal and spatial control (like other photoinitiator systems).

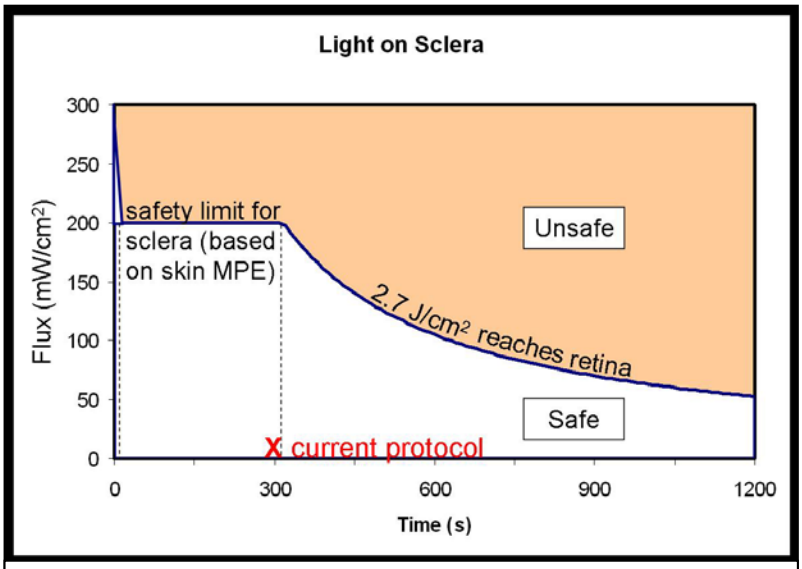

Figure 3.5. Safety calculations based on ANSI standards reveal that treatment using the current protocol of 525 ± 16 nm at 6–8 mW/cm^2 for 5 minutes directed onto the posterior sclera from outside the eye is well below the safety limits.

BIBLIOGRAPHY

1. Spoerl, E., Wollensak, G., Dittert, D.D., Seiler, T. Thermomechanical behavior of collagen-cross-linked porcine cornea. *Ophthalmologica* **218**, 136-140 (2004).
2. Spoerl, E., Wollensak, G., Seiler, T. Increased resistance of crosslinked cornea against enzymatic digestion. *Current Eye Research* **29**, 35-40 (2004).
3. Sporl, E., Genth, U., Schmalfuss, K., Seiler, T. Thermo-mechanical behavior of the cornea. *Klinische Monatsblatter Fur Augenheilkunde* **208**, 112-116 (1996).
4. Sporl, E., Genth, U., Schmalfuss, K., Seiler, T. Thermomechanical behavior of the cornea. *German Journal Of Ophthalmology* **5**, 322-327 (1997).
5. Wollensak, G. Crosslinking treatment of progressive keratoconus: new hope. *Current Opinion In Ophthalmology* **17**, 356-360 (2006).
6. Wollensak, G., Aurich, H., Pham, D.T., Wirbelauer, C. Hydration behavior of porcine cornea crosslinked with riboflavin and ultraviolet A. *Journal of Cataract and Refractive Surgery* **33**, 516-521 (2007).
7. Wollensak, G., Spoerl, E., Reber, F., Seiler, T. Keratocyte cytotoxicity of riboflavin/UVA-treatment in vitro. *Eye* **18**, 718-722 (2004).
8. Wollensak, G., Spoerl, E., Seiler, T. Stress-strain measurements of human and porcine corneas after riboflavin-ultraviolet-A-induced cross-linking. *Journal Of Cataract And Refractive Surgery* **29**, 1780-1785 (2003).
9. Wollensak, G., Spoerl, E., Seiler, T. Riboflavin/ultraviolet-A-induced collagen crosslinking for the treatment of keratoconus. *American Journal Of Ophthalmology* **135**, 620-627 (2003).

10. Wollensak, G., Spoerl, E., Wilsch, M., Seiler, T. Endothelial cell damage after riboflavin-ultraviolet-A treatment in the rabbit. *Journal Of Cataract And Refractive Surgery* **29**, 1786-1790 (2003).

11. Wollensak, G., Spoerl, E., Wilsch, M., Seiler, T. Keratocyte apoptosis after corneal collagen cross-linking using riboflavin/UVA treatment. *Cornea* **23**, 43-49 (2004).

12. Wollensak, G., Sporl, E., Reber, F., Pillunat, L., Funk, R. Corneal endothelial cytotoxicity of riboflavin/UVA treatment in vitro. *Ophthalmic Research* **35**, 324-328 (2003).

13. Wollensak, G., Sporl, E., Seiler, T. Treatment of keratoconus by collagen cross linking. *Ophthalmologe* **100**, 44-49 (2003).

14. Wollensak, G., Wilsch, M., Spoerl, E., Seiler, T. Collagen fiber diameter in the rabbit cornea after collagen crosslinking by riboflavin/UVA. *Cornea* **23**, 503-507 (2004).

15. Nakayama, Y., Kameo, T., Ohtaka, A., Hirano, Y. Enhancement of visible light-induced gelation of photocurable gelatin by addition of polymeric amine. *Journal of Photochemistry and Photobiology a-Chemistry* **177**, 205-211 (2006).

16. Orban, J.M., Faucher, K.M., Dluhy, R.A., Chaikof, E.L. Cytomimetic biomaterials. 4. In-situ photopolymerization of phospholipids on an alkylated surface. *Macromolecules* **33**, 4205-4212 (2000).

17. Cruise, G.M., Hegre, O.D., Scharp, D.S., Hubbell, J.A. A sensitivity study of the key parameters in the interfacial photopolymerization of poly(ethylene glycol) diacrylate upon porcine islets. *Biotechnology and Bioengineering* **57**, 655-665 (1998).

18. Pathak, C.P., Sawhney, A.S., Hubbell, J.A. Rapid Photopolymerization of Immunoprotective Gels in Contact with Cells and Tissue. *Journal of the American Chemical Society* **114**, 8311-8312 (1992).

19. Desmangles, A.I., Jordan, O., Marquis-Weible, F. Interfacial photopolymerization of beta-cell clusters: Approaches to reduce coating thickness using ionic and lipophilic dyes. *Biotechnology and Bioengineering* **72**, 634-641 (2001).

20. Wollensak, G., Spoerl, E. Collagen crosslinking of human and porcine sclera. *Journal Of Cataract And Refractive Surgery* **30**, 689-695 (2004).

21. Elisseeff, J., Anseth, K., Sims, D., McIntosh, W., Randolph, M., Langer, R. Transdermal photopolymerization for minimally invasive implantation. *Proc. Natl. Acad. Sci. USA* **96**, 3104-3107 (1999).

22. Carnahan, M.A., Middleton, C., Kim, J., Kim, T., Grinstaff, M.W. Hybrid dendritic-linear polyester-ethers for in situ photopolymerization. *Journal of the American Chemical Society* **124**, 5291-5293 (2002).

23. Luman, N.R., Kim, T., Grinstaff, M.W. Dendritic polymers composed of glycerol and succinic acid: Synthetic methodologies and medical applications. *Pure and Applied Chemistry* **76**, 1375-1385 (2004).

24. Alleyne, C.J.J., Cawley, C.M., Barrow, D.L., Poff, B.C., Powell, M.D., Sawhney, A.S., Dillehay, D.L. Efficacy and biocompatibility of a photopolyrnerized, synthetic, absorbable hydrogel as a dural sealant in a canine craniotomy model. *Journal of Neurosurgery* **88**, 308-313 (1998).

25. West, J.L., Hubbell, J.A. Separation of the arterial wall from blood contact using hydrogel barriers reduces intimal thickening after balloon injury in the

rat: The roles of medial and luminal factors in arterial healing. *Proclomations of the National Academy of Science* **93**, 13188-13193 (1996).

26. Hill-West, J.L., Chowdhury, S.M., Slepianu, M.J., Hubbell, J.A. Inhibition of thrombosis and intimal thickening by in situ photopolymerization of thin hydrogel barriers. *Proclomations of the National Academy of Science* **91**, 5967-5971 (1994).

27. Wollensak, G., Iomdina, E., Dittert, D.D., Salamatina, O., Stoltenburg, G. Cross-linking of scleral collagen in the rabbit using riboflavin and UVA. *Acta Ophthalmologica Scandinavica* **83**, 477-482 (2005).

28. Bryant, S.J., Nuttelman, C.R., Anseth, K.S. Cytocompatibility of UV and visible light photoinitiating systems on cultured NIH/3T3 fibroblasts in vitro. *Journal Of Biomaterials Science-Polymer Edition* **11**, 439-457 (2000).

29. Williams, C.G., Malik, A.N., Kim, T.K., Manson, P.N., Elisseeff, J.H. Variable cytocompatibility of six cell lines with photoinitiators used for polymerizing hydrogels and cell encapsulation. *Biomaterials* **26**, 1211-1218 (2005).

30. American National Standards Institute. *American National Standard for Safe Use of Lasers.* (Laser Institute of America, Orlando, FL, 2000).

31. [Anon]. Guidelines on limits of exposure to broad-band incoherent optical radiation (0.38 to 3 mu M). *Health Physics* **73**, 539-554 (1997).

32. Hammer, M., Roggan, A., Schweitzer, D., Muller, G. Optical-Properties of Ocular Fundus Tissues - an in-Vitro Study Using the Double-Integrating-Sphere Technique and Inverse Monte-Carlo Simulation. *Physics in Medicine and Biology* **40**, 963-978 (1995).

33. Nemati, B., Rylander, H.G., Welch, A.J. Optical properties of conjunctiva, sclera, and the ciliary body and their consequences for transscleral cyclophotocoagulation. *Applied Optics* **35**, 3321-3327 (1996).

34. Olsen, T.W., Aaberg, S.Y., Geroski, D.H., Edelhauser, H.F. Human sclera: Thickness and surface area. *American Journal of Ophthalmology* **125**, 237-241 (1998).

Chapter 4

INTERPENETRATING POLYMER AND TISSUE NETWORKS

4.1 Tissue Engineering IV-1
4.2 Concentration and Oxygen Dependence of Increases in Scleral Modulus IV-3
4.3 Crosslinking Without PEGDM IV-7
4.4 *In Vivo* Treatment Comparison With and Without PEGDM IV-10
Bibliography IV-14

This work has been done in collaboration with graduate student Joyce Huynh during her first year, who assisted with *in vivo* treatment of rabbit eyes. Undergraduates Dennis Ko and Meredith Wiseman contributed to the study of fluorescent molecules within the sclera.

4.1 Tissue Engineering

Tissue engineering is an attractive approach for treating keratoconus and degenerative myopia because of the potential to replace or reinforce old, diseased, or malfunctioning tissue. Hydrogel based materials are traditionally used in tissue engineering because of their adjustable mechanical and chemical properties, biocompatibility, and biodegradability.[1] These characteristics have been employed in biosensor coatings, drug delivery devices, the encapsulation of cells, cell delivery to tissue, and the creation of biodegradable scaffolding for new tissue growth.[2-4] Photopolymerizable hydrogels can be injected as a liquid and then solidified by exposure to light in a controlled, localized manner.[5] This method has demonstrated usefulness in filling voids in bone,[5-7] in wound

healing, and in creation of an engineered tissue, e.g., cartilage in a specified location and shape.[4, 6-11]

Poly(ethylene glycol) (PEG) or PEG-based materials have been widely used in hydrogel and tissue engineering applications, and PEG-diacrylate has been approved by the FDA for use in the body. PEG-based hydrogels formed by photopolymerization in the body have already shown clinical applicability in treatment of lung and dural tissues.[12, 13] PEG-based macromers may have varying-length PEG chains, which alters the solubility of the macromers and, upon polymerization, can create different crosslink densities (or modulus) of the polymerized network. By incorporating appropriate amino acid sequences along the PEG chains, the matrix can contain cell-binding domains, enzymatically degradable sections, growth factors, etc. This allows for artificial direction of cell growth and behavior. Also, PEG can be functionalized with varying end groups such as methacrylate, to give different reactivities. Radical generation by the photoinitiator initiates reaction of the endgroups, which form bonds with other macromers and/or with the tissue. Because of the customizability of PEG-based macromers, they have been chosen for use in our preliminary treatment mixtures.

While literature on tissue engineering typically focuses on the filling of voids, surface modifications, and temporary support for growing tissue, an alternative approach that we have studied for the cornea and sclera is the creation of an integrated polymer network within the tissue. By first allowing the tissue to imbibe photopolymerizable material, crosslinking incorporates the new material inside the tissue. This interpenetrating network could increase structural support, and through covalent crosslinks, could lock pre-existing

structures in place and prevent tissue reconfiguration. In the present case, it might prevent excessive deformation or tissue remodeling in keratoconus and degenerative myopia. In addition, we have demonstrated that it can be used to anchor labels or other functional moieties into the tissue (illustrated in Chapter 3 using Fluorescein-PEG-methacrylate). In studies of the mechanical properties related to polymerization or grafting of PEG-dimethacrylate (PEGDM) into ocular tissues, we have examined 1) the concentration dependence of modulus increases in sclera, 2) the relationship of oxygen to the modulus increase in sclera, and 3) the stabilization of eye shape with and without an interpenetrating network.

4.2 Concentration & Oxygen Dependence of Increases in Scleral Modulus

The density of the new network (artificial and natural), or the degree of crosslinking is expected to determine the treated tissue modulus. For example, a controlled increase in tissue modulus might be achieved by increasing the concentration of PEGDM, which is expected to increase crosslink formation.

In addition to control of the final modulus, in the case of degenerative myopia, we desire selective polymerization within sclera and not within vessel walls that penetrate the posterior sclera (Figure 4.1a). Oxygen inhibition of radical polymerization is commonly observed,[14, 15] which could be an advantage in this situation. Because sclera is largely avascular, we can exploit the differential concentration of oxygen within vessel walls compared to adjacent sclera to control polymerization. In and around blood vessels where

oxygen tension is higher, polymerization will be inhibited; further away, in avascular portions of the sclera where the oxygen tension is lower, polymerization will occur.

To test these hypotheses regarding the effects of concentration and oxygen on photo-activated incorporation of PEGDM, we use oscillatory shear measurements of the mechanical properties of porcine sclera specimens before and after treatment.

Methods: Eyes from 3–4 month old swine were obtained from Sierra for Medical Science. Tissue was shipped on ice, in saline to maintain proper hydration and freshness. The fresh eyes (< 72 hours post mortem) were dissected to remove orbital fat and muscles, and then cut at the equator to separate the anterior and posterior globe. The episclera, retina, and choroid were removed before cutting a circular disk from the posterior pole with an 8-mm-diameter trephine punch. The center of the circular section was located ~10 mm from the optic nerve on the temporal side. The sections were immediately put on the rheometer for oscillatory shear tests at a frequency of 1 rad/sec and a stress amplitude of 5 Pa.

After initial modulus measurements on the rheometer, tissue sections were soaked for 1 hour in a solution containing a specific concentration (0, 1, 5, 10, or 25 % w/w) of PEGDM (550 Dalton) with 1% 4-benzoylbenzyl trimethylammonium bromide (Initiator A: Figure 3.1a) in Dulbecco's phosphate-buffered saline (DPBS). After soaking for 1 hour, excess solution was removed from the tissue surface by dabbing with a kimwipe. The samples were mounted in a humid chamber that allowed control of oxygen in the atmosphere (Figure 4.1b). The atmosphere was either argon or air during irradiation. After 5 minutes of equilibration in the chamber, a Thermo Oriel 500 Watt mercury xenon arc lamp was

used to irradiate with approximately 4 mW/cm^2 365 nm UV light for 30 minutes. Following irradiation, the samples were rinsed for 4 hours in DPBS to remove unreacted macromer and initiator, and then modulus was measured again.

The storage modulus of each specimen was measured prior to the treatment protocol and again afterward. The same frequency and stress amplitude (1 rad/s, 5 Pa) were used for all measurements. The frequency and stress amplitude were chosen from the range of values where the modulus was in the linear regime. The temperature used for the soak and atmospheric chamber during irradiation was room temperature, and rheological measurements were done at 37ºC. For each specimen, the "% change in G′" was evaluated as $100x(G'_{after}-G'_{before})/G'_{before}$. Four specimens were examined for each condition: the mean and standard deviation are shown by the symbols and vertical bars in Figure 4.1c.

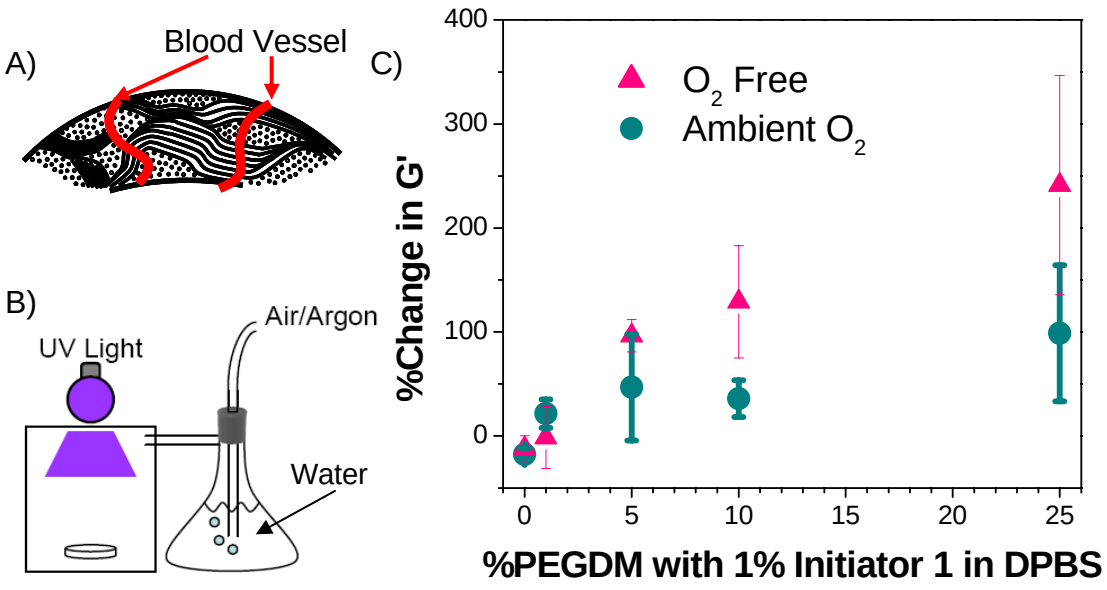

Figure 4.1. A) Schematic illustration of the collagen network of the sclera, depicting oxygen-rich blood vessels that should be avoided during polymerization. B) Humid chamber to provide UV light to tissue samples while maintaining proper hydration in different purge gases. C) Change in storage modulus of porcine sclera tissue sections at a frequency of 1 rad/sec, and oscillatory shear stress amplitude of 5Pa as a function of the concentration of PEGDM (0–25% w/w in DPBS) used in the treatment solution (see text). Samples received UV irradiation in either ambient O_2 (air) or no O_2 (argon). Results indicate a concentration-dependent increase in modulus. Presence of oxygen clearly decreases effectiveness of the reaction. Each data point is an average of 4 samples.

Results: A statistically significant increase in modulus was observed with as little as 5% PEGDM added to the solution. Increasing PEGDM concentration in the mixture generally increases the change in modulus of the sclera (Figure 4.1c). The change in tissue modulus for irradiation in the presence of oxygen is significantly less than that for irradiation under argon. At PEGDM concentrations of 25% w/w, the change in modulus while under argon was 240 ± 110 %, while in the presence of oxygen from air the modulus was 99 ± 65%. The modulus change in the presence of oxygen is less than half that achieved under argon for all concentrations of PEGDM 5% and above.

Discussion: The dose-dependent response of the tissue (increase in modulus with increasing %PEGDM) should enable the adjustment of individual treatments to achieve different desired end properties. The changes that occurred for the ~ 2 hour treatment with 25% w/w PEGDM under argon (240 ± 110 %) were comparable to those for a 24 hour 2% glyceraldehyde crosslinking treatment described in Chapter 2 (330 ± 110 %, Figure 2.16). Such shortening of treatment time would be beneficial for clinical application.

The inability to crosslink efficiently in the presence of oxygen could be a beneficial for this system. For the treatment of degenerative myopia it will be necessary to deliver drug around the back of the eye and close to the retina. The ability of oxygen to inhibit the reaction could provide a method by which strengthening of tissue is done everywhere except in close proximity to oxygen-rich vessels. This is especially relevant to prevention of crosslinking the short posterior ciliary arteries that penetrate sclera in the macular region and around the optic nerve. If drug and light did reach the choroid, the oxygen-rich layer could prevent damaging crosslinking there as well.

4.3 Crosslinking Without PEGDM

In addition to controlling tissue modulus by altering the PEGDM concentration, adjusting the treatment protocols (initiator concentration and soak time) and irradiation parameters (wavelength, intensity, exposure time) can be used to control the reaction. Shorter soak times prevent the drug from penetrating far into the tissue, and the light exposure controls the degree of activation. By examining these parameters, we discovered strengthening of the tissue was possible without any macromer, as illustrated by the following experiments.

Methods: Eyes from 3–4 month old swine were obtained from Sierra for Medical Science. Tissue was shipped on ice, in saline to maintain proper hydration and freshness. The fresh eyes (< 72 hours post mortem) were dissected to remove orbital fat and muscles. The whole eyes were soaked for 60 minutes in one of three solutions prepared in DPBS: a control of only DPBS, 0.3% I2959 in DPBS, or 20% PEGDM (550 MW) with 0.3% I2959 (I2959, Figure 3.1b). Afterward, sections of the eyes were irradiated with UV (~50 mW/cm^2, 315–405 nm, for 5 minutes) using a mask and then 8 mm disks were cut from irradiated and non-irradiated sections of the sclera. The samples were soaked for 24 hours in DPBS and then measured for modulus using oscillatory shear measurements. The difference in modulus between the exposed and unexposed regions was compared.

Results: Specimens from control eyes soaked in DPBS showed little difference in modulus between exposed and unexposed regions (14 ± 33%). The tissue sections from eyes receiving only initiator, or a combination of initiator and PEGDM both displayed increases in modulus in the exposed regions (290 ± 180%, and 150 ± 110% respectively). Due to the large scatter, there is not a significant difference between the treatment with and without PEGDM ($p > 0.05$ as determined using an unpaired t-test) so it is not possible to conclusively determine which treatment was better.

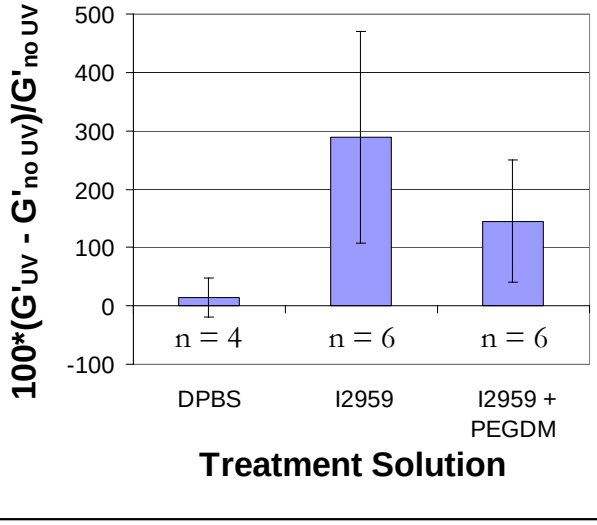

Figure 4.2. Eyes soaked in treatment solutions of DPBS, 0.3% I2959, and a mixture of 0.3% I2959 with 20% PEGDM were partially exposed to UV irradiation. Modulus values from tissue sections of the exposed region, G'_{UV} are compared to those of tissue sections from the unexposed region $G'_{no\ UV}$ to give a % difference of modulus due to treatment. Treatment with I2959 and treatment with the PEGDM initiator mixture both cause increases in modulus.

Discussion: These results indicate that treatments using only initiator and light have the capability of strengthening tissue by inducing crosslinking within the native components of the tissue. While the use of PEGDM allows the incorporation of degradable polymer sections, growth factors, and the possibility to further control stiffness through altering molecular weight, the use of just an initiator would greatly simplify the treatment and reduce the number of variables that must be studied.

4.4 *In Vivo* Treatment Comparison With and Without PEGDM

As discussed in the previous section, it is possible to increase tissue modulus with or without PEGDM present. Although there are advantages to either approach, they appear to have similar effects on modulus and it is not clear which will provide the best treatment *in vivo*. A set of experiments was conducted on rabbits in order to determine the efficacy of *in vivo* treatment with or without PEGDM while using the Eosin Y (EY) and triethanolamine (TEOA) photoinitiator system (Figure 3.1c). This system was chosen based on issues of safety discussed in Chapter 3.

Methods: The detailed methods for *in vivo* treatment delivery and irradiation are given in Chapter 5. For these experiments, 6 rabbits (12 eyes) received a subconjunctival injection of one of the following three solutions (Table 4.1): 1) control solution (DPBS), 2) 0.3 mM Eosin Y and 90 mM Triethanolamine in DPBS (10x EY), or 3) 10x EY with 10% PEGDM, 550 MW (10x EY w/PEGDM). After allowing 5 minutes for drug to diffuse into the sclera, the eyes were irradiated for 5 minutes using ~525 ± 16 nm, ~2 mW/cm^2 light. The animals were sacrificed on the same day that treatment was performed. The eyes were enucleated and then tested using the intact globe expansion method (Chapter 2).

Group	# of eyes	EY concentration	TEOA concentration	PEGDM concentration
1) DPBS	4	None	None	None
2) 10x EY	4	0.3 mM	90 mM	None
3) 10x EY w/PEGDM	4	0.3 mM	90 mM	10 % w/w

Table 4.1 *In Vivo* Treatment Comparison with and without PEGDM

Results: Treatment with either 10x EY or 10x EY w/PEGDM reduces the expansion of the sclera as compared to controls (SP, ED, SL, Figure 4.3). Because drug was only applied to the subconjunctival sclera, the corneas were untreated and changes in CP, CD, and CL are similar in treated and control eyes. The reduction in expansion along CD is most likely due to treatment effects at the limbus which constrain expansion of sclera around the edge of the cornea. Treatment without PEGDM may be slightly more effective at preventing expansion of the eyes, with average values of SP, ED, and SL being lower than those from treatment with PEGDM.

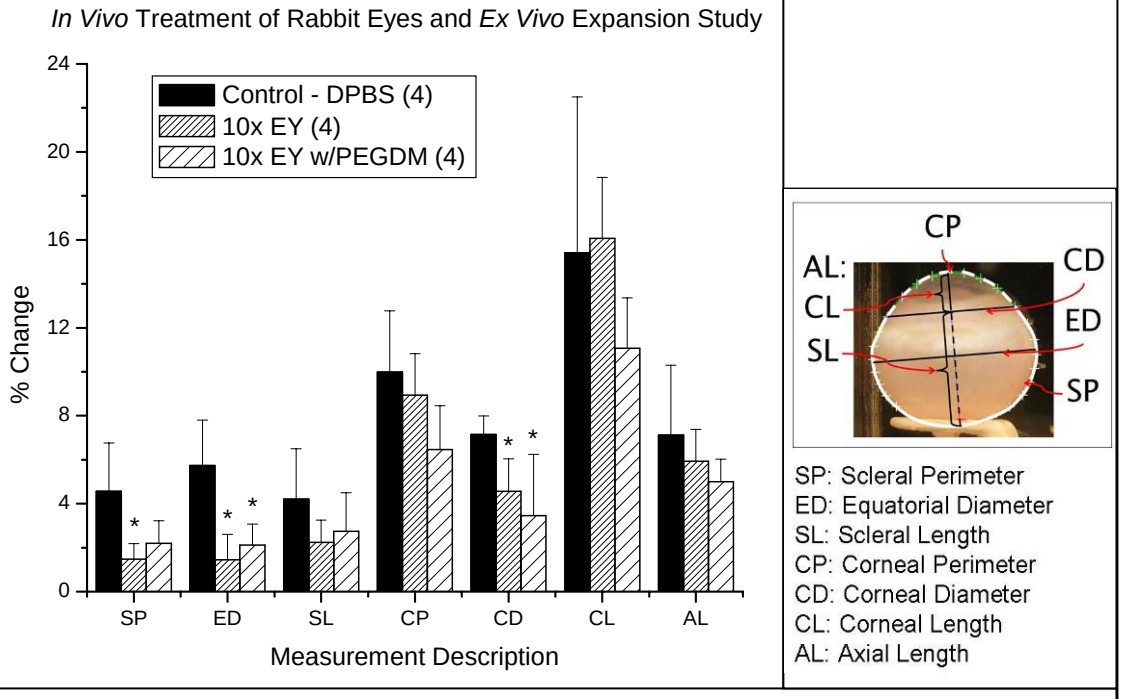

Figure 4.3. Rabbit eyes were treated *in vivo* and then examined using the intact globe method *ex vivo* in order to compare the treatment effects with and without macromer (PEGDM). Changes to scleral dimensions SP, ED, and SL are similar for both treatments, and there is some decrease in expansion along CD. Only the sclera was treated, so SP, ED, and SL are expected to differ from controls, while CP, CD, and CL may show minor changes. The measured ocular dimensions are illustrated in the side figure.

Summary: Previous work involving interpenetrating networks and tissue has demonstrated the use of these systems for ensuring hydrogel-to-tissue adhesion. West and coworkers have reported interfacial photopolymerization of PEGDM networks and tissue where the liquid form of the hydrogel penetrates into crevices in the tissue surface and upon polymerization, enhances adhesion between the final hydrogel coating and the tissue.[16, 17] In contrast to their work, we have demonstrated that interpenetrating networks can be used to increase the strength of tissue. The use of interpenetrating networks to control increases in the modulus of the cornea or sclera could be excellent treatments for keratoconus and degenerative myopia, particularly because of the potential to functionalize the network. Preliminary studies by undergraduate students Meredith Wiseman and Dennis Ko have shown the ability to deliver fluorescein-PEGM molecules within the sclera and immobilize them at a depth within the tissue (Figure 3.4), demonstrating functionalization and crosslinking of molecules inside the tissue.

Confocal microscopy of sclera from eyes soaked in the crosslinkable fluorescent molecule for 10 minutes reveals a gradient in fluorescence that varies with depth (Figure 4.4). The gradient in crosslinking is due to a concentration gradient from diffusion of molecules into the tissue, and due to light attenuation by the tissue. Future work that varies the crosslinking profile may illustrate differences in the mechanical properties (i.e., when PEGDM is present throughout the depth of the tissue instead of just the surface). Changing the soaking time, the time between soaking and irradiation, and the wavelength of light used for activation could all be used to modify the crosslinking.

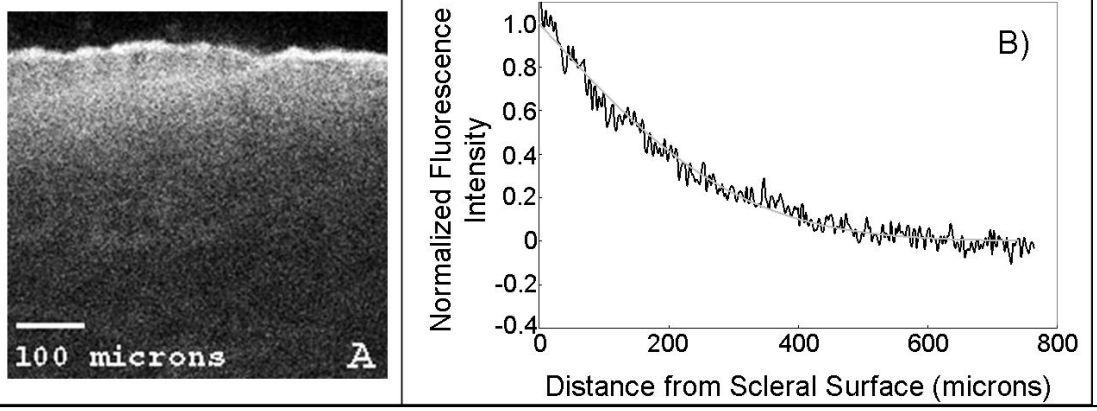

Figure 4.4. A) The confocal fluorescence image of porcine sclera shows fluorescence intensity of crosslinked fluorescein-PEGM within the tissue after a 10 minute soak, and B) a profile of the intensity as a function of depth demonstrates the gradient crosslinking within the tissue.

Results from this chapter indicate that the tissue can be strengthened by crosslinking of the native components of the tissue without the use of photopolymerizable molecules. Future studies could reveal certain conditions at which PEGDM plays the dominant role in strengthening the tissue, or other conditions at which crosslinking of the native tissue components dominates the strengthening. Studies on model systems using simple amino acids could reveal the interactions that are most important in the mechanism of crosslinking for both native tissue and interpenetrating networks.

The simplicity of using a photoinitiator-only system as the treatment is attractive because it can reduce the steps toward clinical use. In Chapters 5 and 6, we will focus discussion primarily on the use of EY/TEOA for treatment of degenerative myopia and keratoconus respectively.

BIBLIOGRAPHY

1. Nguyen, K.T., West, J.L. Photopolymerizable hydrogels for tissue engineering applications. *Biomaterials* **23**, 4307-4314 (2002).
2. Sershen, S., West, J. Implantable, polymeric systems for modulated drug delivery. *Advanced Drug Delivery Reviews* **54**, 1225-1235 (2002).
3. Riley, S.L., Dutt, S., de la Torre, R., Chen, A.C., Sah, R.L., Ratcliffe, A. Formulation of PEG-based hydrogels affects tissue-engineered cartilage construct characteristics. *Journal Of Materials Science-Materials In Medicine* **12**, 983-990 (2001).
4. Park, Y., Lutolf, M.P., Hubbell, J.A., Hunziker, E.B., Wong, M. Bovine primary chondrocyte culture in synthetic matrix metalloproteinase-sensitive poly(ethylene glycol)-based hydrogels as a scaffold for cartilage repair. *Tissue Engineering* **10**, 515-522 (2004).
5. Hou, Q.P., De Bank, P.A., Shakesheff, K.M. Injectable scaffolds for tissue regeneration. *Journal Of Materials Chemistry* **14**, 1915-1923 (2004).
6. Watkins, A.W., Anseth, K.S. Copolymerization of photocrosslinkable anhydride monomers for use as a biodegradable bone cement. *Journal Of Biomaterials Science-Polymer Edition* **14**, 267-278 (2003).
7. Poshusta, A.K., Burdick, J.A., Mortisen, D.J., Padera, R.F., Ruehlman, D., Yaszemski, M.J., Anseth, K.S. Histocompatibility of photocrosslinked polyanhydrides: A novel in situ forming orthopaedic biomaterial. *Journal Of Biomedical Materials Research Part A* **64A**, 62-69 (2003).

8. Halstenberg, S., Panitch, A., Rizzi, S., Hall, H., Hubbell, J.A. Biologically engineered protein-graft-poly(ethylene glycol) hydrogels: A cell adhesive and plasm in-degradable biosynthetic material for tissue repair. *Biomacromolecules* **3**, 710-723 (2002).

9. Zisch, A.H., Lutolf, M.P., Ehrbar, M., Raeber, G.P., Rizzi, S.C., Davies, N., Schmokel, H., Bezuidenhout, D., Djonov, V., Zilla, P., Hubbell, J.A. Cell-demanded release of VEGF from synthetic, biointeractive cell-ingrowth matrices for vascularized tissue growth. *Faseb Journal* **17** (2003).

10. Rice, M.A., Dodson, B.T., Arthur, J.A., Anseth, K.S. Cell-based therapies and tissue engineering. *Otolaryngologic Clinics Of North America* **38**, 199-214 (2005).

11. Rizzi, S.C., Hubbell, J.A. Recombinant protein-co-PEG networks as cell-adhesive and proteolytically degradable hydrogel matrixes. Part 1: Development and physicochernical characteristics. *Biomacromolecules* **6**, 1226-1238 (2005).

12. Allen, M.S., Wood, D.E., Hawkinson, R.W., Harpole, D.H., McKenna, R.J., Walsh, G.L., Vallieres, E., Miller, D.L., Nichols, F.C., Smythe, W.R., Davis, R.D. Prospective randomized study evaluating a biodegradable polymeric sealant for sealing intraoperative air leaks that occur during pulmonary resection. *Annals Of Thoracic Surgery* **77**, 1792-1801 (2004).

13. Boogaarts, J.D., Grotenhuis, J.A., Bartels, R., Beems, T. Use of a novel absorbable hydrogel for augmentation of dural repair: Results of a preliminary clinical study. *Neurosurgery* **57**, 146-151 (2005).

14. Lee, T.Y., Guymon, C.A., Jönsson, E.S., Hoyle, C.E. The effect of monomer structure on oxygen inhibition of (meth)acrylates photopolymerization. *Polymer* **45**, 6155-6162 (2004).

15. Ramis, X., Morancho, J.M., Cadenato, A., Salla, J.M., Fernández-Francos, X. Effect of oxygen on the photopolymerization of a mixture of two dimethacrylates. *Thermochimica Acta* **463**, 81-86 (2007).

16. Hill-West, J.L., Chowdhury, S.M., Slepianu, M.J., Hubbell, J.A. Inhibition of thrombosis and intimal thickening by in situ photopolymerization of thin hydrogel barriers. *Proclomations of the National Academy of Science* **91**, 5967-5971 (1994).

17. West, J.L., Hubbell, J.A. Separation of the arterial wall from blood contact using hydrogel barriers reduces intimal thickening after balloon injury in the rat: The roles of medial and luminal factors in arterial healing. *Proclomations of the National Academy of Science* **93**, 13188-13193 (1996).

Chapter 5

TREATMENT OF MYOPIA

5.1 Introduction V-2
5.2 Materials and Methods V-6
5.2.1 In Vitro *Application* & In Vitro *Expansion* *V-6*
5.2.2 Biocompatibility *V-8*
5.2.3 In Vivo *Application* & In Vitro *Expansion* *V-9*
5.2.4 Animal Model of Myopia *V-12*
5.3 Results V-17
5.3.1 In Vitro *Application* & In Vitro *Expansion* *V-17*
5.3.2 Biocompatibility *V-20*
5.3.3 In Vivo *Application* & In Vitro *Expansion* *V-23*
5.3.4 Animal Model of Myopia *V-24*
5.4 Summary V-31
Bibliography V-32

This work has been done in collaboration with Joyce Huynh at Caltech, Dr. Marco Coassin and Dr. Keith Duncan at University of California at San Francisco, and Dr. Sally McFadden at University of Newcastle. As a first year graduate student, Joyce has assisted with *in vitro* expansion tests and with *in vivo* experiments on rabbits. Marco provided surgical expertise in both rabbits and guinea pigs. Keith has assisted with procurement of rabbits necessary for this work as well as with conduction of biocompatibility studies. Sally provided the guinea pig animal model of myopia and conducted expert measurements and analysis of ocular parameters. The data related to these guinea pig studies are a subset of results from a report provided by Dr. McFadden.

5.1 Introduction

In degenerative myopia, the reduction of collagen fibril diameter, enhanced turnover of scleral collagen, and alteration of scleral glycosaminoglycans results in mechanical changes to the sclera.[1] Progressive elongation of the eye in degenerative myopia is thought to be the result of 1) the tissue being inherently weak, 2) the sclera continuously being remodeled, or 3) a combination of these.[1, 2] From studies of human donor tissue, high myopia is associated with weakening and thinning of the sclera, a reduction in matrix material, and reduction in collagen fibril diameter. While refractive errors induced by progressive myopia are readily corrected by spectacles, contact lenses, corneal refractive surgery, or intraocular lenses, these modalities do not prevent visual loss induced by stretching of chorioretinal tissues. Current means to treat choroidal neovascularization in degenerative myopia, such as photodynamic therapy, are minimally effective,[3] and studies have only recently begun to test injections of anti-angiogenic drugs such as bevacizumab (Avastin®), or Lucentis®.[4-8] Various attempts have been made to treat expansion of the eye due to myopia, including the use of scleroplasty, scleral reinforcement, and even an attempt to polymerize foam around the eye.[9-18] Largely because these modalities remain unproven in well-controlled clinical trials, none have been widely adopted to manage patients with degenerative myopia. Current therapies are essentially palliative, attempting to mitigate visual loss in this condition.

Crosslinking of scleral components has the potential to halt progression of degenerative myopia because it addresses both of the underlying causes that are currently hypothesized: crosslinking increases tissue strength and hinders tissue remodeling.[19-21] As mentioned in

Chapters 1 and 3, Wollensak and Spoerl have reported the use of collagen cross-linking agents, including glutaraldehyde, glyceraldehyde, and riboflavin-UVA treatment, to strengthen both human and porcine sclera *in vitro*.[22] Glutaraldehyde and glyceraldehyde would be difficult to spatially control, and unwanted crosslinking of collagen in vascular and neural structures might have particularly untoward effects. Use of light-activated riboflavin would seem preferable in this regard; however, when testing on a rabbit model, "serious side-effects were found in the entire posterior globe with almost complete loss of the photoreceptors, the outer nuclear layer and the retinal pigment epithelium (RPE)."[23] While crosslinking near the posterior pole would increase scleral modulus and potentially arrest myopic progression, there remains a need for a non-toxic crosslinking agent that could be activated using short exposure to a less-toxic light source. Our research in Chapters 3 and 4 indicates that the visible-light-activated co-initiator system of Eosin Y (EY) and triethanolamine (TEOA) has the potential to fill this need.

For transition of this treatment from the lab to clinical practice, biocompatibility and efficacy must be proven in an animal model of myopia. Current state-of-the-art animal models to study the etiology of myopia rely on 1) visual form deprivation and 2) the eye's tendency to correct refractive errors toward emmetropia.[24] During development, eyes tend to grow excessively upon removal of spatial vision. Form-deprivation models use this response to induce myopia either by placing semitransparent occluders over the eye, or by suturing the eyelid shut.[25] The second animal model makes use of emmetropization of the eye, which is the process by which eyes change to focus images on the retina. When minus

or plus lenses are placed over the eye, the eye adjusts its growth to bring the image into focus.

As is observed in the human disease, form-deprivation animal models (e.g., tree shrew eyes covered with occluders for 12 days) also exhibit weakened sclearl tissue (e.g., increased scleral creep rates). In these animal models, there is also a measurable change in the amount and type of collagen and proteoglycan present in the tissue, indicating abnormal remodeling of the sclera. Sustained form-deprivation in animals induces changes in collagen fibril diameter and spacing analogous to the distinctive structure observed in human donor tissue of high myopes.

Various animal models exhibit similarities to humans and each other. Eutherian mammals, such as humans, monkeys, tree shrews and guinea pigs, share the trait that "the entire sclera consists of the fibrous, type I collagen-dominated extracellular matrix".[2] This feature sets them apart from other vertebrates, which have an inner layer of cartilage (e.g., in chicks). Indeed, the mechanism of emmetropization during form-deprivation in eutherian mammals (remodeling of the fibrous sclera) is different from that in other vertebrates (growth of the inner cartilaginous region). Therefore, eutherian mammals provide a better model for testing treatments related to scleral remodeling for potential application in humans. In light of the fact that tree shrews and monkeys are difficult to obtain and monkeys suffer from high variability of the results, researchers have been establishing other mammalian models. Guinea pigs have recently gained acceptance due to the fact that they rapidly develop myopia, the changes are large and reproducible, and they are easy to care for.[26-32] This animal provides a model that is well suited for research requiring significant numbers of

animals, and at the same time demonstrates physiological and anatomical similarities to humans.

Despite the fact that the mechanism of degenerative myopia in humans is not completely understood, the animal models of myopia do express the weakened sclera and excessive remodeling typical of the disease. As will be demonstrated in this chapter, light activation of Eosin Y/TEOA strengthens the sclera; and as discussed in Chapter 3, non-enzymatic collagen crosslinking is known to decrease enzymatic degradation. Therefore, treatment with Eosin Y/TEOA has the potential to address both putative mechanisms of degenerative myopia.

This chapter illustrates efficacy and biocompatibility of this potential treatment. Stabilization of ocular shape is demonstrated for *in vitro* and *in vivo* drug delivery to rabbit eyes followed by *in vitro* eye expansion using the intact globe method (Chapter 2). Preliminary safety studies in rabbits suggested no ill effect of the treatment. We have also conducted experiments to establish drug and light delivery protocols in guinea pigs and to assess the effect of EY/TEOA on ocular growth and form-deprivation myopia in collaboration with Sally McFadden at the University of Newcastle in Australia. The current results indicate that EY/TEOA has an ability to alter ocular parameters of guinea pig eyes without altering gross ocular function or animal behavior.

5.2 Materials and Methods

5.2.1 In vitro *Treatment &* In Vitro *Expansion*

The following procedures were used for testing the effect of *in vitro* treatment of eyes on preventing expansion of intact rabbit kit globes subjected to an elevated intraocular pressure.

Tissue Preparation: Eyes from 2–3 week old New Zealand White Rabbits (University of California at San Francisco) were stored in saline on ice for use within 48 hours of enucleation. Immediately before testing, the extraocular muscles, the conjunctiva, and the episcleral tissues around the eyes were carefully removed to expose the sclera.

Materials: Treatment solutions of 0.0289 mM EY and 90 mM TEOA in DPBS (henceforth called 1x EY) were prepared fresh. As discussed in Chapter 3, these solutions are activated by visible light and have peak absorption at 514 nm. The measured pH was 7.5 for the solution. Glyceraldehyde (GA) solution was prepared by mixing 2% by weight DL-Glyceraldehyde (Sigma) in distilled water. The pH was adjusted to ~7.5 with HCl and NaOH.

Eosin Procedure: Eyes were soaked for 5 min in 5 mL of treatment (1x EY) or control (DPBS) solution. The eyes were removed from the soak and excess solution was wiped from the surface using a Kimwipe. The treatment was activated by placing the eyes under one of two light sources: a high intensity mercury arc lamp equipped with a 450–550 nm bandpass filter that provided 34 mW/cm^2, or a panel of seven light emitting diodes (LEDs) with a spectral output at 525 ± 16 nm that provided an irradiance of 7–10 mW/cm^2, as

measured at the center position of the eye (Figure 5.1). With the arc lamp, the anterior hemisphere of the eye was exposed for 5 minutes and then the eye was flipped and the posterior globe was exposed for 5 minutes. With the LEDs, the entire eye was irradiated at once for 5 minutes. The eyes were placed in a rinse solution of DPBS for 30–45 min and then loaded on the expansion setup which has been described in detail previously (Chapter 2).

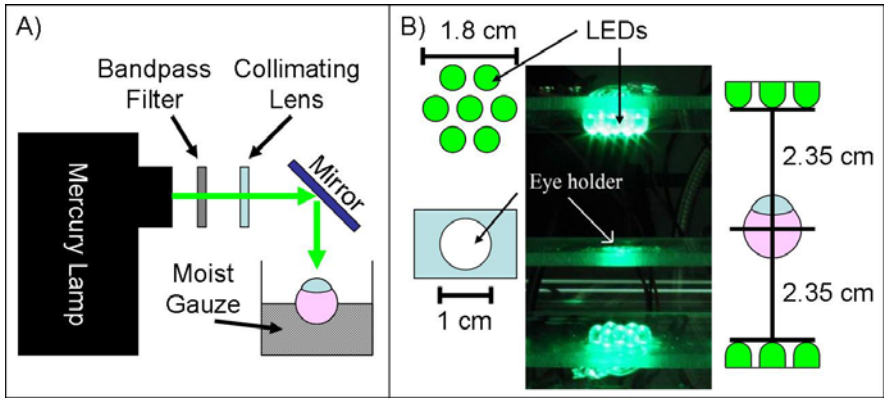

Figure 5.1. A) Schematic of the mercury arc lamp source where light of 450–550 nm passes through a bandpass filter and is collimated onto the eye, which sits on moist gauze. B) Close-packed arrays of 7 LEDs located 2.35 cm above and below the eye direct light onto the eye while it sits in a 1 cm circular hole in the Plexiglas holder.

Glyceraldehyde Procedure: Because of its well-documented effects as a crosslinker, a comparison group was treated with 2% GA solution. To allow GA to penetrate into the cornea (for comparison to keratoconus treatments in Chapter 6), the corneal epithelium of enucleated eyes was removed by scraping with a scalpel blade. The eye was then soaked in 5 mL of 2% GA for 12 hours; when it was removed from the soak, excess solution was removed with a Kim Wipe. The eyes were rinsed in a 20 mL bath of DPBS for ~5 seconds,

and then put in a fresh 40 mL DPBS bath to rinse for 10 hours. The eyes were then loaded on the expansion setup.

As described in Chapter 2, the expansion protocol began with a 1 hour interval at an intraocular pressure (22 mmHg) close to the physiologic value, which allowed the globe to recover from shape distortion that may have occurred during handling post mortem. Then the pressure was raised and held at 85 mmHg for 24 hours. Digital photographs (2272 x 1704) were acquired every 15 min for the duration of the experiment.

5.2.2 Biocompatibility

Toxicity studies were performed at UCSF, to determine if the formulation and light exposure selected from *in vitro* studies would be suitable to use in an animal model for myopia. To test the *in vivo* response to 1x EY and light exposure, the following experiments were performed using topical application of the drug.

Procedure: Four adult New Zealand White rabbits were given general anesthesia with 1–5% inhaled isofluorane administered by mask and topical 0.5% proparacaine to the right eye (OD). The right eye of each animal was sterilized with 5% povidone-iodine (betadyne). Throughout the procedure the eye was washed with sterile ocular balanced saline solution (BSS). A 15 mm incision was made in the conjunctiva close to the limbus and another incision running anterior to posterior allowed the conjunctiva to be pulled away to expose the sclera over approximately 1 cm^2 area. The animal was positioned such that the exposed sclera faced upward and a drop of solution placed on it could remain in contact with the tissue for 5 minutes. Rabbits from Group 1 had 200 microliters of 1x EY

solution applied directly to the exposed sclera. Rabbits from Group 2 had 200 microliters of DPBS (control) applied directly to the exposed sclera.

After 5 minutes, the treated area was rinsed with 1–2 mL of BSS and then photoactivated by exposure to light from an LW Scientific Alpha 1501 Fiber Light Source (~34 mW/cm^2) for 5 minutes.

The conjunctival incision was closed with 7-0 vicryl suture. All animals received subconjunctival injections of celestone (75–150 microliters) and cepahzolin (75–150 microliters). All animals were given injections of carprofen (5 mg/kg) and buprenorphine (0.05 mg/kg) for pain and 2–3 drops of neomycin, polymixin B sulfates, and gramicidin OD to prevent infection.

Eyes were examined for any signs of pain or inflammation such as redness of the eye, discharge, ptosis of the eyelid, blepharospasm, or photophobia once a day for 1 week then once a week for 3 additional weeks.

Histology: After 4 weeks all animals were anesthetized with 30–50 mg/kg ketamine and 5–10 mg/kg xylazine, euthanized, and the eyes were removed, fixed in 10% formalin, and processed for light microscopic examination (Eosin/hematoxylin stain).

5.2.3 In vivo *Treatment* & In Vitro *Expansion*

The following experiments used *in vivo* treatment of the eye followed by *in vitro* expansion on the intact globe setup to test the ability to deliver drug and treatment in a live animal.

Materials: Although *in vivo* treatment does not permit soaking of an entire eye and direct access to the sclera is blocked by conjunctiva and tenon, subconjunctival/subtenon injection is a low-impact surgical procedure that permits drug delivery into the space adjacent to the sclera. Literature on the subconjunctival delivery of mitomycin-C to the sclera indicates that only ~5% of drug present on the surface of sponges is able to diffuse into the sclera, and there is a preferential uptake by the conjunctiva.[33-36] For this reason, a higher drug concentration than that used *in vitro* was used to achieve the desired dose in the sclera. Literature reports excellent cell viability with Eosin Y concentrations up to 20 mM and TEOA concentrations up to 450 mM.[37] Our *in vivo* studies used a solution with 0.289 mM Eosin Y concentration, and 90 mM TEOA concentration, denoted 10x EY from here on. Solutions denoted 10x EY w/PEGDM were a mixture of 10x EY with 10% w/w Poly(ethylene glycol) dimethacrylate. All solutions were adjusted to pH 7.5 and passed through a 0.2 micron filter before use.

Surgical Procedure: The procedures for *in vivo* drug delivery were conducted at UCSF and were performed on 2–3 week old New Zealand White rabbits. The rabbits were given general anesthesia with 1–5% inhaled isofluorane administered by mask and topical 0.5% proparacaine to the eye. The eye of each animal was sterilized with 5% betadyne. Throughout the procedure the eye was washed with sterile ocular balanced saline solution (BSS).

A minimal procedure using subconjunctival injection (0.6–1.2 mL) placed the drug formulation in contact with the sclera. Eight treated eyes were injected with 10x EY, four treated eyes were injected with 10x EY w/PEGDM, and four control eyes received an

injection of DPBS (Table 5.1). The injection formed a pocket of fluid between the conjunctiva and sclera which remained during the 5 minutes given for diffusion (Figure 5.2a). During this time, the lids were closed over the eye. After the 5 minute diffusion time, the lids were retracted and the eye slightly prolapsed. A circular array of 525 nm LEDs was held around the eye for 5 minutes (Figure 5.2b). The control eyes received irradiation of 2 mW/cm^2, four 10x EY treated eyes received 2 mW/cm^2, four 10x EY w/PEGDM treated eyes received 2 mW/cm^2, and the remaining four 10x EY treated eyes received 6 mW/cm^2. After irradiation, the animals were sacrificed, and the eyes were enucleated and stored in DPBS on ice until use on the intact globe expansion setup at Caltech.

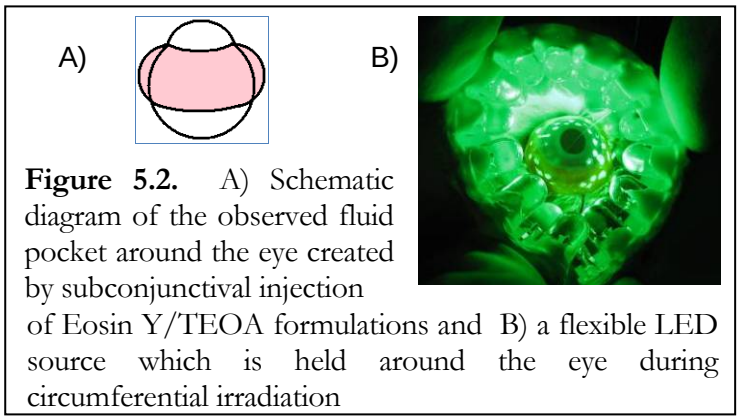

Figure 5.2. A) Schematic diagram of the observed fluid pocket around the eye created by subconjunctival injection of Eosin Y/TEOA formulations and B) a flexible LED source which is held around the eye during circumferential irradiation

***In Vivo* Rabbit Drug Delivery**			
Set	Light Protocol	Drug Formulation	# of Rabbits
A	2 mW/cm^2	DPBS	4
B	2 mW/cm^2	10x EY	4
C	2 mW/cm^2	10x EY w/PEGDM	4
D	6 mW/cm^2	10x EY	4

Table 5.1. Variations for *In Vivo* Rabbit Treatments and *Ex Vivo* Expansion

Expansion Testing: Expansion experiments were performed within 48 hours post mortem. The appearance of the eyes (e.g., clarity of the cornea and size of the globe) was unchanged over this time scale. For the expansion experiment, extraocular tissues were carefully removed from the eye and then the eye was placed into DPBS for ~1 hour to equilibrate to room temperature. The eyes were loaded onto the expansion setup where the intraocular pressure was set to 22 mmHg for 1 hour then increased to 85 mmHg for 24 hours (Chapter 2 for details).

5.2.4 Animal Model of Myopia

These experiments in a guinea pig model were conducted in collaboration with Dr. Sally McFadden at the University of Newcastle, NSW Australia. These tests examine the feasibility and safety of surgery, the safety of drug and irradiation, the effect of treatment on development of form deprivation, and the effect of treatment on normal ocular growth.

Materials: All treatment solutions were prepared at pH 7.5 and passed through a 0.2 micron filter to ensure sterility for surgery. The tests used DPBS, 3x EY (0.1 mM EY & 90 mM TEOA in DPBS), and 10x EY.

Pigmented guinea pigs (*Cavia porcellus*, n = 47) were maternally reared and housed in their natural litters with their mothers in opaque plastic boxes (65 x 45 x 20 cm) with wire mesh lids. Water (supplemented with Vitamin C), guinea pig food pellets, and hay were available *ad libitum*. Light hoods containing incandescent bulbs evenly diffused through a perpex barrier were suspended 30 cm above each box and switched on a 12 h light/12 h dark cycle. All procedures were approved by The University of Newcastle in accordance

with New South Wales Animal Research Act and were in accordance with National Institutes of Health Guidelines.

Procedures: Animals were anesthetized with Ketamine (50 mg/kg) and Xylazine (5 mg/kg) and if necessary, administered a small dose of Bupremorphine (0.1 mg/kg). The eyes received topical anesthetic as needed. On the right eye, drug was delivered through subconjunctival injection (Figure 5.3), which was previously demonstrated as a successful method in rabbits. Some animals received a sham surgery with injection of DPBS instead of drug (Table 5.2). After subconjunctival injection, 10 minutes was allowed for diffusion of drug formulation into the sclera.

***In Vivo* Guinea Pig Drug Delivery**					
Set	Light Protocol	Drug formulation	Form Deprivation	# of Guinea Pigs	Day of Enucleation
A	No Irradiation	10x EY	No	3	Immediate
B	No Irradiation	No Treatment	Yes	7	17 days post surgery
C	3 Trisections	3x EY	Yes	14	
D	3 Trisections	10x EY	No	7	
E	Circumferential	10x EY	No	8	30 days post surgery
F	Circumferential	DPBS (sham)	No	8	

Table 5.2. Treatment Variations for *In Vivo* Guinea Pig Studies

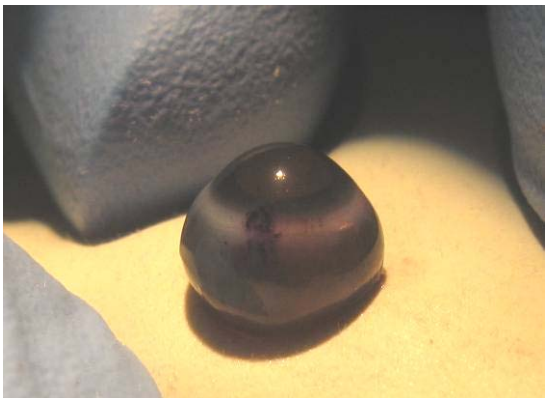

Figure 5.3. Controlled subconjunctival injection of 10x EY delivers treatment to the eye. 10x EY is seen as pink on the right side, and locations where 10x EY has not yet been delivered are seen as grey on the left side.

After the 10 minute diffusion time, the right eyes of Sets C-E were prolapsed and irradiated in two different manners. One group of animals had a superficial suture placed at the limbus for traction while prolapsing the eye (Sets C, D). The eye was irradiated with an LED light source for 5 minutes at each of 3 trisections (Figure 5.4a). The second group of animals had a piece of elastic placed around the eye to hold it prolapsed (Set E, Figure 5.4b). While prolapsed in this manner, a circular array of LEDs was placed around the eye for 5 minutes (Figure 5.4c, d). We built the light sources from 525 ± 16 nm LEDs to provide 6–8 mW/cm2 at the plane of the sclera; the light for trisection illumination consisted of three 5 mm LEDs aligned to irradiate a 120 degree section of the eye while held a distance of ~8 mm from the eye, and the light for circumferential illumination consisted of 2 rows of twelve 3 mm LEDs ~2 mm from the scleral surface that could irradiate 360 degrees of the eye.

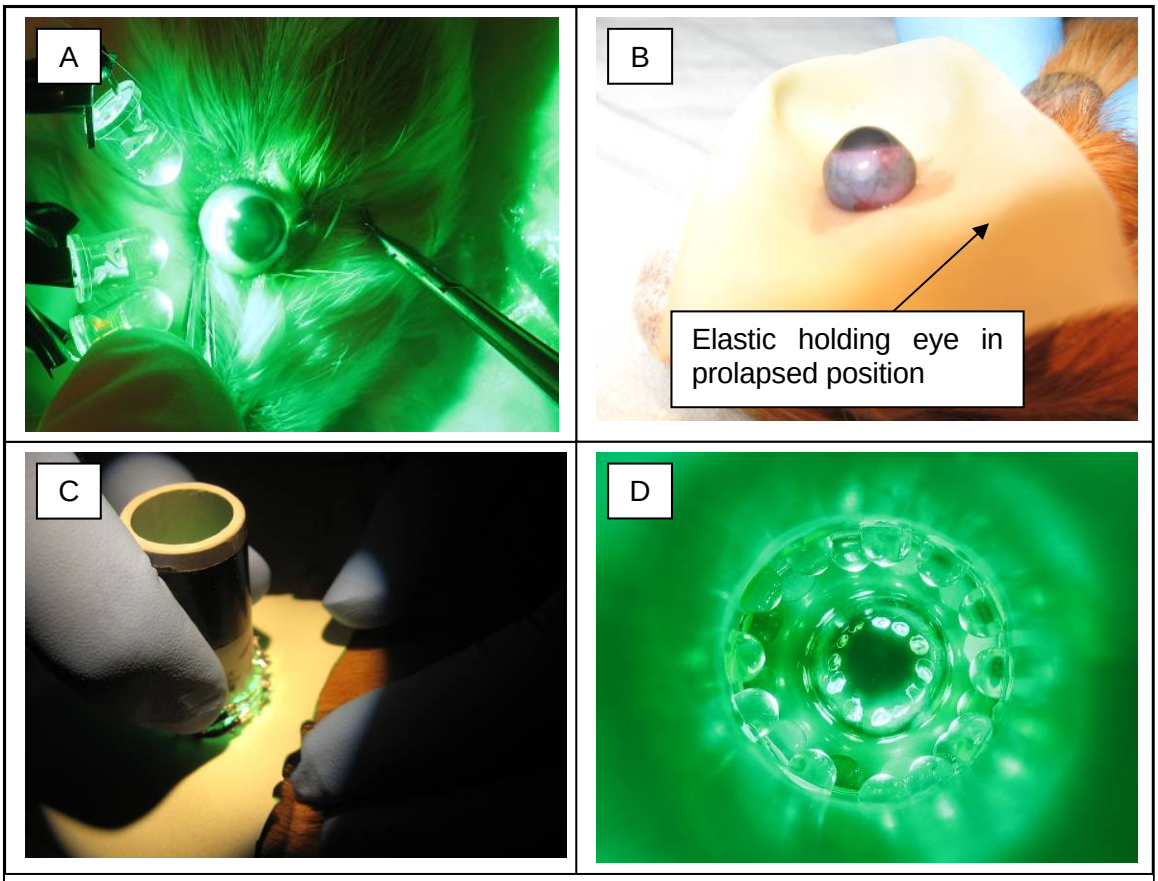

Figure 5.4. A) Group 1—Irradiation of one trisection of a prolapsed guinea pig eye while a suture is used to control the exposed region. B) Group 2—Elastic placed around the eye of an anesthetized guinea pig to hold the eye prolapsed during irradiation. C) The light source is place around the eye for 5 minutes, while D) LEDs provide circumferential irradiation.

After irradiation, the eyes were placed back in the normal position and washed with antibiotic eyedrops. The animals were placed back with their mothers after surgery and monitored to observe behavioral responses.

Animals from Set A were immediately euthanized and the eyes were enucleated. The eyes were examined for the presence of Eosin Y in the sclera.

The animals from Sets B and C included form-deprivation studies. Diffusers were secured with velcro over the right eye when the animals were ~6 days old and the fellow eye was left untreated (Figure 5.5). This was 2–3 days after surgery of animals in Set C. The animals were exposed to a 12h/12h light/dark cycle, and the diffusers were removed for 50–90% of the dark periods overnight. Diffusers were also removed during measurements.

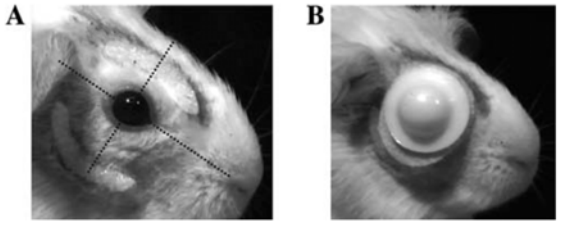

Figure 5.5. Method of attaching a diffuser in the guinea pig. (A) Position of the Velcro arcs. Dotted lines indicate the horizontal and vertical meridians used in retinoscopy. (B) The diffuser held in place by a matching Velcro ring attached to its base (Howlett 2006)

Animals from Sets D, E, & F did not receive diffusers and they were monitored to observe normal growth of the eye.

Measurements were made before surgery, and then periodically after surgery to track changes in eye shape throughout form deprivation and normal growth. Corneal power was measured using IR videokeratometry. The animals were cyclopleged (i.e., dilated) with 2 drops of 1% cyclopentolate, and refractive error was measured using streak retinoscopy. Finally, the animals were anesthetized with 2% isoflurane in oxygen and the axial ocular parameters were measured using high-frequency ultrasound (20 MHz).

Within 2 days of the last ocular measurements, guinea pigs were euthanized and the eyes were prepared for histology. A strip of tissue was dissected from the eye cup, fixed overnight in 4% glutaldehyde, imbedded in resin, cut in 1 μm sections, and then mounted and stained.

5.3 Results

5.3.1 In Vitro *Application and* In Vitro *Expansion*

Treatment with GA was performed as a positive control to demonstrate the ability of crosslinking to prevent creep and the results have previously been discussed in Chapter 2. Motivated by the advantages of using a visible light activated crosslinking system, we chose EY/TEOA for these studies. Digitized images from the expansion studies were analyzed to measure the ocular dimensions labeled in Figure 5.6. Over the 24 hour period, control eyes expand continuously along every dimension (Figure 5.7). This is expected due to the high pressure which induces creep. The treated eyes resist expansion along SP, ED, and SL—dimensions associated with the sclera. Expansion along dimensions associated with the cornea (CP, CD, and CL) increase in the same manner for treated and control eyes. Because the corneal epithelium remained intact during treatment, it provided a protective layer that prevented treatment of the cornea. Removal of this layer in order to treat the cornea will be discussed in Chapter 6. Because we are currently interested in the treatment's ability to strengthen sclera for degenerative myopia, we will focus on results of SP, ED, and SL expansion (all components of the sclera).

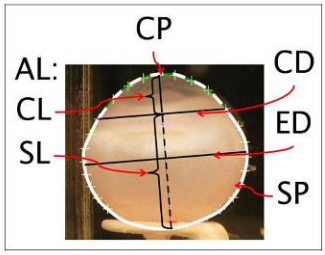

SP: Scleral Perimeter
ED: Equatorial Diameter
SL: Scleral Length
CP: Corneal Perimeter
CD: Corneal Diameter
CL: Corneal Length
AL: Axial Length

Figure 5.6. Measurement of Ocular Dimensions

Treatments tested with a high-intensity, broadband arc lamp source, and with a low-intensity LED light source both show similar results after 24 hours (Figure 5.8). Further reduction in the intensity may be possible using a light source more in tune with the absorption peak of EY (514 nm). The use of low light doses (5 minutes, 6 mW/cm^2) of visible wavelength may avoid the cytotoxic effects on the retina that were seen with larger doses of UV (30 minutes, 3 mW/cm^2) used by Wollensak.

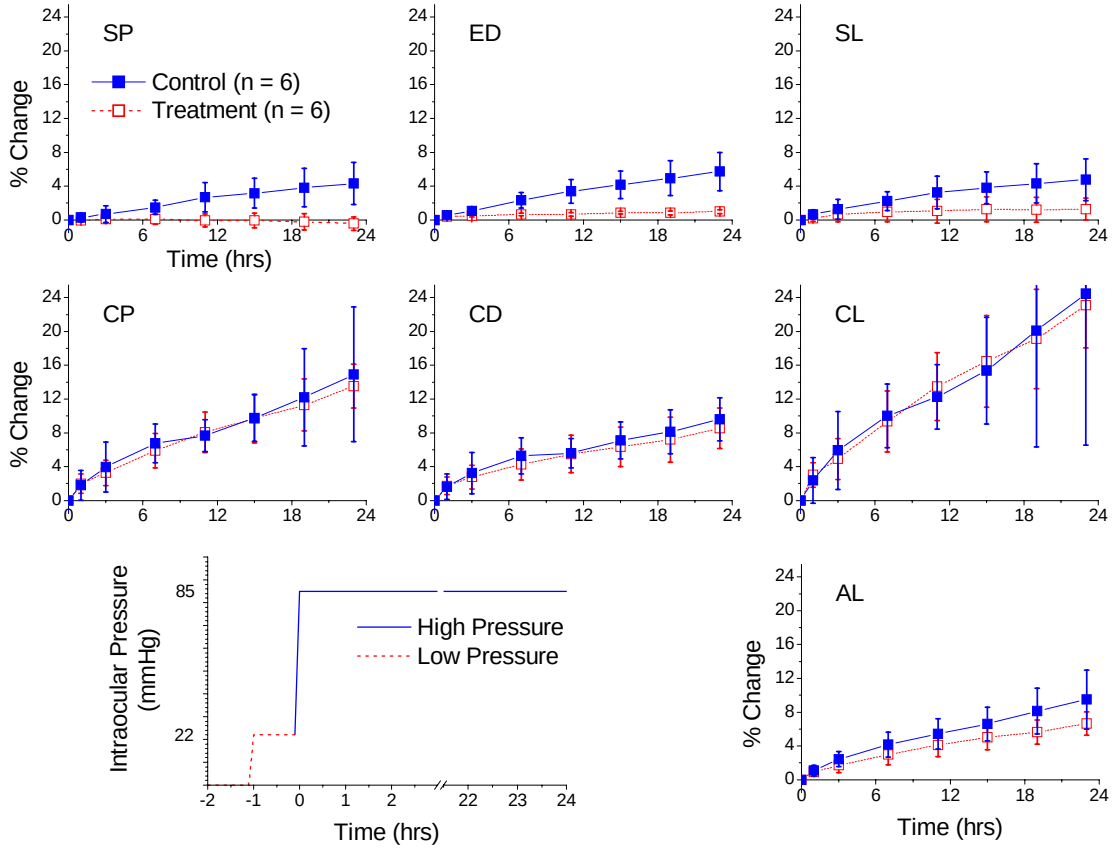

Figure 5.7. Rabbit eyes subjected to a low prestress similar to normal intraocular pressure (22 mmHg) followed by a high (85 mmHg) pressure for 24 hours show the ability of eyes treated with 1x EY to resist creep. The sclera of treated eyes remains stable (top row) while the cornea expands indistinguishably from control cornea (middle row). For values of the overall dimensions, refer to Table 2.2.

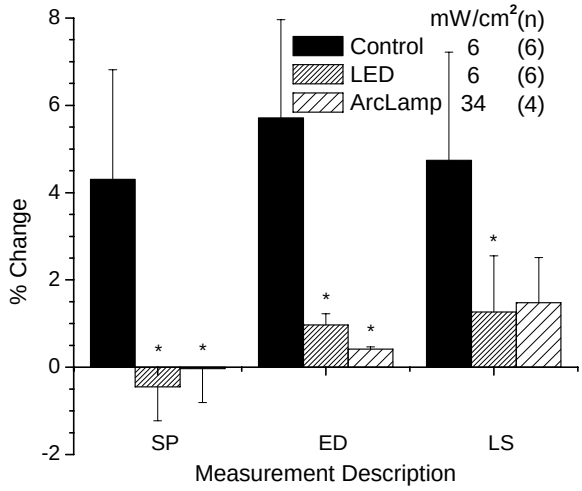

Figure 5.8. *In vitro* treatment: percentage change in scleral dimensions after 24 hour expansion—Eyes treated with 1x EY mixture and irradiation show reduced expansion in the intact globe experiment along SP, ED, and SL (Figure 5) as compared to controls treated with DPBS. Similar efficacy is achieved using narrow-band LEDs (525±16 nm) at a low light dose as with a broadband arc lamp (500±50 nm) at a high light dose. *significant difference from control with $p < 0.05$

5.3.2 Biocompatibility

Biocompatibility studies were performed on albino rabbit eyes because the lack of pigmentation in these eyes allows for easy visualization of toxic or inflammatory responses. In all of the eyes we operated on, there was some observed swelling and inflammation for 2 days following the procedure. This was consistent with what would be expected to result from the surgical procedure itself. There were no clinical signs of pain or inflammation in any of the eyes 3 days after the procedure and on each examination thereafter.

Histological examination revealed that there was mild inflammation and scarring along the conjunctival-sclera junction in the surgical area of all the eyes. The irises, retinas, and ciliary bodies were all normal in all experimental groups. There was no significant difference in the sclera of treated (Figure 5.9a) and control eyes (Figure 5.9c), indicating that the mild inflammation and scarring which occurs is a result of the surgery and not of the treatment. Likewise, the viability of cells in the nearby tissues of the treated eyes matches that of normal eyes.

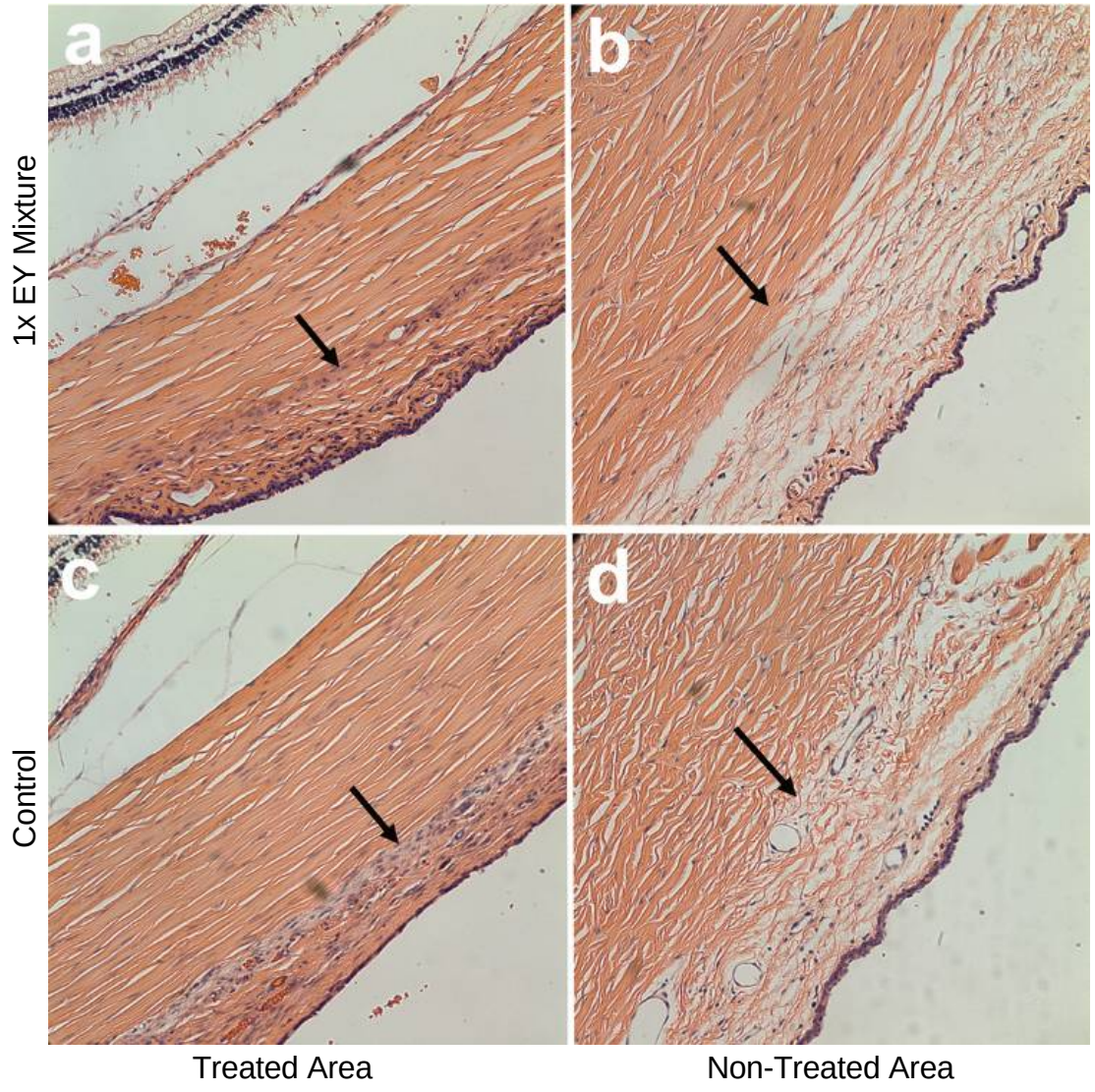

Figure 5.9. Histopathological examination of 1x EY Treatment (Group 1—a, b) and DPBS control vehicle (Group 2—c, d) treated rabbit eyes. The arrows mark the boundary between the sclera and conjunctiva (sclera is to the left of the arrow). All micrographs used 20x magnification. The treated, irradiated area of Group 1 and Group 2 rabbits shows mild inflammation and moderate scarring (darker blue line of staining by the arrow) where the conjunctiva was retracted. For comparison, the untreated, non-irradiated area of a Group 1 and Group 2 rabbits where conjunctiva was *not* retracted shows normal sclera and conjunctiva with no inflammation or scarring. (Greater thickness of the sclera relative to (a) and (c) is characteristic of the location of the section.)

5.3.3 In Vivo *Application and* In Vitro *Expansion*

Average values of changes along ocular dimensions indicate that all injections except the control decrease the expansion of the sclera (Figure 5.10). Values for expansion along SP and ED are significantly smaller compared to controls for the low-intensity treatment, while all values for the high-intensity treatment are significantly smaller than controls. Significance with $p < 0.05$ was determined by comparing values from treatment and control groups using an unpaired t-test. After 24 hours of elevated pressure, *in vivo* treated eyes have an ocular stability comparable to that of the *in vitro* treated eyes (Figure 5.8). This proves that the subconjunctival injection delivers drug to the sclera, and the 5 minute diffusion time is sufficient for 10x EY to penetrate into the live sclera. In addition, the circumferential irradiation with LEDs is able to activate the treatment around the eye.

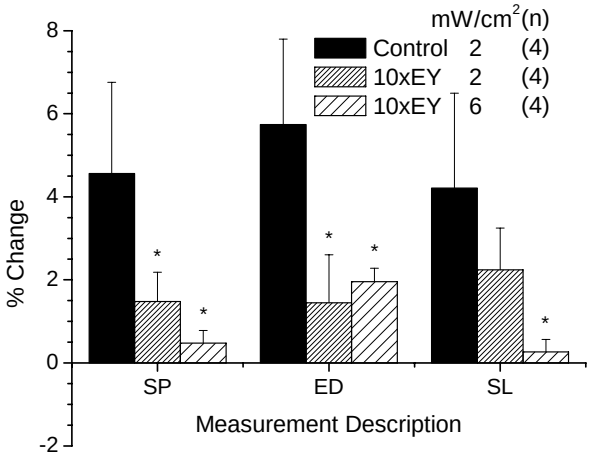

Figure 5.10. *In vivo* treatment after 24 hour expansion—Eyes treated with 10x EY and irradiation show reduced expansion in the intact globe experiment as compared to controls treated with DPBS and irradiation. Treatment with 6 mW/cm^2 may have greater stabilizing effects than with 2 mW/cm^2. Control and treated groups show similar behavior as *in vitro* treated eyes (Figure 5.8).

5.3.4 Animal Model of Myopia

Using a guinea pig model, data was obtained regarding drug delivery, toxicity, and tolerance of surgical procedures. After surgery, there was minimal inflammation of the conjunctiva that disappeared within 2–3 days. The eyes had a normal pupil response and clear ocular media which allowed for streak retinoscopy measurements. Gross ocular function (pupillary reflexes, response to light, blink reflex) appeared normal. Behaviorally, the animals moved about the habitat normally and had normal eating and drinking habits.

Observations of the sham surgery controls indicated that the surgical procedure was well-tolerated by the eyes. The eyes receiving the 3x EY and 10x EY formulations demonstrated no evidence of toxicity problems. Tissue sections from treated and fellow

eyes showed that the sclera was structurally normal (Figure 5.11). The sclera, choroid and retinal pigment epithelium (RPE) had no signs of toxicity from the treatment. There were normal RPE cells and depigmented RPE cells in the treated and untreated eye sections. The sclera of treated and untreated eyes is indistinguishable. Although the retina was removed before fixing the tissue, the overall retinal thickness was within the normal limits and no signs of retinal toxicity were observed. These important findings support our hypothesis that the treatment is safe based on EY/TEOA literature,[1-11] light- and drug-penetration calculations, and rabbit histology.

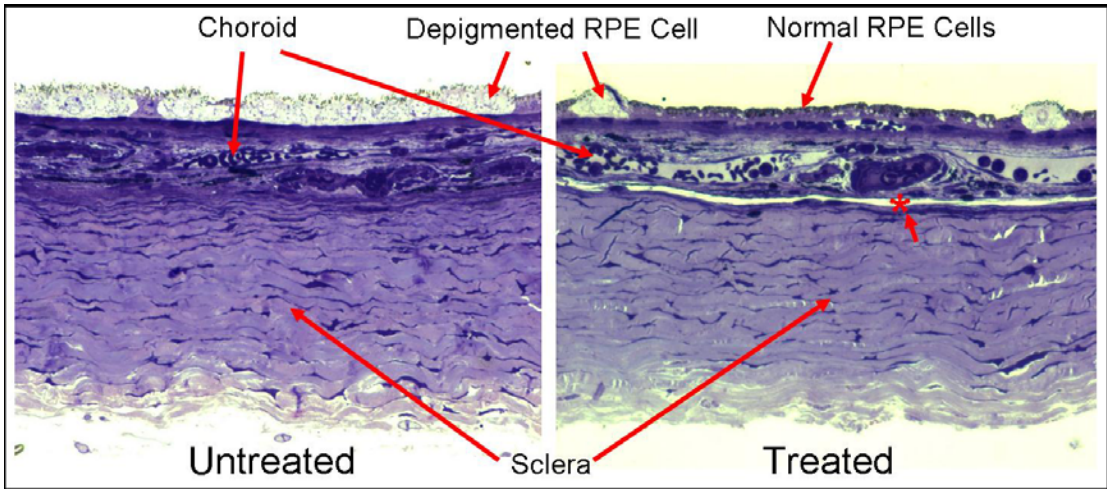

Figure 5.11. Histological sections from 10x EY treated guinea pig eyes and untreated fellow eyes show the sclera but the retina was detached before fixing. There are depigmented RPE cells in both the treated and untreated eyes. There are normal RPE cells present in the treated eye. (*) The choroid is detached from the sclera in the treated eye due to artifacts of the sample preparation. The sclera appears the same in the treated and untreated eye.

Of the three eyes enucleated immediately after treatment (Set A), all showed pink staining from Eosin Y over the entire sclera, including at the posterior pole, indicating that the formulation can be delivered to the entire sclera following subconjunctival injection.

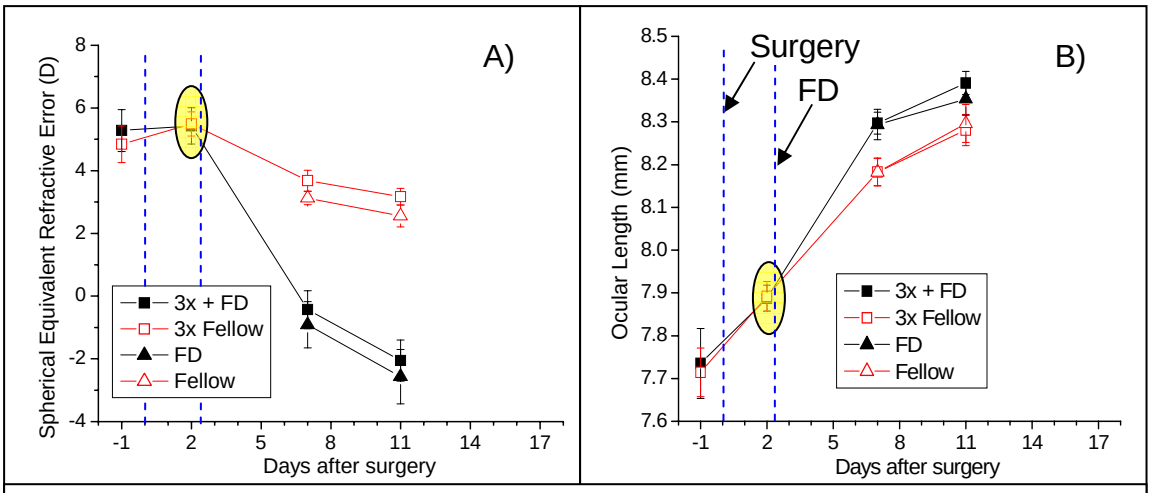

Figure 5.12. *In vivo* measurements of ocular parameters for form-deprived and normal fellow eyes: A) Measurements of refractive error were done by streak retinoscopy and spherical equivalent refractive error is presented as the mean of the measure from the horizontal and vertical meridians. Two days after surgery there is no difference between the 3x EY treated or fellow eyes. The 3x EY form-deprived (3x + FD) eyes exhibit similar responses as untreated form-deprived (FD) eyes in days 7 and 11. The fellow eyes also show similar refractive states. B) Ultrasound measurements of ocular length indicate no difference in the 3x EY treated and fellow eyes 2 days after surgery. The ocular length at days 7 and 11 is similar in both the 3x EY treated animals and the untreated animals for both the FD and fellow eyes. All the animals were approximately the same ages (~6 days old) at the beginning of form deprivation.

Results of normal form-deprivation with untreated eyes (Set B) are presented along with results for form-deprivation of 3x EY treated eyes (Set C). Measurements of refractive state before surgery indicate that the guinea pigs are hyperopic, which is expected for their age (Figure 5.12). Immediately before beginning form-deprivation (2 days after surgery), the treated (3x + FD) and fellow control eyes (3x Fellow) are the same, indicating that surgery had no effect on refractive error. For normal form-deprivation, the differences of refractive error between the form deprived (FD) and fellow eye (Fellow) are -4.04 ± 0.667 D on the first measure (day 7), and -5.12 ± 0.659 D on the second measure (day 11). Nearly identical changes are seen in the treated animals with differences of -4.11 ± 0.675 D and -5.23 ± 0.612 D on the matching days. Measurement of ocular length (from the front

of the cornea to the back of the sclera) by ultrasound also reveals similar behavior in the treated and untreated animals (Figure 5.12b). On day 7, the myopic eye was 111 ± 20.4 μm greater in length than the fellow eye. By day 11, this length difference reduced some in the untreated animals, but remained the same in the 3x EY treated animals. The similarities between the 3x EY treated (Set C) and the normal animals (Set B) indicates that this treatment does not have an effect on the eye. We hypothesize that insufficient EY diffused into the tissue, motivating experiments with 10x EY (below).

Although this treatment was not able to prevent myopia, the results were encouraging due to the lack of cytotoxic effects using 3x EY and irradiation, and the resilience of animals to the surgery. Before examining higher doses in form-deprived animals, we began tests of higher doses in normal eyes to observe if they could tolerate the dose (Sets D & E). At this time, analysis from Sets E and F is incomplete and only results from the other sets are presented.

Eyes from Set D received the same irradiation protocol as those from Set C, but were given higher doses of drug (10x EY instead of 3x EY). Measures of refractive error indicate that 2 days after surgery there is a difference between the treated eye and untreated fellow eye of -3.11 ± 0.714 D (Figure 5.13a). The treatment causes the eye to become more myopic. Over the course of the experiment, the treated eye becomes more hyperopic. The fellow eye emmetropizes normally during this period. The 10x EY treatment also causes an increased ocular length, and the difference between treated and untreated fellow eyes reduces over time (Figure 5.13b). These initial differences were not seen in the 3x EY

treated eyes and they indicate that significant changes have occurred due to treatment with 10x EY.

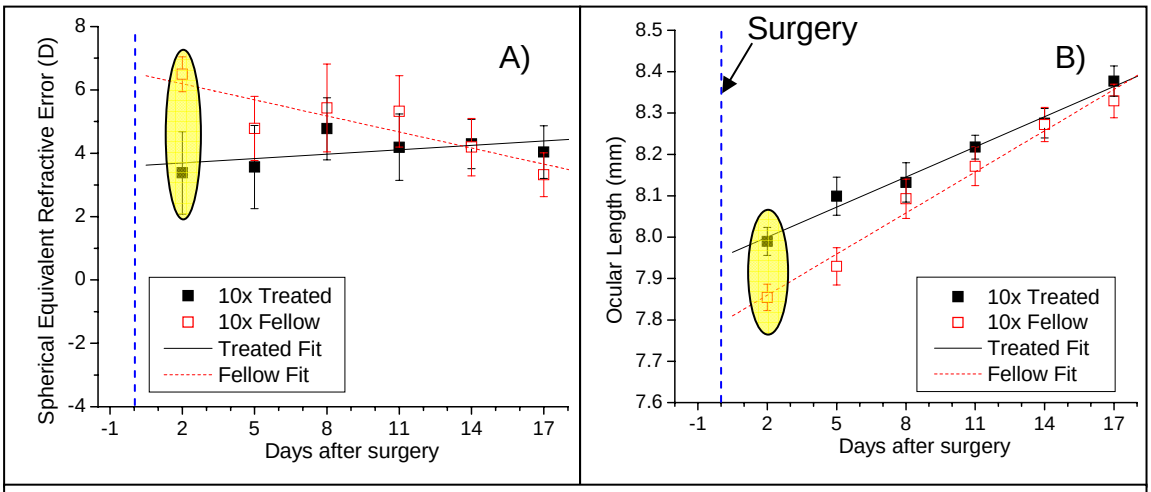

Figure 5.13. Guinea pigs eyes undergoing normal growth were treated at day 0 with 10x EY and irradiation in the right eye and the fellow eye remained untreated. Dotted lines are shown to guide the eye. A) Two days after the surgery, the refractive state of the treated eyes is significantly different from that of the untreated eye. During normal growth, the fellow eye progresses toward emmetropia whereas the 10x EY treated eye maintains a stable refractive state, and becomes slightly more hyperopic over 17 days. B) Measurements of ocular length are different at two days after surgery, with the treated eye being longer than the fellow eye. Over 17 days, the rate of ocular length change is larger in the fellow eye than in the 10x EY treated eye. Linear fits are used to illustrate the growth trends.

The change in ocular length is examined in greater detail using ultrasound biometry to evaluate all the ocular dimensions that contribute to ocular length (Figure 5.14). The cornea and anterior chamber thickness (CAC) grows normally for both eyes (Figure 5.14a). The lens grows normally despite an initial difference at day 2 (Figure 5.14b). The variability in day-to-day lens thickness suggests that the uncertainty in the measurement is greater than the error bars indicate. The vitreous chamber elongates more slowly in the treated eye than in the untreated eye (Figure 5.14c). There is no difference in retinal thickness (Figure 5.14d). The choroid and sclera are both thicker in the treated eye (Figure

5.14d). The sum of these individual components gives the ocular length reported in Figure 5.13b:

$$CAC + Lens + Vit + Ret + Scl + Chr = OL.$$

$$1.06\ mm + 3.53\ mm + 3.02\ mm + 0.16\ mm + 0.11\ mm + 0.11\ mm = 7.99\ mm.$$

The slight differences in corneal power dissipate over the growth period (Figure 5.14e).

The differences in the sclera, choroid, and vitreous chamber of the treated and fellow eyes persist over 15 days of observation. Choroid thickness is known to increase with inhibitory growth signals, and the drug treatment may have triggered an inhibitory response. The initial change in vitreous chamber depth may be explained by crosslinking of the sclera in an extended state. The intraocular pressure increases during prolapsing, which could induce stretching of the sclera. After prolapsing, the pressure decreases, and the sclera relaxes back to normal. However, in a treated eye, the stretched state of the sclera might be crosslinked in place, causing noticeable shape differences. Further tests such as MRI may be capable of examining the shape of the eye before and after prolapsing, with and without treatment.

The data also suggests that the cornea grows in a normal manner in a treated eye despite the abnormal changes in vitreous chamber depth. This is also seen with the normal growth of the lens. The growth of the cornea and lens may not be coupled to axial length. Using this method of crosslinking tissue, whether it is cornea or sclera, might enable researchers to

determine if there is a coupled feedback for growth of the ocular components in these animals.

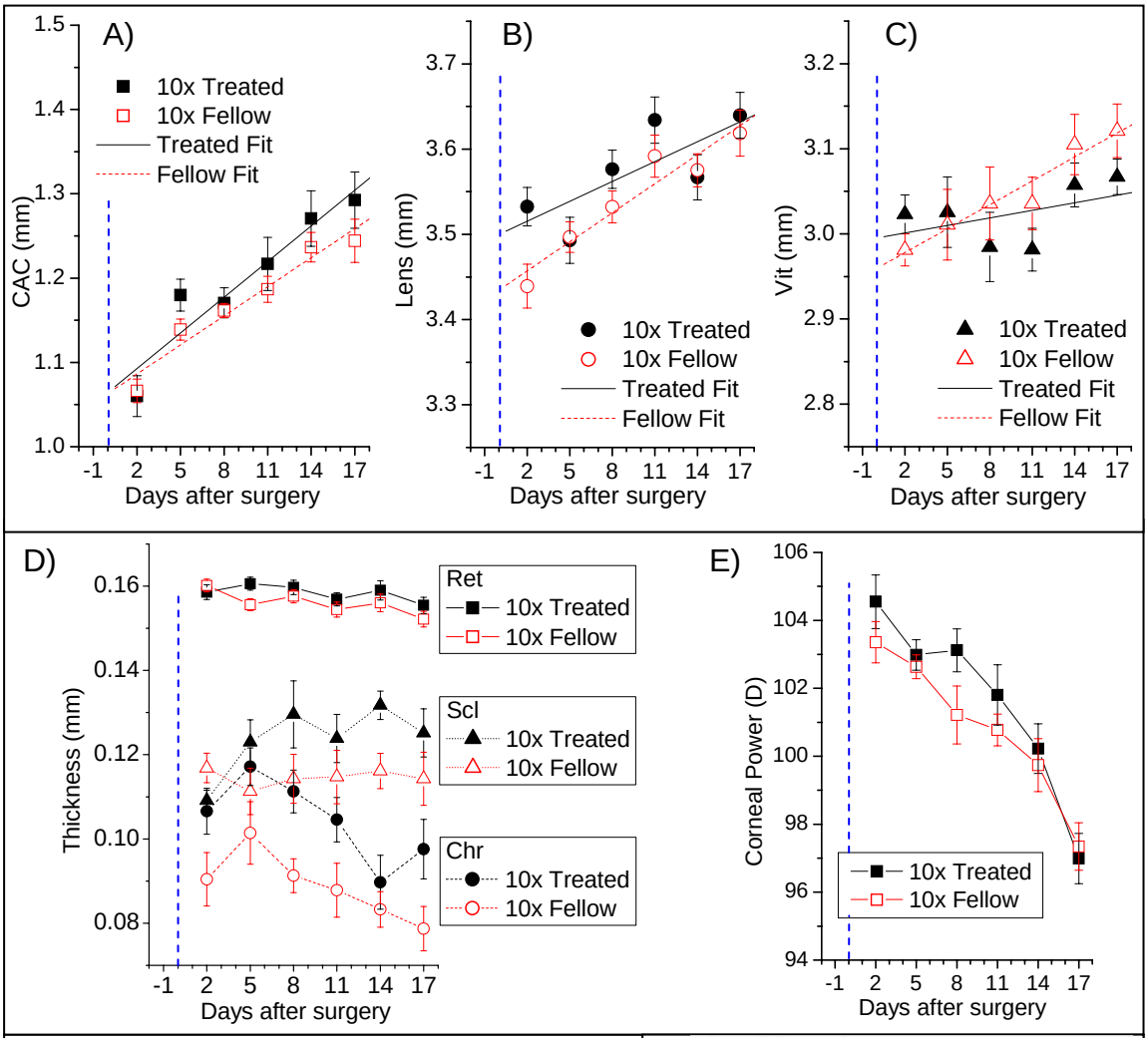

Figure 5.14. The ultrasound measurements are analyzed to measure corneal thickness and anterior chamber depth (CAC), lens thickness (Lens), vitreous chamber depth (Vit), retina thickness (Ret), choroid thickness (Chr), and sclera thickness (Scl) as F) illustrates. There are no differences between the 10x EY treated and untreated fellow eyes for A) CAC, B) Lens, D) posterior layers, and E) corneal power. C) The vitreous chamber elongates faster in the untreated fellow eye than in the treated eye and D) the sclera and choroid are thicker in treated eyes.

5.4 Summary

Were it possible to retard or prevent abnormal axial elongation of the globe in degenerative myopia, visual loss might be prevented. Use of the expansion model in this study has allowed us to measure the progressive enlargement of the eye due to creep in the sclera. The ability of 1x EY and 10x EY to halt expansion *in vitro* in rabbit eyes indicates that the change in tissue properties upon treatment might prevent creep *in vivo*. Results from the biocompatibility studies in rabbits and guinea pigs show only minor inflammation from the surgery, and no adverse responses due to treatment concentrations up to 10x EY. Results from *in vivo* guinea pig studies demonstrate that the treatment with 3x EY did not alter ocular shape or prevent form-deprivation myopia. However, the higher dose of 10x EY did substantially alter ocular parameters during normal growth, possibly due to elevated intraocular pressure during prolapsing at the time of irradiation. The experiments establish protocols that may be extended to form-deprivation studies of 10x EY, perhaps with modification of the irradiation step to ensure that the globe is at normal intraocular pressure. Future treatments of the entire eye, or specifically the posterior pole, are also recommended to test their ability to prevent form-deprivation myopia in the guinea pigs.

BIBLIOGRAPHY

1. McBrien, N.A., Gentle, A. Role of the sclera in the development and pathological complications of myopia. *Progress In Retinal And Eye Research* **22**, 307-338 (2003).
2. Rada, J.A.S., Shelton, S., Norton, T.T. The sclera and myopia. *Experimental Eye Research* **82**, 185-200 (2006).
3. Blinder, K.J., Blumenkranz, M.S., Bressler, N.M., Bressler, S.B., Donati, G., Lewis, H., Lim, J.I., Menchini, U., Miller, J.W., Mones, J.M., Potter, M.J., Pournaras, C., Reaves, A., Rosenfeld, P., Schachat, A.P., Schmidt-Erfurth, U., Sickenberg, M., Singerman, L.J., Slakter, J., Strong, H.A., Virgili, G., Williams, G.A. Verteporfin therapy of subfoveal choroidal neovascularization in pathologic myopia - 2-year results of a randomized clinical Trial - VIP report no. 3. *Ophthalmology* **110**, 667-673 (2003).
4. Chan, W.M., Ohji, M., Lai, T.Y.Y., Liu, D.T.L., Tano, Y., Lam, D.S.C. Choroidal neovascularisation in pathological myopia: an update in management. *British Journal of Ophthalmology* **89**, 1522-1528 (2005).
5. Buys, Y.M. Bevacizumab: the need for controlled studies to move forward. *Canadian Journal of Ophthalmology-Journal Canadien D Ophtalmologie* **42**, 789-789 (2007).
6. Rosenfeld, P.J. Intravitreal Avastin for choroidal neovascularisation in pathological myopia: the controversy continues. *British Journal of Ophthalmology* **91**, 128-130 (2007).

7. Yamamoto, I., Rogers, A.H., Reichel, E., Yates, P.A., Duker, J.S. Intravitreal bevacizumab (Avastin) as treatment for subfoveal choroidal neovascularisation secondary to pathological myopia. *British Journal of Ophthalmology* **91**, 157-160 (2007).

8. Sakaguchi, H., Ikuno, Y., Gomi, F., Kamei, M., Sawa, M., Tsujikawa, M., Oshima, Y., Kusaka, S., Tano, Y. Intravitreal injection of bevacizumab for choroidal neovascularisation associated with pathological myopia. *British Journal of Ophthalmology* **91**, 161-165 (2007).

9. Avetisov, E.S., Tarutta, E.P., Iomdina, E.N., Vinetskaya, M.I., Andreyeva, L.D. Nonsurgical and surgical methods of sclera reinforcement in progressive myopia. *Acta Ophthalmologica Scandinavica* **75**, 618-623 (1997).

10. Chua, W.H., Tan, D., Balakrishnan, V., Chan, Y.H. Progression of childhood myopia following cessation of atropine treatment. *Investigative Ophthalmology & Visual Science* **46** (2005).

11. Tarutta, Y.P., Iomdina, Y.N., Shamkhalova, E.S., Andreyeva, L.D., Maximova, M.V. Sclera Fortification In Children At A High-Risk Of Progressive Myopia. *Vestnik Oftalmologii* **108**, 14-17 (1992).

12. Politzer, M. Experiences In Medical-Treatment Of Progressive Myopia. *Klinische Monatsblatter Fur Augenheilkunde* **171**, 616-619 (1977).

13. Belyaev, V.S., Ilyina, T.S. Late Results Of Scleroplasty In Surgical Treatment Of Progressive Myopia. *Eye Ear Nose And Throat Monthly* **54**, 109-113 (1975).

14. Chauvaud, D., Assouline, M., Perrenoud, F. Scleral reinforcement. *Journal Francais D Ophtalmologie* **20**, 374-382 (1997).

15. Jacob, J.T., Lin, J.J., Mikal, S.P. Synthetic scleral reinforcement materials .3. Changes in surface and bulk physical properties. *Journal Of Biomedical Materials Research* **37**, 525-533 (1997).

16. Korobelnik, J.F., D'Hermies, F., Chauvaud, D., Legeais, J.M., Hoang-Xuan, T., Renard, G. Expanded polytetrafluoroethylene episcleral implants used as encircling scleral buckling - An experimental and histopathological study. *Ophthalmic Research* **32**, 110-117 (2000).

17. Mortemousque, B., Leger, F., Velou, S., Graffan, R., Colin, J., Korobelnik, J.F. S/e-PTFE episcleral buckling implants: An experimental and histopathologic study. *Journal Of Biomedical Materials Research* **63**, 686-691 (2002).

18. Jacoblabarre, J.T., Assouline, M., Conway, M.D., Thompson, H.W., McDonald, M.B. Effects Of Scleral Reinforcement On The Elongation Of Growing Cat Eyes. *Archives Of Ophthalmology* **111**, 979-986 (1993).

19. Bailey, A.J. Molecular mechanisms of ageing in connective tissues. *Mechanisms of Ageing and Development* **122**, 735-755 (2001).

20. Singh, R., Barden, A., Mori, T., Beilin, L. Advanced glycation end-products: a review. *Diabetologia* **44**, 129-146 (2001).

21. Spoerl, E., Wollensak, G., Seiler, T. Increased resistance of crosslinked cornea against enzymatic digestion. *Current Eye Research* **29**, 35-40 (2004).

22. Wollensak, G., Spoerl, E. Collagen crosslinking of human and porcine sclera. *Journal Of Cataract And Refractive Surgery* **30**, 689-695 (2004).

23. Wollensak, G., Iomdina, E., Dittert, D.D., Salamatina, O., Stoltenburg, G. Cross-linking of scleral collagen in the rabbit using riboflavin and UVA. *Acta Ophthalmologica Scandinavica* **83**, 477-482 (2005).

24. Norton, T.T. Animal Models of Myopia: Learning How Vision Controls the Size of the Eye. *ILAR* **40**, 59-77 (1999).

25. Gao, Q.Y., Liu, Q., Ma, P., Zhong, X.W., Wu, J.S., Ge, J. Effects of direct intravitreal dopamine injections on the development of lid-suture induced myopia in rabbits. *Graefes Archive For Clinical And Experimental Ophthalmology* **244**, 1329-1335 (2006).

26. Howlett, M.H.C., McFadden, S.A. Emmetropization and schematic eye models in developing pigmented guinea pigs. *Vision Research* **47**, 1178-1190 (2007).

27. Zhou, X.T., Qu, J., Xie, R.Z., Wang, R.Q., Jiang, L.Q., Zhao, H.L., Wen, J.Q., Lu, F. Normal development of refractive state and ocular dimensions in guinea pigs. *Vision Research* **46**, 2815-2823 (2006).

28. Lu, F., Zhou, X.T., Zhao, H.L., Wang, R.Q., Jia, D., Jiang, L.Q., Xie, R.Z., Qu, J. Axial myopia induced by a monocularly-deprived facemask in guinea pigs: A non-invasive and effective model. *Experimental Eye Research* **82**, 628-636 (2006).

29. Howlett, M.H.C., McFadden, S.A. Form-deprivation myopia in the guinea pig (Cavia porcellus). *Vision Research* **46**, 267-283 (2006).

30. McFadden, S.A., Howlett, M.H.C., Mertz, J.R. Retinoic acid signals the direction of ocular elongation in the guinea pig eye. *Vision Research* **44**, 643-653 (2004).

31. McFadden, S.A. Partial occlusion produces local form deprivation myopia in the guinea pig eye. *Investigative Ophthalmology & Visual Science* **43**, U34 (2002).

32. Lodge, A., Peto, T., McFadden, S.A. Form deprivation myopia and emmetropization in the guinea pig. *Proceedings of the Australian Neuroscience Society* **5**, 123 (1994).

33. Georgopoulos, M., Vass, C., El Menyawi, I., Radda, S., Graninger, W., Menapace, R. In vitro diffusion of mitomycin-C into human sclera after episcleral application: Impact of diffusion time. *Experimental Eye Research* **71**, 453-457 (2000).

34. Vass, C., Georgopoulos, M., El Menyawi, I., Radda, S., Nimmerrichter, P. Intrascleral concentration vs depth profile of mitomycin-C after episcleral application: Impact of applied concentration and volume of mitomycin-C solution. *Experimental Eye Research* **70**, 571-575 (2000).

35. Vass, C., Georgopoulos, M., El Menyawi, I., Radda, S., Nimmerrichter, P., Menapace, R. Intrascleral concentration vs depth profile of mitomycin-C after episcleral application: Impact of irrigation. *Experimental Eye Research* **70**, 139-143 (2000).

36. Vass, C., Georgopoulos, M., El Menyawi, I., Radda, S., Nimmerrichter, P. Impact of Mitomycin-C application time on the scleral Mitomycin-C concentration. *Journal of Ocular Pharmacology and Therapeutics* **17**, 101-105 (2001).

37. Cruise, G.M., Hegre, O.D., Scharp, D.S., Hubbell, J.A. A sensitivity study of the key parameters in the interfacial photopolymerization of poly(ethylene glycol) diacrylate upon porcine islets. *Biotechnology and Bioengineering* **57**, 655-665 (1998).

Chapter 6

TREATMENT OF KERATOCONUS

6.1 Introduction VI-1
6.2 Materials and Methods VI-3
6.2.1 Penetration of Molecules—Epithelial Barrier *VI-3*
6.2.2 In Vitro *Application and* In Vitro *Expansion* *VI-6*
6.3 Results VI-9
6.3.1 Penetration of Molecules—Epithelial Barrier *VI-9*
6.3.2 In Vitro *Application and* In Vitro *Expansion* *VI-10*
6.4 Summary VI-14
Bibliography VI-16

This work has been done with Joyce Huynh, Heejae Kim, and Muzhou Wang. Graduate student Joyce Huynh assisted with *in vitro* expansion experiments, and undergraduates Heejae and Muzhou assisted with penetration studies.

6.1 Introduction

Keratoconus is a disorder that results in corneal thinning and is named for the conical shape that the cornea develops.[1-3] The progressive distortion of corneal shape usually becomes noticeable in early adulthood, causing increasingly severe astigmatism, myopia, and higher-order aberrations that become difficult to correct by spectacles or contact lenses. A number of different therapies have been tested in keratoconus as alternatives to contact lenses. These include, thermokeratoplasty[4], epikeratophakia[5], and intracorneal ring segments (Intacs).[6, 7] These treatments do not appear to stop progression of the disease; rather, they are alternatives to manage the refractive abnormalities induced by irregular

corneal thinning and ectasia, or expansion. When distortions reach the point that refractive correction is no longer possible, corneal transplant is the only option.

Recently, the pioneering work of Wollensak, Seiler, Spoerl, and co-workers demonstrated a potential treatment to arrest progression of keratoconus using photoactivated crosslinking.[8-21] Deriving from presumed weakened mechanical integrity of the cornea in keratoconus,[22] this novel crosslinking therapy is directed at increasing the cornea's strength. The procedure uses ultraviolet light (370 nm) to activate radical generation of riboflavin in the cornea. The treatment consists of removing the corneal epithelium over a 7 mm diameter and then applying 0.1% riboflavin solution 5 minutes before, and then every 5 minutes thereafter, during a 30 minute UV-A irradiation. Other than post-operative pain from corneal epithelial removal, the procedure is well tolerated. In a series of 22 patients with progressive keratoconus, progression was stopped by treatment with UV-A and riboflavin.[16] Mean follow up was nearly 2 years. In 16 patients there was actual regression of the keratoconus with dioptric corneal flattening of 2 diopters. After the epithelium regenerated, no adverse effects, e.g., on corneal transparency, were observed.

Despite these encouraging results, there are several potential drawbacks to the current method. First, removal of the epithelium is not desirable because the tight junctions of epithelial cells provide the first protective barrier for the cornea and prevent many molecules from penetrating this cell layer. To avoid difficulties of delivering drug through the lipophilic epithelium and into the hydrophilic stroma, the epithelium is typically removed. Although it re-grows, the epithelium is home to nearly 325,000 nerve endings[23] and its removal risks impaired sensation, leading to complications due to reduced blinking

reflex (failure to maintain proper corneal hydration and to sense foreign particles on the eye). For this reason, the present study examines the ability of our chosen light-activated drug, Eosin Y, to penetrate into the cornea with and without the epithelium present. Second, UV light is potentially toxic, and when combined with riboflavin activation, has produced toxic effects on keratocytes, the cells responsible for ongoing repair and remodeling of the corneal stroma. We study the ability to induce corneal crosslinking with a visible-light-activated system. Finally, the UV treatment lasts 35 minutes, a relatively long time compared to refractive procedures that last only about two minutes. Our demonstration of crosslinking uses a shorter treatment time totaling 10 minutes (only 5 minutes of irradiation). We compare treatment efficacy of the brief, visible-light protocol to the > 30 minute, UV-activated method using our intact globe expansion test.

6.2 Materials and Methods

6.2.1 Penetration of Molecules—Epithelial Barrier

We have modified a slit lamp with filters and a digital camera to observe the depth profile of the fluorescence of drug molecules in enucleated porcine corneas (Figure 6.1). A sheet of light, sent through a bandpass filter chosen to select light that efficiently excites Eosin Y (Filter 1 passes 500±20 nm), is incident on the cornea and both emitted and scattered light are viewed from an angle. Scattered light, imaged without a filter between the specimen and the camera, is used to record the shape and position of the cornea. The fluorescence of Eosin Y (EY), imaged through Filter 2 (which passes 560±25 nm) as shown in Figure 6.1a,

facilitates visualization of its penetration profile in the stroma (Figure 6.2b). Untreated corneas show no fluorescence (field appears dark with Filter 2 in place). In this manner, we are able to examine the amount of drug that crosses the epithelium and its distribution in the stroma.

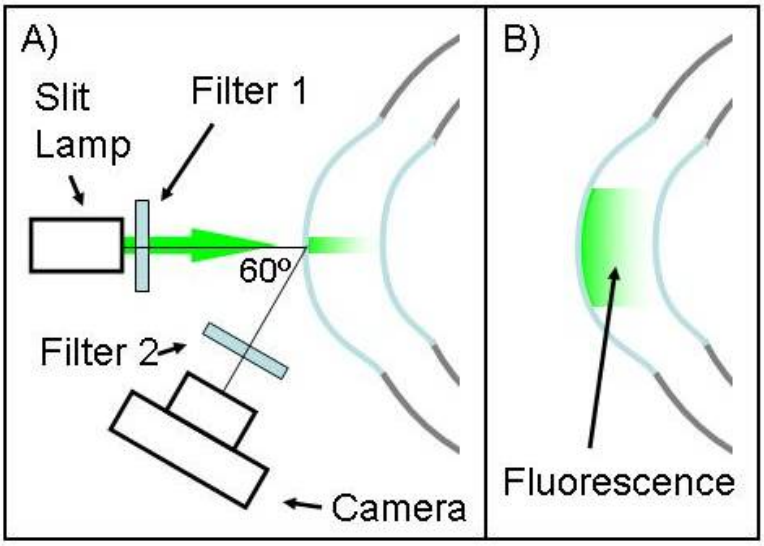

Figure 6.1. A) Apparatus for imaging the cornea uses a slit lamp to provide a sheet of light and uses a band pass filter (500±20 nm) to reject light outside the absorption band of Eosin Y (EY). Filter 2 (560±25 nm) is only used to image the fluorescence of EY; it is removed when images of scattered light are acquired. B) Photographs reveal a cross section of the cornea with the fluorescence profile inside the stroma.

Enucleated eyes from 3–4 month old swine were obtained from Sierra for Medical Science. Fresh eyes were shipped in saline, on ice. On arrival, the eyes were immediately (< 42 hours post-mortem) cleaned by removing the tissue still attached to the eye. Then the cornea was photographed in scattering mode, providing initial dimensions of the cornea,

and fluorescence mode, providing baseline measures of background fluorescence. The epithelium was either removed with a scalpel or left intact before the eye was placed in 2 ml of treatment solution (Table 1). Eyes were left in solution for 1 hour and then removed, rinsed with approximately 4 ml of Dulbecco's PBS and photographed in both scattering and fluorescence mode on the slit lamp. After this treatment, eyes with intact epithelium were found to have very strong absorption and fluorescence associated with their epithelium. To image fluorescence in their stroma, the epithelium was removed by scraping with a scalpel and they were photographed again. Removal of the epithelium at this step allows excitation light to reach the stroma.

Treatment Solutions	**EosinY (mM)**	**Triethanolamine (mM)**
1x EY	0.0289	90
35x EY	1	90
350x EY	10	225

Table 6.1. Treatment Solutions in Dulbecco's Phosphate-Buffered Saline.

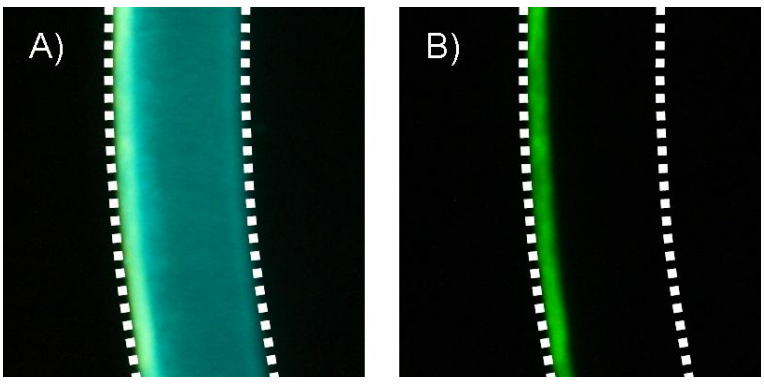

Figure 6.2. Slit lamp images of A) scattered light, revealing the full thickness of the treated cornea (without Filter 2), and B) filtered light, isolating the fluorescence emission of Eosin Y (with Filter 2, as shown in Figure 1A)

6.2.2 In Vitro *Application and* In Vitro *Expansion*

We use the intact globe method, established in Chapters 2 and 5, to quantitatively compare treated and control eyes with respect to their resistance to corneal expansion.

Tissue Preparation: Eyes from 2–3 week old New Zealand White Rabbits (provided by collaborator Dr. Keith Duncan at the University of California at San Francisco) were stored in saline on ice for use within 48 hours of enucleation. The epithelium was removed by scraping a scalpel blade across the cornea. Removal was confirmed by visual inspection of the corneal surface. The extraorbital tissues were removed to expose the sclera and ensure accurate analysis of the eye shape. The eyes were then put into DPBS until treatment (at least 30 minutes and not more than 120 minutes).

Materials:

We tested three treatment solutions:

"1x EY": 0.0289 mM EY with 90 mM TEOA in DPBS,

"10x EY": 0.289 mM EY with 90 mM TEOA and 2% w/w hyaluronic acid (HA) in DPBS, and

"R/UVA": 2.09 mM (0.1% w/w) riboflavin-5′-phosphate sodium salt hydrate and 20% w/w T-500 Dextran in DPBS.

Respective controls for each group used the treatment vehicle without EY or TEOA (i.e., DPBS, 2% HA in DPBS, and 20% T-500 Dextran in DPBS, respectively).

The addition of 2% HA and dextran are to increase viscosity so that the treatment could be applied topically and to maintain hydration of the cornea while doing so (Table 6.2).

	Treatment Formulation	Vehicle	Delivery Method
1x EY Treated	0.0289 mM EY and 90 mM TEOA	DPBS	Soaking
1x EY Control	None		
10x EY Treated	0.289 mM EY and 90 mM TEOA	2% HA in DPBS	Gel
10x EY Control	None		
R/UVA Treated	2.09 mM riboflavin-5′-phosphate	20% Dextran in DPBS	Viscous Drops
R/UVA Control	None		

Table 6.2. Treatments and Respective Controls Used for Corneal Expansion Studies

Procedure: The intact globes for 1x EY treated and control (fellow eye from the same animal) were placed cornea down in a holder such that 750 μL of their respective solutions just covered the cornea. The eyes were soaked in this manner for 5 minutes in the dark. The eyes were removed from solution and dabbed with a Kimwipe to remove excess solution from the corneal surface. Then the treated and fellow control eyes were placed cornea up in two identical holders, each equipped with a circle of green light-emitting diodes (seven 5-mm LEDs at 525 ± 16 nm, 6–8 mW/cm^2 in the plane of the cornea). An aluminum foil mask was place over each specimen to cover the sclera, while leaving the cornea exposed. Then the irradiation was applied for 5 minutes.

The 10x EY treated and control corneas had the gel treatment solution spread over the cornea. After allowing 5 minutes of diffusion time, the solution was removed with a spatula and the corneal surface was rinsed with DPBS. Each of the eyes was placed under a green light source consisting of seven 5-mm LEDs at 525 ± 16 nm and 6–8 mW/cm^2.

Using the same protocol described above, the corneas of the treated and fellow control eyes were irradiated simultaneously for 5 minutes while the remainder of the eye was protected from light exposure using an aluminum foil mask.

The R/UVA treated and control eyes received drops of solution on the cornea for 5 minutes prior to irradiation, and then received fresh drops every 5 minutes during the 30 minute irradiation with 3 mW/cm^2 of 370±5 nm ultraviolet light for 30 minutes. Both eyes were irradiated at the same time.

After irradiation, all the eyes were placed in DPBS for 30 minutes. Treated and fellow control eyes were mounted into an intact globe expansion apparatus with two sites to ensure that both experienced the same ambient pressure and temperature, and the same imposed intraocular pressure, as described in Chapter 2. To restore the native shape of the globes, they received a "prestress" of 22 mmHg for one hour, based on observations that showed that shape recovery required up to 45 minutes for some specimens. Images were recorded at 15 minute intervals during the prestress period. Then the imposed intraocular pressure was increased to 85 mmHg, a first image was required within a few seconds of the inception of elevated pressure and subsequent images were acquired at 15 minute intervals for 24 hours.

6.3 Results

6.3.1 Penetration of Molecules—Epithelial Barrier

Fluorescence emission from the stroma of eyes treated with the epithelium present is much weaker than that observed in specimens that had the epithelium removed prior to treatment (Figure 6.3): 1x EY penetrates the stroma of eyes with removed epithelium within an hour, but in eyes with the epithelium intact, 1x EY cannot be detected after 6 hours of soaking. This observation accords with prior literature indicating that the epithelium inhibits penetration of compounds closely related to EY (e.g., fluorescein). Nevertheless, significant penetration of EY across the epithelium is evident in corneas treated with high concentration solutions (35x EY and 350x EY). These results indicate that EY penetration through the epithelium is possible. Clinically, it is significant that removal of the epithelium may not be necessary for treatment.

Note that this method has very low sensitivity relative to, for example, laser scanning confocal fluorescence microscopy. Due to low sensitivity, soaking for at least 1 hour was needed to achieve detectable levels of fluorescence for 1x EY even without the epithelium present (Figure 6.3, left, second row). The next section of this chapter discusses treatments with 1x EY that successfully stabilize deepithelialized corneas using a 5 minute soaking time. While slit lamp photography may be used to make qualitative judgments of epithelial penetration, it cannot be used to quantify changes with the sensitivity required for our treatments. Future studies with the more sensitive approach of confocal microscopy could be used to reveal the diffusion rates through the epithelium and within the stroma.

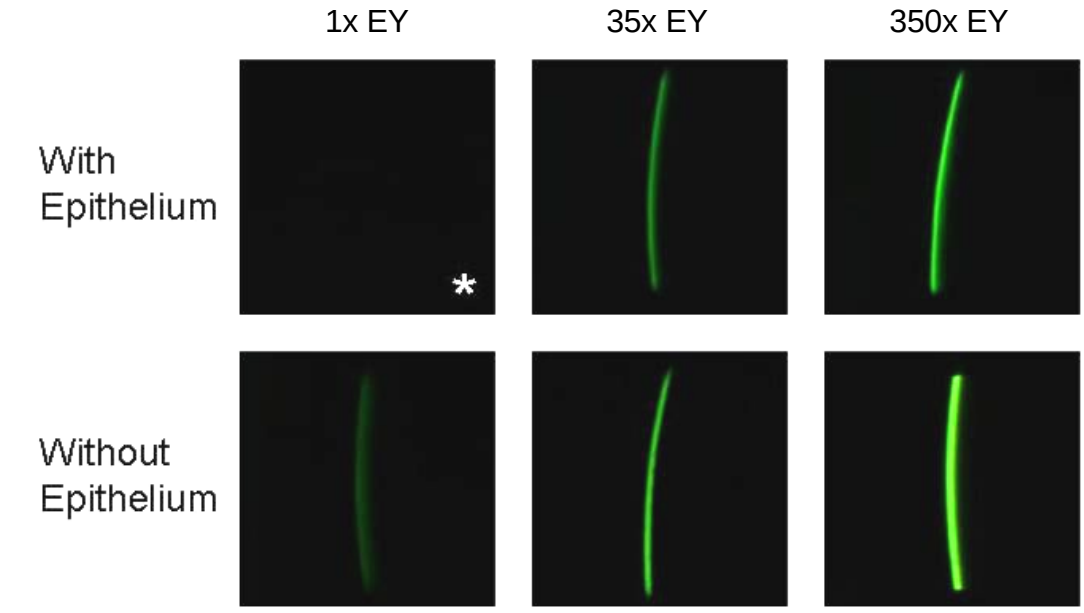

Figure 6.3. Slit lamp images of the stroma of enucleated porcine eyes that were treated either with their epithelium left intact (top row) or after de-epithelialization (bottom row) by immersion for 1 hour (or *6 hours) in treatment solutions (formulation described in Table 1). Increasing the EY concentration increases the fluorescence inside the stroma.

6.3.2 In Vitro *Application and* In Vitro *Expansion*

All quantitative comparisons of treated and control eyes were performed using deepithelialized specimens. This decision was based on observations made on intact globes with the epithelium present. An illustration is presented in Figure 6.4 (a and b) where the epithelium was left intact: the cornea behaves similarly for treated and control globes, while the expansion of the sclera is lower for the treated globe than for the fellow control. In contrast, if the epithelium is removed (Figure 6.4c, d), sufficient drug enters the cornea during the 5 minute soak to prevent corneal expansion (Figure 6.4c). The behavior evident for this pair of eyes is statistically significant: results for a group of 6 treated eyes and their

6 fellow controls (Figure 6.5) show that both cornea and sclera of deepithelialized globes are stabilized by treatment (further information on this set of data is given in Chapter 5).

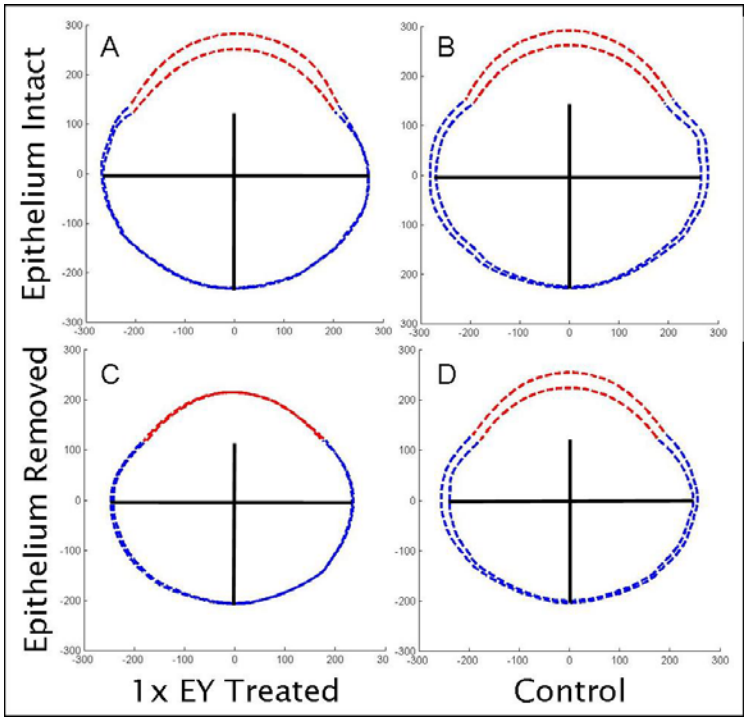

Figure 6.4. Traces of the globe perimeter show the initial shape and final shape after 24 hours of high pressure (85 mmHg) for representative specimens that were fully immersed for 5 minutes in either 1x EY (treated) or DPBS control followed by irradiation of the entire globe for 5 minutes (see Chapter 5 for further details). The epithelium was left in place for the upper pair of eyes (A treated and B control). The epithelium was removed prior to soaking the lower pair of eyes (C treated and D control). Effective stabilization of the cornea is observed in C, but not in A.

Although they are not from the same animal, comparison of the control eyes (Figure 6.4b and d) shows that control eyes with epithelium removed expand similarly to control eyes with epithelium intact. Removal of the epithelium, used in the remainder of this section,

allows drug to penetrate into the corneal stroma with no other discernible effect on the intact globe expansion behavior.

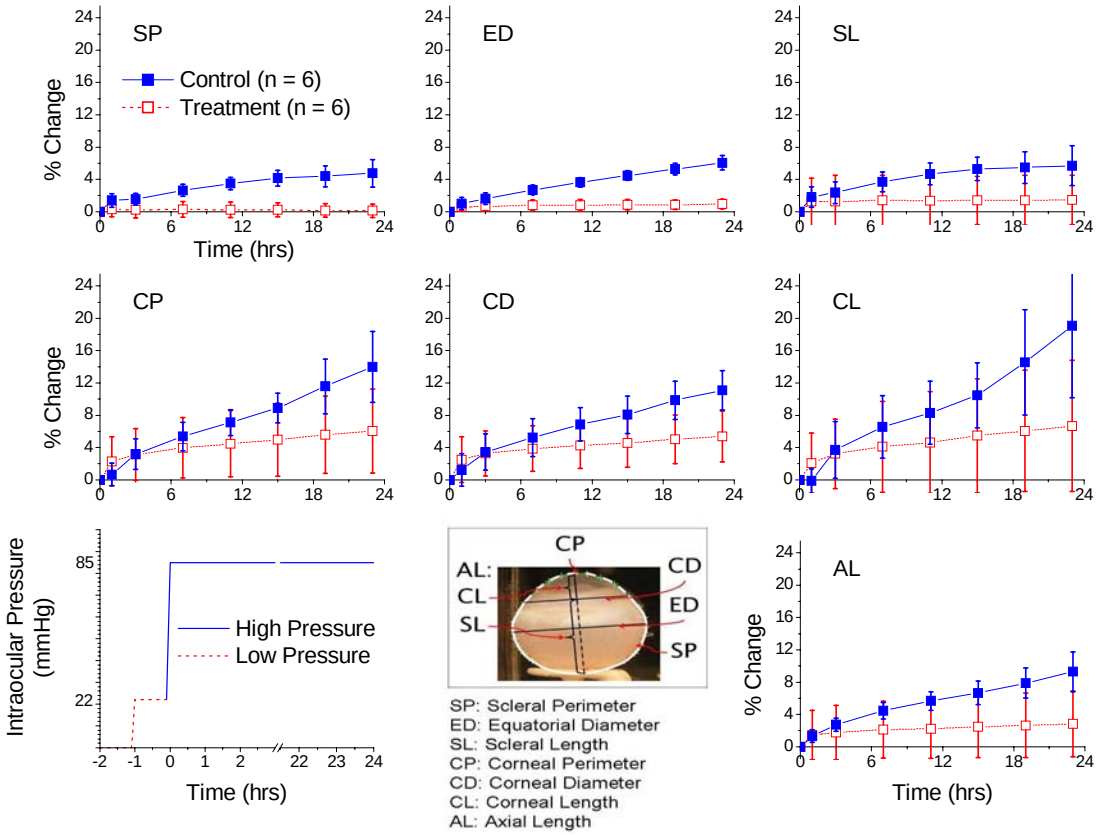

Figure 6.5. Rabbit eyes with removed epithelium are subjected to a high pressure (85 mmHg) for up to 24 hours, showing the ability of treatment of the entire eye with 1x EY to prevent the expansion of the sclera (top row) and cornea (middle row). The relevant ocular dimensions are illustrated in the inset figure, and n is the number of eyes in each group.

In relation to keratoconus, we examine the changes in dimensions of the cornea (CP, CD, and CL, defined in Figure 6.5). In the control specimens, each of the three dimensions expands significantly under the influence of elevated pressure (approximately 12% for CP, 10% for CD and 18% for CL). The three groups of controls do not differ significantly, indicating that the formulation vehicles do not play a direct role in mechanical stabilization.

Soaking the cornea in 1x EY for 5 minutes and irradiating with visible light for 5 minutes reduces expansion of the cornea as compared to DPBS controls (Figure 6.6). In anticipation of topical application of a viscous solution or gel on the cornea to administer the drug, a more concentrated solution (10x EY) was made with a "viscoelastic" surgical aid (2% HA) that creates a gel. It was applied to form a coating on the cornea. This treatment showed enhanced ability to prevent expansion (Figure 6.6), consistent with the increased EY concentration. For comparison to the treatment that is currently in FDA clinical trials for the treatment of keratoconus, we include a protocol that uses the same parameter values described for that clinical procedure. The treated eyes in the R/UVA group show similar resistance to expansion as the 10x EY treated group (Table 6.3). The treatment of the whole eye with GA (Figure 2.26) gives an extreme degree of crosslinking that is presented here for comparison (Figure 6.6).

Importantly, the intact globe expansion method provides a way to compare treatments for efficacy. Tests using a few animals (8–10) are able to distinguish treatments and to screen variations on the procedure to improve the treatment. Further, the results of the R/UVA treatment provide a benchmark for identifying clinically relevant treatments.

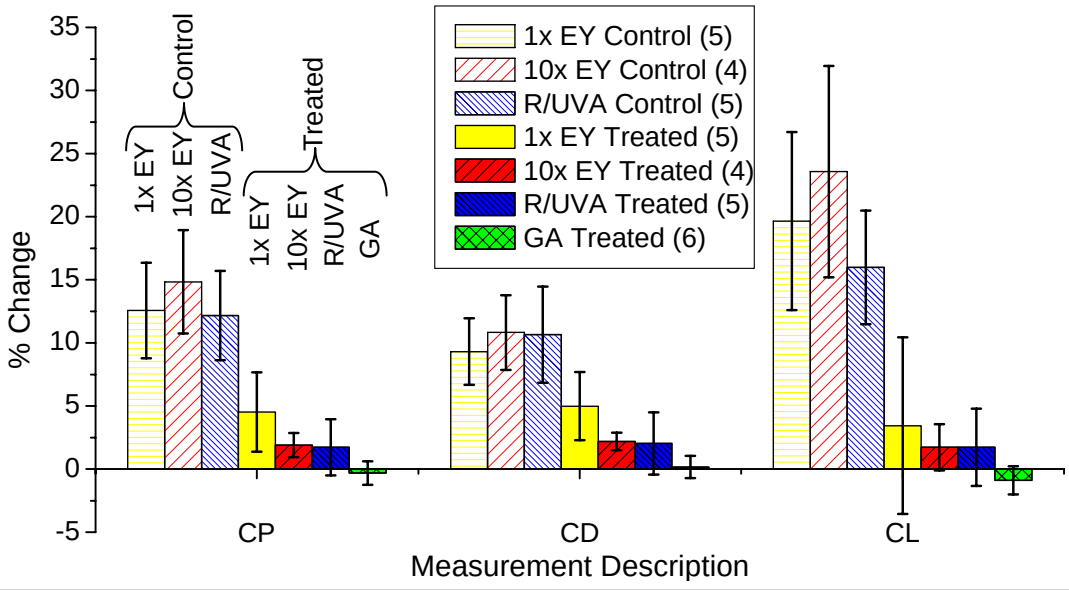

Figure 6.6. *In vitro* treated cornea after 24 hour expansion—Corneas treated with 1x EY in DPBS and visible light, 10x EY in 2% HA and visible light, R/UVA in 20% dextran and ultraviolet light, and GA all show reduced expansion compared to their respective controls (DPBS, 2% HA, and 20% dextran). Treatment effectiveness increases from left to right, with 1x EY least effective and GA most effective. In the middle, 10x EY and R/UVA are nearly equivalent. Numbers in parentheses indicate the number of eyes.

Corneal	**1x EY**		**10x EY 2% HA**		**Riboflavin**		**GA**
Dimension	Treated	Control	Treated	Control	Treated	Control	Treated
# samples	5	5	4	4	5	5	6
CP	4.5±3.14	12.6±3.80	1.9±0.96	14.8±4.09	1.7±2.22	12.2±3.53	-0.3±0.93
CD	5.0±2.70	9.3±2.63	2.2±0.69	10.8±2.96	2.0±2.47	10.6±3.80	0.2±0.88
CL	3.4±6.99	19.7±7.05	1.7±1.84	23.6±8.38	1.7±3.06	16.0±4.50	-0.9±1.11

Table 6.3. Keratoconus Treatments—Numerical Values of Data Presented in Figure 6.6

6.4 Summary

Successful treatment of keratoconus by crosslinking the constitutents of the cornea depends on penetration of the photoactivated formulation into the tissue and the activation of the

drug with safe doses of light to produce a therapeutically significant stabilization of the tissue. The *in vitro* studies presented in this chapter address each of these requiremements. It is shown that EY readily penetrates into the cornea if the epithelium is removed. If the epithelium remains on the cornea, partitioning of Eosin Y into the cornea is greatly reduced. Nevertheless, with sufficiently high driving force (high EY concentration), EY does penetrate into the cornea. Furthermore, it penetrates to an extent visible with a relatively insensitive imaging system—representing a large excess over the concentration required to achieve an effect similar to the riboflavin/UVA treatment. Therefore, it may be possible to deliver treatment to the cornea without removing the epithelium, and future studies on increasing concentrations could achieve the desired mechanical stability. Without the epithelium present, the 10x EY treatment shows strengthening capabilities comparable to the R/UVA treatment. Clinically, the R/UVA treatment involves removing the epithelium, applying topical drops of treatment solution for 5 minutes, and irradiating for 30 minutes with ~3 mW/cm^2 370 nm ultraviolet light while applying drops every 5 minutes. The 10x EY treatment we have developed involves removing the epithelium, applying a viscous drug solution for 5 minutes, cleaning off excess drug, and irradiating with ~6 mW/cm^2 514 nm visible light for 5 minutes. The 10x EY treatment is shorter and uses visible light instead of UV in order to achieve the same effective prevention of expansion. If the treatment also proves to be non-toxic and the cornea maintains optical clarity *in vivo*, this would be a potential treatment option for keratoconus.

BIBLIOGRAPHY

1. Bron, A.J. Keratoconus. *Cornea* **7**, 163-169 (1988).
2. Krachmer, J.H., Feder, R.S., Belin, M.W. Keratoconus And Related Noninflammatory Corneal Thinning Disorders. *Survey Of Ophthalmology* **28**, 293-322 (1984).
3. Rabinowitz, Y.S. Keratoconus. *Survey Of Ophthalmology* **42**, 297-319 (1998).
4. Kaufman, H.E., Werblin, T.P. Epikeratophakia for the Treatment of Keratoconus. *American Journal of Ophthalmology* **93**, 342-347 (1982).
5. Spitznas, M., Eckert, J., Frising, M., Eter, N. Long-term functional and topographic results seven years after epikeratophakia for keratoconus. *Graefes Archive for Clinical and Experimental Ophthalmology* **240**, 639-643 (2002).
6. Colin, J., Cochener, B., Savary, G., Malet, F. Correcting keratoconus with intracorneal rings. *Journal of Cataract and Refractive Surgery* **26**, 1117-1122 (2000).
7. Kymionis, G.D., Siganos, C.S., Tsiklis, N.S., Anastasakis, A., Yoo, S.H., Pallikaris, A.I., Astyrakakis, N., Pallikaris, I.G. Long-term follow-up of intacs in keratoconus. *American Journal of Ophthalmology* **143**, 236-244 (2007).
8. Spoerl, E., Wollensak, G., Dittert, D.D., Seiler, T. Thermomechanical behavior of collagen-cross-linked porcine cornea. *Ophthalmologica* **218**, 136-140 (2004).
9. Sporl, E., Genth, U., Schmalfuss, K., Seiler, T. Thermo-mechanical behavior of the cornea. *Klinische Monatsblatter Fur Augenheilkunde* **208**, 112-116 (1996).
10. Sporl, E., Genth, U., Schmalfuss, K., Seiler, T. Thermomechanical behavior of the cornea. *German Journal Of Ophthalmology* **5**, 322-327 (1997).

11. Spoerl, E., Wollensak, G., Seiler, T. Increased resistance of crosslinked cornea against enzymatic digestion. *Current Eye Research* **29**, 35-40 (2004).

12. Wollensak, G. Crosslinking treatment of progressive keratoconus: new hope. *Current Opinion In Ophthalmology* **17**, 356-360 (2006).

13. Wollensak, G., Aurich, H., Pham, D.T., Wirbelauer, C. Hydration behavior of porcine cornea crosslinked with riboflavin and ultraviolet A. *Journal of Cataract and Refractive Surgery* **33**, 516-521 (2007).

14. Wollensak, G., Spoerl, E., Reber, F., Seiler, T. Keratocyte cytotoxicity of riboflavin/UVA-treatment in vitro. *Eye* **18**, 718-722 (2004).

15. Wollensak, G., Spoerl, E., Seiler, T. Stress-strain measurements of human and porcine corneas after riboflavin-ultraviolet-A-induced cross-linking. *Journal Of Cataract And Refractive Surgery* **29**, 1780-1785 (2003).

16. Wollensak, G., Spoerl, E., Seiler, T. Riboflavin/ultraviolet-A-induced collagen crosslinking for the treatment of keratoconus. *American Journal Of Ophthalmology* **135**, 620-627 (2003).

17. Wollensak, G., Spoerl, E., Wilsch, M., Seiler, T. Endothelial cell damage after riboflavin-ultraviolet-A treatment in the rabbit. *Journal Of Cataract And Refractive Surgery* **29**, 1786-1790 (2003).

18. Wollensak, G., Spoerl, E., Wilsch, M., Seiler, T. Keratocyte apoptosis after corneal collagen cross-linking using riboflavin/UVA treatment. *Cornea* **23**, 43-49 (2004).

19. Wollensak, G., Sporl, E., Reber, F., Pillunat, L., Funk, R. Corneal endothelial cytotoxicity of riboflavin/UVA treatment in vitro. *Ophthalmic Research* **35**, 324-328 (2003).

20. Wollensak, G., Sporl, E., Seiler, T. Treatment of keratoconus by collagen cross linking. *Ophthalmologe* **100**, 44-49 (2003).

21. Wollensak, G., Wilsch, M., Spoerl, E., Seiler, T. Collagen fiber diameter in the rabbit cornea after collagen crosslinking by riboflavin/UVA. *Cornea* **23**, 503-507 (2004).

22. Andreassen, T.T., Simonsen, A.H., Oxlund, H. Biomechanical Properties of Keratoconus and Normal Corneas. *Experimental Eye Research* **31**, 435-441 (1980).

23. Oyster, C.W. *The Human Eye: Structure and Function*. (Sinauer Associates, Inc., Sunderland, Massachusetts, 1999).